ÉCOLE DE TECHNOLOGIE SUPÉRIEURE
UNIVERSITÉ DU QUÉBEC

MANUSCRIPT-BASED THESIS PRESENTED TO
ÉCOLE DE TECHNOLOGIE SUPÉRIEURE

IN PARTIAL FULFILLMENT OF THE REQUIREMENTS
FOR THE DEGREE OF DOCTOR OF PHILOSOPHY
Ph.D.

BY
Mohamed LATEB

NUMERICAL STUDY OF NEAR-FIELD POLLUTANT DISPERSION AROUND A BUILDING COMPLEX EMITTED FROM A ROOFTOP STACK

MONTREAL, NOVEMBER 13, 2013

BOARD OF EXAMINERS

THIS THESIS HAS BEEN EVALUATED

BY THE FOLLOWING BOARD OF EXAMINERS:

Prof. Christian Masson, Thesis director
Department of Mechanical Engineering, École de Technologie Supérieure

Prof. Claude Bédard, Thesis co-director
Dean of research, École de Technologie Supérieure

Prof. François Brissette, Committee president
Department of Construction Engineering, École de Technologie Supérieure

Prof. Horia Hangan, External examiner
Wind Engineering, Energy and Environment Research Institute,
The University of Western Ontario

Prof. François Morency, Examiner
Department of Mechanical Engineering, École de Technologie Supérieure

Prof. Theodore Stathopoulos, Invited examiner
Department of Building, Civil and Environmental Engineering, Concordia University

THIS THESIS WAS PRESENTED AND DEFENDED

IN THE PRESENCE OF A BOARD OF EXAMINERS AND PUBLIC

ON OCTOBER 28, 2013

AT ÉCOLE DE TECHNOLOGIE SUPÉRIEURE

ACKNOWLEDGEMENTS

The author expresses his deepest gratitude to Prof. Christian Masson and Prof. Claude Bédard for their guidance and invaluable advice. Special thanks are also given to Prof. Ted Stathopoulos for his collaboration, constructive comments and support during this research. I would like to highlight the interest of all of them to this present work that has been a constant source of motivation.

The author would also like to thank the anonymous reviewers of the various conferences[1] and journals[2] – where portions of this work have been presented and published – for thoroughly reading the manuscripts and for their valuable comments.

I wish to express my deep indebtedness to the Fonds québécois de la recherche sur la nature et les technologies (FQRNT) for their financial support without which this research would not have been possible.

Many thanks to all those who shared their valuable time with me to discuss matters related to the research. I would also like to thank all my friends, colleagues and fellow researchers of the department of mechanical engineering for the enlightening discussions and with whom I spent a very enjoyable time.

Last, but not least, my warmest and most sincere thanks are especially given to my family whose help, support and encouragement have given me motivation to carry out this research, and without which this study could have never been completed.

[1] Conferences are: AWAS'08, CWE2010 and 12ACWE.

[2] Journals are: Building and Environment, Atmospheric Environment and Journal of Wind Engineering and Industrial Aerodynamics.

NUMERICAL STUDY OF NEAR-FIELD POLLUTANT DISPERSION AROUND A BUILDING COMPLEX EMITTED FROM A ROOFTOP STACK

Mohamed LATEB

ABSTRACT

The topic of environmental pollution is of special significance in the atmospheric boundary layer (ABL) especially in urban areas as it is one of the significant sources of poor indoor air quality due to contamination of fresh-air intakes. In city centres where external air pollution levels are relatively high, it is usually assumed that natural ventilation may not be able to provide adequate indoor air quality. Therefore mechanical ventilation and air-conditioning systems are thus being solicited to "clean" the incoming air (Kukadia and Palmer, 1998). There is evidence that such systems do not always provide clean fresh-air to the occupants of the building since several contaminants from nearby outside sources exist (e.g. vehicle exhaust, rooftop stack exhaust, wind-blown dust). Control of the pollutant sources and understanding the dispersion mechanisms, therefore, shall be considered as the first alternative to evaluate better these harmful phenomena.

This thesis focuses on dispersion and transportation of pollutant emissions from a building rooftop stack situated in the wake of a neighbouring tower using numerical simulation approach. The main objective of this work is to contribute to the "best-practice" of numerical modelling for dispersion studies. For that, wind tunnel tests as well as full-scale experiments are numerically reproduced to shed light on the uncertainties related to the complex dispersion phenomenon when using CFD simulations.

In the first study of this thesis, the behaviour of the flow and pollutant concentration fields around the two-building configuration are investigated by means of various $k-\epsilon$ turbulence models (i.e. standard, re-normalization group (RNG) and realizable $k-\epsilon$ models). The results show that the realizable $k-\epsilon$ model yields the best agreement with wind tunnel experimental data for lower stack height and smaller momentum ratio, while the RNG $k-\epsilon$ model performs best for taller stacks. Despite an overestimation of concentrations using the realizable $k-\epsilon$ model, it remains the only model that provides the correct trend of concentration distribution in the lower region between the two buildings. Based on this finding, the second study deals with the ability of CFD to simulate controlled (wind tunnel scale) and non-controlled (full-scale) environments using realizable $k-\epsilon$ model. This study details also the main steps for conducting consistent and reliable numerical simulations for dispersion studies. Additionally, CFD is shown to simulate better controlled environments than non-controlled environments.

The third study investigates the influence of two important parameters related to the pollutant exhaust source, i.e. stack height and pollutant exhaust velocity, on the concentration fields measured in the wind tunnel. The results show that increasing the stack height has an effect that is similar to increasing the pollutant exhaust velocity on the concentration distributions and that such effect depends upon the wall of the building under consideration. In addition,

recommendations on fresh-air intake locations for the two buildings are provided. In the final study, an unsteady turbulence model (i.e. detached-eddy simulation) is tested to evaluate the flow-field and the dispersion field around the two-building configuration. The results show that the flow fluctuation capture is crucial to address better the dispersion in the wake of buildings. Consequently, the strengths of using an unsteady approach are compared to RANS methodology which provides however good results far from the exhaust source. The results of this extensive research support the use of an unsteady methodology in future works.

Keywords: Computational fluid dynamics (CFD), atmospheric boundary layer (ABL), rooftop stack emissions, RANS $k - \epsilon$ turbulence models, dispersion modelling, numerical simulation, stack height, detached-eddy simulation (DES) turbulence model, pollutant exhaust velocity, urban environment.

NUMERICAL STUDY OF NEAR-FIELD POLLUTANT DISPERSION AROUND A BUILDING COMPLEX EMITTED FROM A ROOFTOP STACK

Mohamed LATEB

RÉSUMÉ

Le sujet de la pollution environnementale est d'une importance significative dans la couche limite atmosphérique, particulièrement dans les zones urbaines où elle est l'une des principales sources de la mauvaise qualité de l'air intérieur des habitations due à la contamination au niveau des prises d'air neuf. Dans les centres-villes où le niveau de la pollution de l'air extérieur est relativement élevé, on suppose généralement que la ventilation naturelle est incapable d'assurer une qualité d'air adéquate à l'intérieur des édifices. Par conséquent, les systèmes de ventilation mécaniques et d'air climatisé sont de plus en plus sollicités pour la "purification" de l'air introduit dans le bâtiment (Kukadia and Palmer, 1998). Il est évident que de tels systèmes n'arrivent pas toujours à produire de l'air propre à l'intérieur des édifices car plusieurs sources de pollution existent dans le voisinage extérieur (ex. gaz d'échappement des automobiles, émissions des cheminées de toit, poussières et débris transportés par le vent). Il est donc nécessaire de prendre en compte le contrôle de ces sources polluantes et la compréhension des mécanismes de dispersion en premier lieu afin d'évaluer correctement ces phénomènes nocifs.

Cette thèse porte sur la dispersion et le transport des émissions polluantes de cheminée de toit d'un immeuble situé dans le sillage d'une tour voisine obtenus à l'aide de la modélisation numérique. L'objectif principal de ce travail est d'apporter une contribution vers une meilleure modélisation numérique de la dispersion des polluants atmosphériques. Pour ce faire, des expériences menées en soufflerie et sur le terrain ont été numériquement reproduites pour mettre en évidence les incertitudes relatives à la modélisation numérique du phénomène de dispersion.

Dans la première étude de cet ouvrage, le comportement du champ de l'écoulement et du champ de concentration a été examiné autour du site considéré à l'aide de différents modèles de turbulence $k-\epsilon$ (c.-à-d. les modèles standard, re-normalization group (RNG) et realizable $k-\epsilon$). Les résultats montrent que le modèle realizable $k-\epsilon$ donne de meilleurs résultats, comparés à ceux de la soufflerie, pour de petites hauteurs de cheminée et faibles vitesses d'émission du polluant. Le modèle RNG $k-\epsilon$ performe mieux pour de grandes hauteurs de cheminée, quelle que soit la vitesse d'émission du polluant. Cependant, malgré la surestimation de la concentration par le modèle realizable $k-\epsilon$, ce dernier reste le seul capable de reproduire correctement l'évolution de la concentration dans la basse région entre les deux immeubles. Se basant sur ce résultat, la deuxième étude est consacrée à la capacité de la CFD à simuler un environnement contrôlé (essais de soufflerie) et non contrôlé (essais de terrain) à l'aide du modèle realizable $k-\epsilon$. Dans cette partie, les différentes étapes principales et nécessaires pour réaliser une étude numérique fiable et consistante de la dispersion sont détaillées. L'étude démontre que la CFD reproduit mieux un environnement contrôlé qu'un environnement non contrôlé.

La troisième étude de cet ouvrage examine l'influence de deux paramètres importants reliés à la source de pollution, c.-à-d. la hauteur de cheminée et de la vitesse d'émission du polluant, sur les concentrations mesurées dans une soufflerie. Les résultats indiquent que l'augmentation de la hauteur a un effet similaire à l'augmentation de la vitesse d'émission sur la distribution des concentrations et que la nature de ces effets dépend de la façade de l'immeuble considérée. Par la suite, des recommandations sur les emplacements des entrées d'air frais sont formulées. Dans la dernière étude, le modèle de turbulence instationnaire "detached-eddy simulation" est analysé pour évaluer le champ de l'écoulement et le champ de la dispersion. Les résultats révèlent que la capture des fluctuations de l'écoulement est cruciale pour mieux reproduire la dispersion dans la région du sillage des immeubles. Par conséquent, l'avantage de l'approche instationnaire est illustré comparé aux méthodes stationnaires RANS qui donnent toutefois de bons résultats loin de la source de pollution. Les résultats de cette vaste recherche suggèrent d'exploiter d'avantage la modélisation numérique instationnaire pour les futurs travaux de recherche.

Mot-clés : Modélisation de la dynamique des fluides, couche limite atmosphérique, émissions de cheminées de toit, modèles de turbulence RANS $k - \epsilon$, modélisation de la dispersion, simulation numérique, hauteur de cheminée, modèle de turbulence "detached-eddy simulation" (DES), vitesse d'émission de polluant, environnement urbain.

CONTENTS

LIST OF TABLES

LIST OF FIGURES

LIST OF ABBREVIATIONS

ABL	Atmospheric boundary layer
ADMS	Atmospheric dispersion modelling system
AIAA	American institute of aeronautics and astronautics
AP	Aspiration probe measurements
ASHRAE	American society of heating, refrigerating and air-conditioning engineers
ASME	American society of mechanical engineers
CFD	Computational fluid dynamics
CFL	Courant-Friedrichs-Lewy
CPU	Central processing unit
CWE	Computational wind engineering
DES	Detached-eddy simulation
EPA	United state environmental protection agency
FFT	Fast Fourier transform
GCI	Grid convergence index
IAWE	International association for wind engineering
IRSST	Institut de recherche Robert-Sauvé en santé et sécurité du travail
ISL	Inertial sublayer
LES	Large-eddy simulation
LS-PIV	Large scale-particle image velocimetry
LST	Light scattering technique

MDS	Modelled-stress depletion
PSD	Power spectral density
QUICK	Quadratic upstream interpolation for convective kinetics
RANS	Reynolds-averaged Navier–Stokes
RLZ	Realizable $k - \epsilon$ turbulence model
RNG	Re-normalized group $k - \epsilon$ turbulence model
RSL	Roughness sublayer
RSM	Reynolds stress model
SGDH	Standard gradient-diffusion hypothesis
SGS	Sub-grid scale
SIMPLE	Semi-implicit method for pressure-linked equations
SKE	Standard $k - \epsilon$ turbulence model
SL	Surface layer
UBL	Urban boundary layer
UCL	Urban canopy layer
URANS	Unsteady Reynolds-averaged Navier–Stokes

LIST OF SYMBOLS

c	Pollutant concentration [ppb]
c_o	Pollutant reference concentration [ppb]
c'	Fluctuating pollutant concentration [ppb]
C	Mean pollutant concentration [ppb]
C_e	Mean pollutant concentration at the stack exit [ppb]
C_{des}	DES model constant
C_1	$k-\epsilon$ model coefficient
C_2	$k-\epsilon$ model coefficient
C_μ	$k-\epsilon$ model coefficient
d_s	Diameter of the stack [m]
D_t	Turbulent mass diffusivity [m^2 s^{-1}]
e_a	Average relative error
$\langle f \rangle$	Time averaged value of f
$f^{'}$	Fluctuating value of f
H_{BE}	Height of the BE building [m]
H_{Fb}	Height of the Faubourg tower [m]
k	Turbulent kinetic energy [m^2 s^{-2}]
K	Non-dimensional pollutant concentration
l_{des}	Length scale for DES model (= min[l_{rke}, l_{les}]) [m]
l_{les}	Length scale for LES model (= $C_{des}\Delta x_{i_{\max}}$) [m]

l_{rke}	Length scale for $k-\epsilon$ model ($= k^{3/2}/\epsilon$) [m]
l_λ	Taylor microscale ($= [10\nu k/\epsilon]^{1/2}$) [m]
M	Momentum ratio
P	Mean pressure [kg m^{-1} s^{-2}]
P_k	Turbulent production term [m^2 s^{-3}]
Q_e	Pollutant emission rate [m^3 s^{-1}]
Re	Reynolds number
Re_s	Reynolds number at the stack exit
Sc_t	Turbulent Schmidt number
S_{ij}	Strain rate tensor [s^{-1}]
S'	Mean volume contaminant source generation rate
t	Time [s]
t^*	Non-dimensional time unit
TI	Turbulence intensity
TI_s	Pollutant turbulence intensity at the stack exit
u_i	Velocity components along the three directions x, y and z [m s^{-1}]
u_i'	Fluctuating velocity components along the three directions x, y and z [m s^{-1}]
u^*	Friction velocity [m s^{-1}]
U_H	Mean wind Velocity at the roof height of the BE building [m s^{-1}]
U_i	Mean velocity components along the three directions x, y and z [m s^{-1}]
$\overline{u_i'u_j'}$	Reynolds stress components [m^2 s^{-2}]

w_e	Pollutant exhaust velocity [m s^{-1}]
x, y, z	Space coordinates [m]
Y_k	Turbulent dissipation term [m^2 s^{-3}]
z_o	Roughness length [m]
κ	Von Karman constant ($= 0.42$)
ϵ	Turbulent dissipation rate [m^2 s^{-3}]
ρ	Air density [kg m^{-3}]
ρ_e	Pollutant density [kg m^{-3}]
σ_k	$k - \epsilon$ model coefficient
σ_ϵ	$k - \epsilon$ model coefficient
μ	Air dynamic viscosity [kg m^{-1} s^{-1}]
μ_e	Pollutant dynamic viscosity [kg m^{-1} s^{-1}]
ν	Air kinematic viscosity [m^2 s^{-1}]
ν_e	Pollutant kinematic viscosity [m^2 s^{-1}]
ν_t	Turbulent eddy viscosity [m^2 s^{-1}]
δ_{ij}	Kronecker delta
Δx_i	Grid spacing in the three directions ($= \Delta x$, Δy, Δz) [m]
$\Delta x_{i_{\max}}$	Maximum grid spacing for a given cell ($=$ max[Δx, Δy, Δz]) [m]
$\Delta x_{i_{\min}}$	Minimum grid spacing for a given cell ($=$ min[Δx, Δy, Δz]) [m]
Δt	Time step [s]

INTRODUCTION

Background of the problem

The field of wind engineering is defined by the International Association for Wind Engineering (IAWE) as a multi-disciplinary subject matter concerned with multifold topics including the atmospheric dispersion of pollutants which is the main subject of the present work. This topic, especially in the urban environment is concerned with the transportation of pollutants in the lower atmospheric boundary layer by wind flows. Dispersion of pollution represents an important environmental problem with respect to human health. The subject is of great concern especially when the crucial issues of the well-being and human comfort are considered. Investigation of pollutant transport and dispersion have received a lot of attention in recent years and become a focal point in environmental research because of an increasing interest for the protection of air quality (Assimakopoulos *et al.*, 2003). In urban areas, several sources of pollution (e.g. wind-blown dust, vehicle exhaust, toxic and odorous emissions) may be unpleasant and dangerous where health and safety are of concern (ASHRAE, 2007). Among them, pollutant emissions from rooftop stacks is a factor that can seriously affect the quality of fresh-air at intakes of the emitting and/or surrounding buildings, and potentially compromising the well-being of these buildings' occupants. Additionally, inside cities – where building density increases – the problem of air quality becomes critical; indeed, stack emissions can accumulate between buildings, thus inducing an increase of the contaminant concentrations because reduced airflow passes through the zone's boundaries as compared to free-stream flow (Rock and Moylan, 1999). Therefore, the risk of their possible ingestion at fresh-air intakes remains highly likely and dangerous for the occupants' health. Current standards for building ventilation systems recommend that rooftop stacks be designed such that their emissions do not contaminate the fresh-air intakes of the emitting building or the nearby buildings (Stathopoulos *et al.*, 2004). The scientific community has responded to the need to contribute to daily life quality by controlling and maintaining air quality, in buildings and offices, above the acceptable norms typically established and authorised either by governments or within the respective professional organizations (Sterling, 1988).

Urban air quality is directly related to the atmospheric boundary layer (ABL) flows and their interactions with obstacles, which are themselves strongly dependent on many aspects of meteorology, wind engineering and environmental science (Salim, 2011). Turbulent wind flows have long presented a considerable challenge to the accuracy in the applicability of calculations (Mockett and Thiele, 2007). The types of flows encountered in the field of wind engineering are no exception, and consist of many complex flow features that may contain recirculation zones and stagnation points (Easom, 2000). Indeed, in the lower atmospheric boundary layer, specifically in cities around individual and/or groups of buildings, the superposition and interaction of the flow patterns induced by the buildings and structures strongly affect the dispersion and govern the movement of pollutants (Chang and Meroney, 2001). Consequently, complicated dispersion phenomena and highly unpredictable effects are created. Besides, the state-of-the-art, as noticed by Stathopoulos *et al.* (2004), is not sufficiently advanced to allow building engineers to find appropriate design criteria to avoid this problem – ingestion of stack emissions at fresh-air intakes – for new construction or to help alleviate for existing buildings. Therefore, finding a way to resolve this harmful phenomenon and understanding the mechanisms and characteristics of the pollutant dispersion process still remain a challenge for scientific researchers in wind engineering.

Sites and cases under investigation

The present numerical study takes its origin from previous full-scale experimental work completed in downtown Montreal and thereafter at the boundary layer wind tunnel of Concordia University by Stathopoulos *et al.* (2004). The specific experiments reproduced in this numerical study were carried out between August 12th and 26th, 2002, in full-scale, on the roof of the BE building, a 3-storey building[3] which used to house the department of Building, Civil and Environmental Engineering at Concordia University in downtown Montreal. A pollutant was emitted by means of a rooftop stack, located in the upwind part of the BE building roof, with various stack heights and various exhaust velocities. This building was situated 25 m away from a 12-storey tower[4] located on its south-west side. The wind came from the south-west

[3] Hereafter referred to as BE building.
[4] Hereafter referred to as Faubourg tower.

perpendicularly to the windward wall of the Faubourg tower, thus placing the BE building in its wake. The field tests were performed in strong winds ($U_{Dorval} > 4$ m s^{-1}) according to measurements taken at Dorval airport provided by Environment Canada (Stathopoulos *et al.*, 2004). Wind speeds of this magnitude correspond, according to stability classes defined by Pasquill (1961), to a neutral or slightly unstable atmosphere and lend themselves well to wind tunnel modelling according to Stathopoulos *et al.* (2004). The laboratory tests were carried out at the boundary layer wind tunnel of Concordia University. The models of the BE building, Faubourg tower, and surroundings were reproduced at 1:200 scale. In the windward direction, the surroundings were reproduced up to a distance of 250 m. In the leeward direction, the neighbouring buildings were included up to a distance of 50 m.

This research complements the experimental works described above by applying numerical modelling techniques. Since the wind comes perpendicularly to the upstream Faubourg tower, the latter seems to be the only main obstacle capable of producing major effects on the overall behaviour of the wind flow and concentration fields around the building of interest downstream. Therefore, only the BE building and the Faubourg tower are considered at the site under investigation (see Fig. 2.1 in Chapter 2). Three structures are situated on the roof of the BE building. A penthouse is located at the back of the roof, along the downstream wall, a skylight in the north-east part and an elevator in the upwind south-east part of the roof. The stack, from which the pollutant is exhausted, is at the upstream edge of the roof near the windward wall of the BE building. Only one structure exists at the centre of the Faubourg tower roof. It should be noted that all these structures are taken into account in the geometric model. Not taken into account in the geometric model are the entry of the BE building, located on the ground floor on the windward wall, and a small wall of height 1 m (parapet) that runs along the perimeter of the BE roof. Since the entry of the BE building and the parapet have not been reproduced either in the wind tunnel experiments, it was decided not to reproduce them in this numerical study.

Among the various parameters that affect the dispersion of pollutants from rooftop stacks, two of them – namely stack height and pollutant exhaust velocity – are investigated in this

study, since these two parameters have been considered and examined in the experimental tests. Tables 1 and 2 list the different cases of stack height, h_s, and momentum ratio, M, tested at field and wind tunnel scale experiments, respectively. Since densities of air and pollutant gas are assumed equal, the momentum ratio represents the ratio between the exhaust velocity of the pollutant, w_e, and wind velocity, U_H, at height H_{BE} of the BE building. The height of the stack is given in metre [m].

Table 1 Summary of simulation test cases selected from full-scale experiments (1:1 scale).

Stack height (h_s) [m]	Momentum ratio ($M = w_e/U_H$)
1	2.3
	4.9
3	1.7
	3.9

Table 2 Summary of simulation test cases selected from wind tunnel experiments (1:200 scale).

Stack height (h_s) [m]	Momentum ratio ($M = w_e/U_H$)
1	2.2
	5
3	2.2
	4.5
	5
4	2.2
	5
7.2	2.2
	5

Objectives of the thesis

This work is primarily concerned with developing a better understanding of the numerical modelling of pollutant transport in urban areas in the case of pollutants emitted from a rooftop stack, therefore contributing to the "best-practice" of numerical modelling for dispersion studies. According to Stathopoulos *et al.* (2008), it is of prime importance to reduce the potential risk of exhaust ingestion at the location of fresh-air intakes, due to flow recirculation around buildings in city centres where external air pollution levels are relatively high. The behaviour of the flow and pollutant concentration fields around a two-building configuration is therefore investigated and the results of simulations are compared to wind tunnel data as well as actual in situ measurements.

The first study reported in this thesis compares different turbulence models. Various steady-state RANS $k-\epsilon$ turbulence models (i.e. standard $k-\epsilon$, RNG $k-\epsilon$ and realizable $k-\epsilon$ models) which are the most widely used models for many applications (e.g. Assimakopoulos *et al.*, 2003; Xie *et al.*, 2005; Salim *et al.*, 2011) including wind engineering (Huang *et al.*, 2011) and pollutant transport (Xie and Castro, 2006) are tested to evaluate their accuracy in reproducing the dispersion process. Special attention is given to the evolution of the wind-flow field and distribution of the pollutant concentrations around the two-building configuration. In addition, the distribution of the turbulent kinetic energy, k, has been also investigated, since many authors (e.g. Murakami, 1993; Rodi, 1997; Wright and Easom, 2003; Tominaga *et al.*, 2008) have noticed that an inaccurate wind-flow pattern can be induced by an excessive k-production which, in turn, is generated by some RANS models.

Reproduction of the full-scale and wind tunnel tests using the realizable $k-\epsilon$ turbulence model, following previous findings and recommendations of Wang (2006) and Blocken *et al.* (2007), permits first to emphasize the performance of the numerical approach and to validate the results obtained with the two simulation scales against experimental data. Thus, the ability of CFD to simulate controlled (i.e. wind tunnel tests) and non-controlled (i.e. full-scale experiments) environments is highlighted.

Several simulations using various stack heights and pollutant exhaust velocities are performed to seek, on the one hand, the effects of these two parameters on pollutant concentration fields. On the other hand, determining the high concentration locations highlights where to locate fresh-air intakes in order to avoid a re-ingestion of the pollutants into the emitter building as well as into the upstream tower. Therefore, this study should provide recommendations on the appropriate fresh-air intake locations.

In order to evaluate the performance of RANS $k - \epsilon$ models and to take into account the transient characteristics of the flow, an unsteady-state model is also tested to evaluate the flow-field structure and the dispersion field around the considered configuration since no information of the flow-field pattern is available from experimental data. The detached-eddy simulation turbulence model is selected as the most appropriate model since it combines the most favourable aspects of the URANS and LES techniques (Squires, 2004). It permits to evaluate the recirculation region of the wake, to visualize the horseshoe structure around the upstream tower, and to estimate the Reynolds stress components. The contribution of unsteadiness in reproducing accurately the wind-flow structure and the dispersion process is finally highlighted.

Structure of the thesis

In the present research, dispersion of exhaust pollutants from a building rooftop stack situated in the wake of a neighbouring tower is studied by means of computational fluid dynamics. The results of different simulations are compared against experimental results obtained by Stathopoulos *et al.* (2004). This thesis is therefore composed of five chapters and structured as follows:

Chapter 1 is devoted to the state-of-the-art. This part gathers the most important research works that have been carried out to date on pollutant dispersion in urban areas. Studies related to this topic and that bring explanations and solutions to the encountered issues in modelling the dispersion of pollutant emissions are also added to better understand how the dispersion mechanisms occur.

Regarding the prediction accuracy of the wind-flow field around buildings, which is highly dependent on the performance of the turbulence model used, and the dispersion field, which is highly related to the wind-flow field, the choice of the turbulence model appears important and crucial to reproduce an accurate dispersion mechanism and process. The objective of Chapter 2 is therefore to assess various types of RANS $k-\epsilon$ turbulence models (i.e. standard $k-\epsilon$ model, RNG $k-\epsilon$ model and realizable $k-\epsilon$ model) in order to determine the best turbulence model to reproduce pollutant plume dispersion around the two-building configuration under study. The simulation results are compared to those of wind tunnel tests.

In Chapter 3, the necessary different steps for carrying out high quality simulations are detailed, including full descriptions of the geometric model, mathematical model, numerical model and evaluation of the grid refinement as well as the results error analysis. Finally, the performance of the numerical approach using two different scales[5] is emphasized, the validation of results is presented, and the error analysis of the CFD modelling is evaluated.

Chapter 4 complements the simulations previously reported in Chapter 3 at wind tunnel scale (1:200). This study deals with the influence of the stack height and pollutant exhaust velocity on the pollutant plume and dispersion, in order to determine the best fresh-air intake locations where outdoor pollutant concentrations are the lowest.

Finally to shed light on the steadiness of the turbulence models in reproducing the wind-flow structure as well as the dispersion process, complementary simulations are reported in Chapter 5 using an unsteady-state turbulence model. In this case, the detached-eddy simulation (DES) model is employed because of the simplicity of its implementation with a wide range of existing RANS models in industrial and commercial CFD codes (Bunge *et al.*, 2007). The results are again compared to wind tunnel measurements.

[5] The two different scales of concern are full scale (1:1) and wind tunnel scale (1:200).

CHAPTER 1

LITERATURE REVIEW

1.1 Introduction

This chapter deals with the state-of-the-art as well as previous studies – both experimental and numerical methodologies – carried out regarding the area of the air pollutant dispersion in urban environment. Since the simulation of the dispersion field around buildings depends strongly on the correct simulation of the wind-flow structure (Zhang *et al.*, 2005), the studies performed during the past years on the wind-flow field around buildings are reviewed. This chapter also identifies errors that can produce poor results when numerically modelling wind flow and dispersion fields around buildings in urban environments. Finally, particular attention is paid to the practical guidelines developed by researchers and organizations to establish a common methodology for verification and validation of numerical simulations and/or to assist and support the users for a better implementation of the computational fluid dynamics (CFD) approach.

1.2 Literature survey

To counter the pollutant transportation problem, several studies have been carried out during the past few decades in the dispersion field, because of the growing concern about air pollution in urban environments (Tseng *et al.*, 2006) and the increasing interest for protecting air quality (Assimakopoulos *et al.*, 2003). The topic is of prime importance since it is directly related to the protection of human health and the conservation of the living environment (Kawamoto *et al.*, 2011). To ensure a high quality of urban life, it is necessary to understand and predict the flow of urban air as well as emissions and distribution of air pollutants (Fernando *et al.*, 2010). Furthermore, in urban areas the pollutant plume arising is highly affected by the complex flows induced by the surrounding buildings (Pournazeri *et al.*, 2012). Consequently, understanding how the emission of particles is influenced by turbulence and transported from the source to the neighbourhood environment presents a very important challenge for modelling air pollu-

tant transport and dispersion with good accuracy. Additionally, the strong relations existing between the dispersion and wind-flow structures make essential the understanding of the physical processes that characterize the airborne environment in and around urban areas (Philips, 2011). Therefore, the following sections focus on the studies performed on the wind-flow field as well as on the pollutant dispersion around buildings in urban areas. These provide the context for this work and emphasize the contributions of the present thesis. Before reviewing and discussing the main past works related directly to the topic of this thesis, it seems necessary to introduce readers to what the atmospheric boundary layer and its characteristics consist of.

1.2.1 Atmospheric boundary layer (ABL)

The atmospheric boundary layer is defined as the lowest region of the atmosphere directly influenced by the proximity of the earth's surface (Bonner *et al.*, 2010), and where physical quantities such as flow velocity, temperature, moisture, etc. display rapid fluctuations and vertical mixing is strong (Georgoulias and Papanastasiou, 2009). The height of the atmospheric boundary layer is an important parameter in the dispersion of air pollution and its modelling (Gryning *et al.*, 1987; Van-Pul *et al.*, 1994). It can incessantly change both in space and time, and may vary from less than one hundred to several thousand metres depending on the orography, surface cover, season, daytime and weather (Hennemuth and Lammert, 2006).

The ABL is almost always continuously turbulent over its entire depth (Stull, 1998), particularly in urban environment where the main disturbing features are the buildings of different height and shapes which introduce a large amount of vertical surfaces and high roughness elements, and generate complex local flows between buildings (Piringer *et al.*, 2007). In this particular area, the vertical structure of the atmospheric boundary layer – also called urban boundary layer (UBL) – is composed of a roughness sublayer (RSL) near the ground and an inertial sublayer (ISL) above (Fisher *et al.*, 2006) as can be seen in Fig. 1.1. Both the roughness sublayer and the inertial sublayer are encompassed within the surface layer (SL), and above which the urban outer layer – commonly referred to as gradient height – extends to a height where the wind is unaffected by the earth's surface (Easom, 2000). In the surface layer, strong vertical gradients controlling the transfer of momentum, mass and heat

occur (Kaimal and Finnigan, 1994) and the turbulence, which transports the heat, momentum, gaseous constituents and aerosols from and to the earth's surface (Georgoulias and Papanastasiou, 2009), is mainly driven by wind shear and is not enhanced or suppressed by stability effects in neutral stratification (Van-Pul *et al.*, 1994). In the urban outer layer and free atmosphere, the Coriolis force, friction and pressure gradients are responsible for the wind flow whereas in the surface layer, the roughness of the surface becomes the significant parameter affecting the velocity profile (Crasto, 2007).

The roughness sublayer is the region at the bottom of the boundary layer and can be defined as the layer where flow is dynamically influenced by the characteristic length scales of the roughness elements (Barlow and Coceal, 2009). This region is of great importance due to its vertical extension over large roughness elements (Fisher *et al.*, 2006). Near the ground surface, the buildings form an urban canopy layer (UCL) and the dispersion is determined by a number of factors including the configuration of the building and the location of the source (Huq and Franzese, 2012). The urban dispersion is governed by the characteristic length scales of atmospheric boundary-layer turbulence, rather than urban canopy length scales that are more likely to affect dispersion only in the vicinity of the source (Franzese and Huq, 2011). It is worth mentioning that this urban outdoor pollutant dispersion is classified as micro-scale dispersion and refers to small scale meteorological phenomena that affect very small areas (horizontal length scales smaller than 10 km) compared to large scale meteorological phenomena (macro-scale and meso-scale) as detailed by Blocken *et al.* (2013). Within this micro-scale dispersion, two different dispersion regimes are distinguished in the literature since it has been already pointed out that turbulent diffusion differs in the near and the far regions from a continuous point source (Efthimiou and Bartiz, 2011): (i) the near-field dispersion that concerns the near-vicinity of the pollutant source and for which the relevant turbulence time and length scales controlling dispersion are related to the mean building height and to the spacing between buildings (Huq and Franzese, 2012), and (ii) the far-field dispersion of interest in plumes with a flow-structure and a vertical dimension larger than the urban canopy height for which the dispersion is governed by the ABL scales (Hajra *et al.*, 2011). Owing to the main purpose and characteristics of this work, only the near-field dispersion regime is relevant. In the near-field dispersion case, the

pollutant particles released from various sources inside the urban canopy, are mixed and dispersed over and around buildings because of the interactions between many physical processes that contribute to its evolution (White and Senff, 1999) including the dynamics of flow over urban topography and the building configurations.

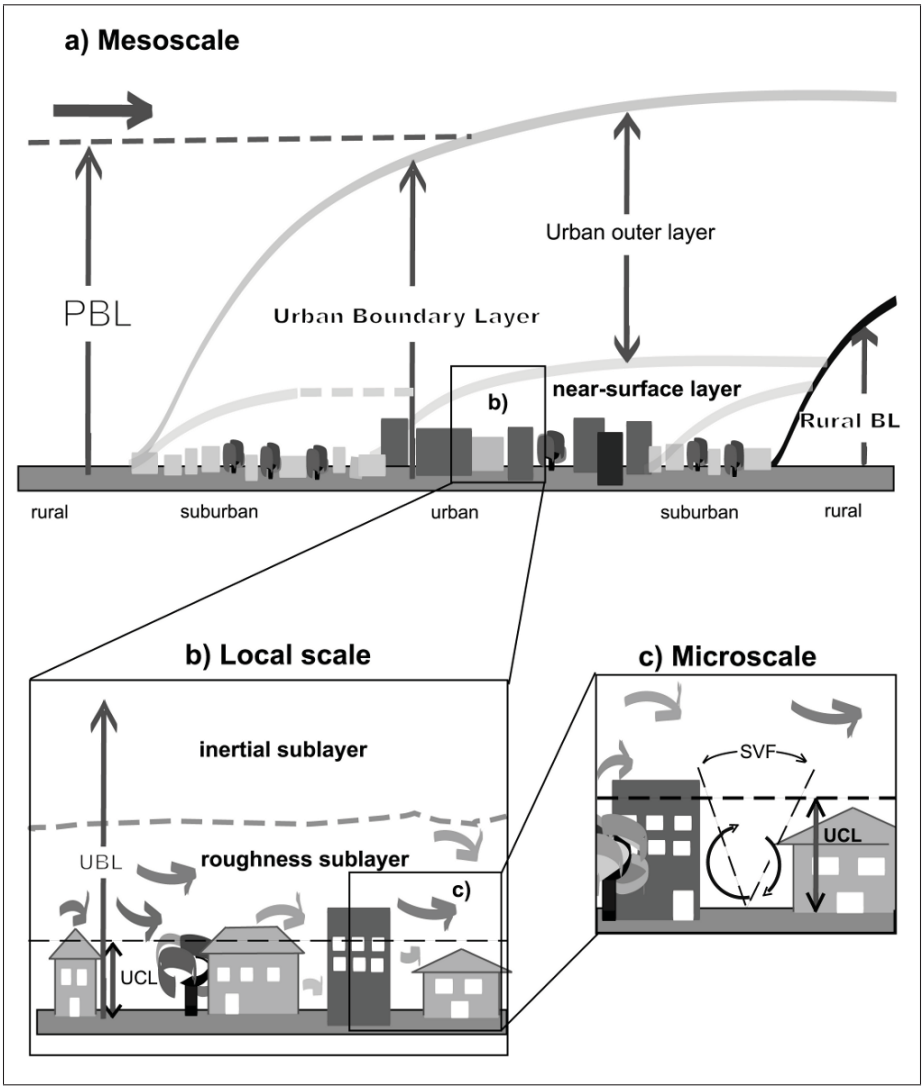

Figure 1.1 Sketch of the urban boundary-layer structure indicating the various sublayers and their names (from Piringer *et al.* (2007)).

1.2.1.1 Homogeneity of the ABL

In recent few decades, the interests and efforts of boundary-layer researchers have been increasingly directed towards problems of surface-atmosphere interaction over complex surfaces including the homogeneous surface-layer relationships used to describe the mean and turbulence properties (Roth, 2000). The homogeneity is defined by Panofsky and Dutton (1984) as one of special characteristics of the turbulence and that the vertical homogeneity is almost never valid near the ground, whereas the assumption of horizontal homogeneity is more easily realized in the surface layer than elsewhere in the ABL (Kaimal and Finnigan, 1994). The flow can be considered horizontally homogeneous if the density, height and distribution of roughness elements do not vary over the upwind area of influence (Rotach, 1999). Under the hypothesis of horizontal homogeneity, the average values of temperature, flow field and heat flux turn out to depend only on the height over the ground (Antonacci, 2005), and there are no streamwise gradients in neither the mean wind speeds nor the turbulent quantities (O'Sullivan *et al.*, 2011). For modelling wind engineering problems within the atmospheric surface layer, several authors (e.g. Richards and Hoxey, 1993; Blocken *et al.*, 2007; Hargreaves and Wright, 2007; Yang *et al.*, 2009) pointed out the need of modelling the flow as a homogeneous flow essentially by well reproducing the turbulence profiles including the wind velocity profile. Therefore, the velocity profile which varies with the nature of the surface and the magnitude of the wind is one of the most important parameters (Kossmann *et al.*, 1998) when modelling the surface boundary layer.

1.2.1.2 Wind velocity profile

According to Varshney and Poddar (2011), the simulation of the wind velocity profile within the atmospheric boundary layer (ABL) is relatively simple, but an accurate prediction of wind-induced loads and contaminant transport needs an accurate simulation of the level of turbulence and the integral length scales. The wind profile can be assumed to be almost always logarithmic for most applications very close to the ground (Kaimal and Finnigan, 1994), and for ABL that are of interest in building studies, Straw (2000) emphasized that the logarithmic law is capable to predict wind velocities more accurately within the lower regions than the power law.

On the other hand, the power law proves adequate for modelling wind velocities in the upper regions (Iyengar and Farell, 2001). Furthermore, Barlow and Coceal (2009) concluded that the mean velocity profile is logarithmic in the inertial sublayer and deviates appreciably from log behaviour within the roughness sublayer. Although, Cheng and Castro (2002) noted that spatially averaged profiles still have a logarithmic form in the above-roof region of the roughness sublayer (RSL) over regular urban-type roughness, while the few extant studies (MacDonald, 2000) have indicated that the mean velocity within the urban canopy layer obeys an exponential decay law. In addition, Rotach (1993a) characterized the ABL as an almost always turbulent layer having a logarithmic profile. White (2000) concluded that many authors observed that the ABL also obeys the logarithmic law during a neutral stratification which occurs when thermal effects are negligible, and Kaimal and Finnigan (1994) underlined that the logarithmic wind profile is strictly valid only for the neutral atmosphere. In addition, for cases where the convection is negligible and the mechanical turbulence prevails, the stratification is nearly neutral; Panofsky and Dutton (1984) noted that the velocity profile follows more the logarithmic law than the power law. Holmes (2001) has detailed the two approaches (i.e. logarithmic and power laws) and concluded that: (i) in strong wind conditions the logarithmic law is the most accurate mathematical expression, but has some characteristics which may cause problems since the logarithms of negative numbers do not exist, thus it is less easy to integrate; (ii) the power law is often preferred by wind engineers to avoid some of these problems, and it is quite adequate for engineering purposes. Finally, according to all the previous statements, one can say that the mean velocity profile can be best represented by a logarithmic law in the inertial sublayer (ISL), while the power law is more appropriate within the urban canopy (Barlow and Coceal, 2009). Xie *et al.* (2013) have recently concluded that turbulent fluctuations and mean velocities are not affected substantially by a change of mean temperature profile below canopy height and that the pollution problems are more severe under stable atmospheric conditions. However, when modelling a neutral atmospheric boundary layer for outdoor environmental applications (e.g. pedestrian wind environment around buildings, wind-driven rain on building facades and air pollutant dispersion around buildings), the mean velocity profile is expressed either by a logarithmic law or a power law (Blocken *et al.*, 2011).

1.2.2 Wind-flow field around buildings

The prediction of effects of wind flow around buildings is of primary importance to a wide variety of engineering applications such as designing durable building envelopes, dispersion of air pollutants, natural ventilation, wind loading, etc. (Tutar and Ogguz, 2004). The wind flows in the atmospheric boundary layer over buildings are inherently complex and exhibits a wide range of physical phenomena including large low-speed areas, strong pressure gradients, unsteady flow regions, three-dimensional effects, and confluence of boundary layers and wakes (Deck, 2005). Therefore, modelling wind flow over buildings is a complicated and challenging process (O'Sullivan *et al.*, 2011). In the case of the present study, the prediction of the nature of a turbulent flow through the urban environment is in principle pre-requisite to the solution of the problem of contaminant dispersion in the urban complex (Lien *et al.*, 2008). The complexity of the flow around an obstacle or group of obstacles has been recognized (Cheng *et al.*, 2003), and turbulent flow remains one of the unresolved problems of classical physics (Qu, 2011). Consequently, a complete understanding of the wind-flow processes and structures over buildings in urban areas has not yet been attained, despite the many years of intensive research (Davidson, 2004).

For studies which involve wind loading, structures and dispersion of contaminants around buildings, the flows with high Reynolds numbers are more closely matching the atmospheric flows characterizing flows in an urban environment (Haupt *et al.*, 2011). These flow patterns around buildings within urban canopy layer are influenced by a large number of parameters (e.g. the thickness of the boundary layer, the layout of the buildings, characteristics of the approach flow) that have been identified and investigated in detail (Cheng *et al.*, 2003) during the last few decades. However many of these studies have produced very interesting comments and conclusions which are only applicable to the studied sites due to physical parameters and configuration details, but not appropriate to other configuration cases. It is generally the case when planning future buildings (e.g. housing project, rebuilding and/or extension of a city, new urban developments) and installing and/or renovating existing ventilation systems (e.g. ventilation inlets and outlets on building facades or roofs). In these cases, the flow patterns are characterized

by complex flow phenomena due to the interactions produced between the various buildings already existing within the site, and some of the results from these trials cannot be generalised, since they are influenced by the presence of secondary structures (Mavroidis *et al.*, 2003).

From this viewpoint and in order to simplify the structure of the flow field and its interaction with the encountered obstacles, many researchers have studied the well documented case of flow around the three-dimensional surface of a cube (Castro and Robins, 1977; Murakami and Mochida, 1988, 1989; Paterson and Apelt, 1990; Zhou and Stathopoulos, 1997; Lakehal and Rodi, 1997; Straw *et al.*, 2000; Krajnovic and Davidson, 2002; Wright and Easom, 2003; Hoxey *et al.*, 2005; Gao and Chow, 2005; Yakhot *et al.*, 2006; Lim *et al.*, 2007; Richards and Hoxey, 2008; Paik *et al.*, 2009; Bitsuamlak *et al.*, 2010; Köse and Dick, 2010; Vardoulakis *et al.*, 2011; Richards and Hoxey, 2012). For this case, the features of the wind-flow pattern are well established in the wind engineering community as detailed by several authors (e.g. Oke, 1988; Martinuzzi and Tropea, 1993; Meinders and Hanjalic, 1999; Blocken and Stathopoulos, 2008; ASHRAE, 2009; Blocken *et al.*, 2011; Moonen *et al.*, 2012a) who contributed to a better understanding of the wind-flow behaviour and its effects on certain parameters such as wind direction, wake region, recirculation zones, etc. The surface-mounted cube case is defined as the geometrically simplest 3D case commonly called "generic case" and has proven quite suitable for validation, verification and sensitivity analyses (Blocken *et al.*, 2011). Other studies, commonly called "applied studies", investigated much more complex configurations that consist of real sites or building blocks (Häggkvist *et al.*, 1989; Rotach, 1993b; Johnson and Hunter, 1998; Roth, 2000; Cheng *et al.*, 2003; Lien and Yee, 2004; Calhoun *et al.*, 2005; Ricciardelli and Polimeno, 2006; Van-Hooff and Blocken, 2010; Fernando *et al.*, 2010; Huang *et al.*, 2011; Hang and Li, 2012; Moonen *et al.*, 2012b; Razak *et al.*, 2013). Such studies were primarily directed towards the influences of neighbourhood buildings, wind directions, wind velocities, Reynolds stress components, etc. on a specific obstacle or building under study.

Through this brief section, the urban flows are mainly dominated by a complex interplay between meteorological conditions and urban morphology (Moonen *et al.*, 2012a), thus their "correct" prediction is currently an unresolved issue (Hsieh *et al.*, 2007). In addition, owing

to the strong relation existing between the flow-field pattern and the transportation of pollutant contaminants in the urban environment (Huang *et al.*, 2009), it is clear that accurately predicting the pollutant dispersion around buildings – that is the topic of the following section – seems to be far from straightforward.

1.2.3 Dispersion field around buildings

Regarding the previous section dedicated to wind flows around buildings where the complexity of understanding the behaviour of atmospheric flows over urban areas is highlighted, it is clear that modelling correctly the pollutant dispersion within a group of buildings remains a very complex challenge, since the wind flow in an urban area may strongly affect the dispersion of pollutants around buildings (Zhang *et al.*, 2005). Indeed, the disturbance of atmospheric flows by various building configurations – often with irregular geometry and spacing – can change the local concentrations by an order of magnitude (Lien *et al.*, 2006). Therefore, to understand well the processes governing the dispersion of pollutants, an accurate concentration prediction of contaminants released into the urban environment is needed (Tseng *et al.*, 2006).

In view of this important need, a number of different approaches have been widely used for studying pollutant dispersion around buildings in urban environments: full-scale field measurements (Wilson and Lamb, 1994; Lazure *et al.*, 2002; Mavroidis *et al.*, 2003; Stathopoulos *et al.*, 2004; Yassin *et al.*, 2005; Santos *et al.*, 2009; Finn *et al.*, 2010; Baldauf *et al.*, 2013), laboratory-scale physical modelling (Li and Meroney, 1983b; Poreh and Cermak, 1990; Saathoff *et al.*, 1995; Sini *et al.*, 1996; Delaunay *et al.*, 1997; White, 2003; Chang and Meroney, 2003; Aubrun and Leitl, 2004; Gomes *et al.*, 2007; Nakiboglu *et al.*, 2009; Liu *et al.*, 2010a; Pournazeri *et al.*, 2012; Carpentieri *et al.*, 2012; Yassin, 2013), semi-empirical methods (Saathoff and Stathopoulos, 1997; Ratcliff and Sandru, 1999; Stathopoulos *et al.*, 2002; ASHRAE, 2007; Hajra *et al.*, 2010; Chavez *et al.*, 2011; Gupta *et al.*, 2012), and computational fluid dynamics (CFD) simulations (Adair, 1990; Li and Stathopoulos, 1997; Riddle *et al.*, 2004; Cai *et al.*, 2008; Hefny and Ooka, 2009; Yoshie *et al.*, 2011; Weil *et al.*, 2012; Rodriguez *et al.*, 2013). Such approaches have improved the understanding of many environmental problems (Gavrilov *et al.*, 2013) that have a direct impact on human health, such as the outdoor pollu-

tion sources (e.g. emissions from rooftop stacks, motor vehicle exhausts, industrial applications, etc.).

Field measurements are conducted under real atmospheric conditions and the full complexity of the problem is taken into account (Blocken *et al.*, 2013). However, full-scale measurements are usually performed on a limited number of points in space (Montazeri and Blocken, 2013). In addition, there is no control over the variation of the wind and weather conditions, therefore repeating an experiment under identical conditions is not possible (Schatzmann and Leitl, 2011). Consequently, this leads to a wide scatter in measured data (Moonen *et al.*, 2012a).

Reduced-scale experiments give an important advantage, in comparison to the field tests, such that the boundary conditions can be chosen to be appropriate to the problem being solved (Schatzmann *et al.*, 1997). However, wind tunnel experiments also suffer from the limited set of points in space (Stathopoulos, 1997) despite new techniques – such as particle image velocimetry (PIV) and laser-induced fluorescence (LIF) which in principle allow planar or even full 3D data to be obtained – in certain applications where the complicated geometries can induce laser-light shielding due to obstructions from the urban model (Blocken and Stathopoulos, 2008). In addition to the high cost of these useful techniques, wind tunnel testing can be time-consuming and requires adherence to similarity criteria that can be a problem for many applications such as multi-phase flow problems and buoyant flows (Blocken *et al.*, 2011).

The semi-empirical methods, such as the Gaussian models and the so-called ASHRAE models (ASHRAE, 2007, 2011) – which apply Gaussian-based models (Hajra and Stathopoulos, 2012) – are based on a Gaussian distribution of the plume in the vertical and horizontal directions under steady conditions (Holmes and Morawska, 2006). Their prediction is based on concentration measurements obtained in wind tunnel simulations and provide little information on dispersion (Tominaga and Stathopoulos, 2009). These models usually need some empirical or semi-empirical parameters from observation and make crude simplifications (Li *et al.*, 2006). While Gaussian models are successfully employed in simplified flow configurations and useful for landscape that is approximately flat and unobstructed, they are wholly inadequate for surface-atmosphere interactions over "complex" surfaces such as cities and other built-up areas

(Lien *et al.*, 2006); the prediction of scalar dispersion over complex and realistic geometries remains challenging, because of additional flow features arising such as separated regions, secondary flows or three-dimensional effects which cannot be properly accounted for (Rossi and Iaccarino, 2009). For instance, Gaussian models are unable to model the effect of upstream and adjacent buildings (Hajra *et al.*, 2011), and are not designed to model the dispersion under low wind conditions or at sites close to the source for which the distance is less than 100 m (Holmes and Morawska, 2006). It is accepted that these models are not suited for predicting concentration in complex structured urban or industrial areas, which is, unfortunately, where pollutants that are of major concern at present are emitted (Schatzmann and Leitl, 2011).

Numerical simulations with CFD offer some advantages compared to other methods; they are less expensive than experimental methods, they provide results of flow features at every point in space simultaneously (Moonen *et al.*, 2012a) and they do not suffer from potentially incompatible similarity because simulations can be conducted at full scale (Montazeri and Blocken, 2013). In addition, at the micro-scale, the CFD technique is the preferred way of investigation (Britter and Schatzmann, 2007) and very suitable for parametric studies for various physical flow and dispersion processes (Gousseau *et al.*, 2011a). Due to the rapid development in computer hardware and numerical modelling, CFD has been increasingly used and adopted to simulate the flow development and pollutant dispersion (Wang and Mu, 2010). Many studies have shown that the approach is capable of reproducing the qualitative features of airflow and pollutant distributions (Huang *et al.*, 2009). However, the accuracy and reliability of CFD are of concern, thus solution verification and validation studies are imperative (Blocken *et al.*, 2013). Since experience has already shown that numerical results do not compare among themselves (Stathopoulos, 1997), experimental tests (i.e. field and wind tunnel measurements) appear unquestionably necessary for fulfilling the requirements of assessing the quality of CFD simulation (Abohela *et al.*, 2013). In addition, one of the objectives of laboratory studies has frequently been to aid the development of dispersion algorithms that can be used in dispersion modelling packages to predict behaviour near and around buildings (Robin, 2003), therefore to place computational results into the right perspective for future improvements (Stathopoulos, 1997).

According to the same author (Stathopoulos, 1997), the principal and most significant areas for improvement in CWE are: (i) the numerical accuracy which requires high-order approximations, (ii) boundary conditions that depend on the specific problem under consideration and (iii) refined turbulence models capable to perform well beyond the specified flow conditions for which they have been developed. All these parameters are the main subjects of the following section which deals with the significant errors that can compromise the accuracy and reliability of numerical simulations.

1.2.4 Errors and quality assurance in CWE

The use of CFD to predict pollutant dispersion properties has been successful in many ways, but also leads to many problems since an accurate prediction of these properties is challenging due to the complex nature of turbulence modelling, the assumptions that are made and the resulting uncertainties (Rohdin and Moshfegh, 2011). For instance, the assumptions commonly used when modelling pollutant dispersion to understand the wind flow and dispersion field behaviours around individual and/or groups of buildings are: (i) the contaminants are mostly treated as a chemically and dynamically passive gases (Sini *et al.*, 1996) – i.e. inert and having the same constant density as air – therefore the effect of contaminant particles on the flow field may be neglected (Wang and James, 1999) and their diffusion process is quite weaker than the turbulent diffusion process (Ma *et al.*, 2012), and (ii) the atmosphere is taken to be horizontally homogeneous, adiabatic and without vertical motion (Cermak and Cochran, 1992).

In computational wind engineering analysis, two types of errors are classified and recognised as critical (Franke *et al.*, 2011). One is the physical modelling arising from the employed turbulence models and the applied boundary conditions, and the other one stems from numerical simulation such as computational domain size, grid design, truncation of discretization scheme, numerical iteration algorithm, etc. (Yang *et al.*, 2005). In addition, these two types of errors are directly related to the large number of computational parameters that have to be set by the user (Ramponi and Blocken, 2012b). Indeed, in a typical CFD simulation, the user has to choose the approximate equations describing the flow (steady RANS, unsteady RANS (URANS), LES or hybrid URANS/LES), the level detail of the geometrical representation of

the buildings, the size and the mesh of the computational grid, the boundary conditions, the discretization schemes, the initialization data and iterative convergence criteria (Blocken *et al.*, 2012). Therefore, detailed and generic sensitivity analyses are important to provide guidance for the execution and evaluation of the CFD studies (Ramponi and Blocken, 2012a).

In this context, many sensitivity tests and detailed verification and validation exercises have been conducted (Blocken and Gualtieri, 2012) during the past decades, and many important best practice guidelines have been developed and/or published (EPA, 1978, 1981; Snyder, 1981; Meroney, 1987; Roache, 1994, 1997; AIAA, 1998; Casey and Wintergerste, 2000; Franke *et al.*, 2004; Oberkampf *et al.*, 2004; Hadjisophocleous and McCartney, 2005; Roy, 2005; Franke *et al.*, 2007; Tominaga *et al.*, 2008; Celik *et al.*, 2008; ASME, 2009; Roy, 2010; AIAA, 2010; Franke *et al.*, 2011) in order to establish a common methodology for verification and validation of CFD simulations in certain cases, and/or to assist and support the users for a better implementation of the CFD in other cases. This can be considered as a milestone in the acceptance process of CFD as a tool for the evaluation of wind flow and pollutant dispersion around buildings in urban areas (Blocken *et al.*, 2012). Among these studies, some of them (Casey and Wintergerste, 2000; Schatzmann and Leitl, 2002; Franke *et al.*, 2007; Tominaga *et al.*, 2008; Franke *et al.*, 2011; Blocken and Gualtieri, 2012) have detailed the main steps that must be addressed when it is question of conducting numerical simulations. Other studies are devoted to how to avoid and/or to reduce the errors and uncertainties that can be induced by a specific factor such as turbulence modelling (Nallasamy, 1987; Cheng *et al.*, 2003; Xie and Castro, 2006; Tominaga and Stathopoulos, 2010; Salim *et al.*, 2011; Rohdin and Moshfegh, 2011; Tominaga and Stathopoulos, 2012), cell geometry (Murakami, 1998; Hefny and Ooka, 2009), boundary conditions (Richards and Hoxey, 1993; Hargreaves and Wright, 2007; Gorlé *et al.*, 2009; Richards and Norris, 2011; An *et al.*, 2013), near-wall treatment (Blocken *et al.*, 2007; Parente *et al.*, 2011), discretization scheme (Stern *et al.*, 2001; Celik *et al.*, 2008; Galvàn *et al.*, 2011), etc.

In recent years, many interesting works have been gathered in the international workshops on quality assurance of micro-scale meteorological models organized by the European Science

Foundation. According to the authors (Schatzmann and Britter, 2005), the reason that most of the models used to predict the micro-scale dispersion lack quality assurance is mainly due to the lack of: (i) a generally accepted quality assurance procedure and (ii) data sets that are quality checked and generally accepted as a standard for model validation purposes. However, the workshop has reviewed the present practices for model validation and data that are available and can be made accessible for micro-scale evaluation. Finally, recommendations have been made to develop coherent and structured procedures which give clear guidance to developers and users as to how properly assure their quality and their proper application. Notwithstanding, it should be noted that CFD solution verification and validation and complete reporting of the followed procedure are essential components of quality assurance (Blocken *et al.*, 2011). Consequently, each study has to respect the different steps of the procedure – for instance, the detailed and recommended procedure by Tominaga *et al.* (2008) and Franke *et al.* (2011) – and to report the grid-sensitivity analysis and validation by comparison with high-quality wind tunnel data and/or on-site measurements (Janssen *et al.*, 2013) to make the study reliable and credible from a quality assurance perspective.

1.3 Justification of the present study

In spite of the large amount of valuable CFD dispersion studies performed in the past, the topic of micro-scale dispersion still requires further investigation (Ramponi and Blocken, 2012a) to understand the effect of all the physical parameters on wind flow and pollutant dispersion in urban areas (Huang *et al.*, 2009), in order to prevent locating fresh-air intakes in zones of high concentrations. Indeed, the increase in knowledge of the flow structure within the urban canopy and of the transport by advection and turbulent diffusion, as well as the development of operational pollutant dispersion models, require more systematic studies of their dependence on factors such as geometry and external flow dynamics (Sini *et al.*, 1996). In addition to the importance of the topic and advances in computational resources (Blocken *et al.*, 2013), since the validation of such models has not always been satisfactory (Meroney *et al.*, 1999) and such systematic studies are too difficult to realize in real sites and still relatively costly in wind tunnels, computational modelling offers an appealing alternative (Sini *et al.*, 1996) and thus

becomes a practical method for predicting the flow and dispersion around buildings (Wang and Mu, 2010). In other words, there is a clear need for the development of computational methods for wind engineering applications utilizing three-dimensional numerical modelling of flow and dispersion fields around buildings (Tutar and Ogguz, 2004) as well as for more validation studies (Blocken *et al.*, 2007).

The present work is classified by Blocken *et al.* (2013) as an applied study, and this kind of research is highly valued by the research community since it attempts to reproduce real cases of existing sites. Chapter 2 as preliminary work will compare among the most widely used turbulence models (i.e. steady RANS $k - \epsilon$ models) in simulating pollutant transport against wind tunnel data. Chapter 3 of this research will present the solution verification and validation of the studied cases to establish the reliability and credibility of results and to shed light on the shortcomings of current computational methods and models as well as possible improvements to produce reasonable predictions and acceptable results. Chapter 4 will investigate the effects of stack height and pollutant exhaust velocity parameters on pollutant concentrations, thus on suitable fresh-air intake locations. In Chapter 5, the comparison between steady and unsteady turbulence approaches highlights the importance of flow fluctuation capture to address better the dispersion in the wake of buildings.

It appears now clearly that the originality of this research stems from the fact that only few studies have investigated so far a building arrangement such that the pollutant emitter building, by means of a rooftop stack, is completely engulfed in the wake zone of another higher building, in spite of the fact that such configuration is frequently met in large downtown areas where tall buildings and high densities of population are mostly concentrated. In addition, to the knowledge of the author, the originality of this study resides also in the fact that very few studies have investigated specifically the effects of stack height and pollutant exhaust velocity on pollutant distribution and fresh-air intake locations, which are among the well-known parameters influencing pollutant distribution in the case of stack emissions (ASHRAE, 2011).

CHAPTER 2

COMPARISON OF VARIOUS TYPES OF $k-\epsilon$ MODELS FOR POLLUTANT EMISSIONS AROUND A TWO-BUILDING CONFIGURATION

Mohamed Lateb[1], Christian Masson[1], Ted Stathopoulos[2] and Claude Bédard[1]

[1]Department of Mechanical Engineering, École de technologie supérieure,

1100 Notre-Dame West, Montreal, Qc, Canada H3C 1K3

[2]Department of Building, Civil and Environmental Engineering, Concordia University,

1455 de Maisonneuve Blvd. West, Montreal, Qc, Canada H3G 1M8

Portions of this chapter were presented at the *Fifth International Symposium on Computational Wind Engineering* (CWE2010) – May 2010, Chapel Hill, NC, USA – and the entire chapter is published April 2013 by Elsevier in *Journal of Wind Engineering and Industrial Aerodynamics*, vol. 115, p. 9−21.

Abstract

The dispersion of pollutants exhausted from a building roof stack located in a tower was investigated using various types of $k-\epsilon$ turbulence models, i.e. a standard $k-\epsilon$ model, a RNG $k-\epsilon$ model and a realizable $k-\epsilon$ model, all implemented using Fluent software. In order to determine the turbulence model that best helped reproduce pollutant plume dispersion, the most critical case was considered, namely, when wind blew perpendicularly towards the upstream tower, then placing the building in its wake. When numerical results were compared to wind tunnel experiments, it was found that the realizable $k-\epsilon$ turbulence model yielded the best agreement with wind tunnel results for the lowest stack height, while for the highest stack height, the RNG $k-\epsilon$ turbulence model provided greater concordance with experimental results. The realizable $k-\epsilon$ model was the only model able to provide the correct trend for the concentration distribution in the lower region between the two buildings; however, none of the models reproduced the trend in the upper regions. The standard $k-\epsilon$ model was generally found to be inadequate for reproducing vertical concentration distribution.

Keywords: Numerical modelling, pollutant emissions, computational fluid dynamics (CFD), $k-\epsilon$ turbulence models, roof stack pollution.

2.1 Introduction

Nowadays, application of Computational Fluid Dynamics (CFD) for atmospheric dispersion processes in the lower region of the Atmospheric Boundary Layer (ABL) is becoming a significant research subject, due to increasing interest in air quality modelling. Full-scale measurement and physical modelling in wind tunnels, have been widely used in studying the dispersion of pollutants (Li and Meroney, 1983a,b; Saathoff *et al.*, 1995; Meroney *et al.*, 1999; Mavroidis *et al.*, 2003; Stathopoulos *et al.*, 2004; Gomes *et al.*, 2007; Stathopoulos *et al.*, 2008; Contini *et al.*, 2009; Nakiboglu *et al.*, 2009; Hajra *et al.*, 2011; Hajra and Stathopoulos, 2012) and most of these experimental studies serve to validate CFD modelling (Murakami *et al.*, 1991; Li and Stathopoulos, 1997; Sada and Sato, 2002; Blocken *et al.*, 2008; Tominaga and Stathopoulos, 2009; Gousseau *et al.*, 2011a,b; Lateb *et al.*, 2011). CFD modelling has already been considered as a powerful tool for predicting the atmospheric dispersion around buildings (Yang and Shao, 2008; Blocken *et al.*, 2011), because it allows for easy control of individual parameters for detailing the process analysis of dispersion. Furthermore, CFD modelling can provide a three-dimensional distribution of the concentration, unlike field and wind tunnel experiments, which only allow to obtain a limited number of point measurements.

The performance of CFD modelling predictions for pollutant concentration fields around buildings is crucial to evaluating air quality, and contributing to the comfort, health and the well-being of building occupants in the vicinity of pollutant sources (e.g. rooftop stacks, vents, vehicle exhausts). Its accuracy depends on several parameters that are used in numerical simulations such as turbulence models, grid resolutions, boundary conditions, geometrical representations, and numerical approximations. In this study, the turbulence model was the primary parameter of interest.

Over the past few decades, many CFD simulations of pollutant dispersion have been carried out regarding turbulence modelling parameters for different buildings and stack configurations.

Murakami *et al.* (1991) have compared the computational results obtained using Reynolds-averaged Navier–Stokes (RANS) standard $k-\epsilon$ and large-eddy simulation (LES) turbulence models with the results of wind tunnel experiments. The accuracy of the flow and diffusion fields around a single building and around a complex building has been confirmed via comparison with experimental results. Meroney *et al.* (1999) compared the Reynolds Stress Model (RSM) and standard and Re–Normalized Group (RNG) $k-\epsilon$ turbulence models with wind tunnel test results, and found that the RSM produced more realistic results than the other two $k-\epsilon$ models. Recently, Blocken *et al.* (2008) studied pollutant dispersion from a rooftop vent on an isolated cubic building using a combination of the realizable $k-\epsilon$ model and RSM for different turbulent Schmidt numbers. Both turbulence models correctly predicted upstream dispersion, but lateral dispersion was underestimated, compared to wind tunnel results. Tominaga and Stathopoulos (2009) studied the prediction accuracy of the flow and dispersion around a cubic building, using four types of turbulence models (the standard $k-\epsilon$ model, a RNG $k-\epsilon$ model, a $k-\epsilon$ model with Launder and Kato modification, and a realizable $k-\epsilon$ model). They concluded that the standard $k-\epsilon$ model provided inadequate results for the concentration field, and that the RNG $k-\epsilon$ model was the best at providing results that were in general agreement with the experimental data. All turbulence models tested showed poor prediction accuracy for the concentration distribution at the side and leeward walls of the building. More recently, Tominaga and Stathopoulos (2010) compared the performance of RNG $k-\epsilon$ model and LES model for flow and concentration fields around a cube with vent emission in the surface boundary layer. They concluded that, compared to the experimental results, the LES model reproduced concentration distribution better than the conventional RNG $k-\epsilon$ model. In addition, horizontal diffusion was reproduced, since the instantaneous concentration fluctuations were available using the LES approach. The RNG $k-\epsilon$ model underestimated the turbulent diffusion near the cube, which was mainly significant for the reproduction of concentration distribution. Computing time for the unsteady simulations in LES model was 25 times greater than it was in simulations using a RNG $k-\epsilon$ model. For this reason, this parameter must be taken into account when using such a model. Gousseau *et al.* (2011a) recently evaluated the performance of two different modelling approaches: a standard $k-\epsilon$ and a LES turbulence model, applied to pollutant dispersion in an urban environment. They concluded that the performance of the

standard $k-\epsilon$ model strongly depended on the turbulent Schmidt number, and in contrast, the LES model provided better performance without requiring any parameter input in order to solve the dispersion equation. The effects of the near-field pollutant dispersion characteristics of upstream and downstream buildings in an urban environment have recently been examined by Hajra *et al.* (2011) and Hajra and Stathopoulos (2012), using a wind tunnel simulation and ASHRAE modelling. Both studies showed that height and spacing between the emitter building and its adjacent buildings were critical parameters in the pollutant dispersion process. The authors emphasize the inability of ASHRAE (2007) to model the effect of adjacent buildings, and recommend further investigations of its formulation, whereas they found the ASHRAE (2011) model suitable only for use in specific, limited cases.

In this paper, the results of CFD simulations of pollutant dispersion exhausted from a building roof stack located in the wake of a tower will be described. The simulations were implemented using Fluent CFD software and investigated using various steady RANS $k-\epsilon$ models (standard $k-\epsilon$, RNG $k-\epsilon$ and realizable $k-\epsilon$ turbulence models) which are the models most widely used for many applications (Assimakopoulos *et al.*, 2003; Xie *et al.*, 2005; Salim *et al.*, 2011) including wind loading (Huang *et al.*, 2011) and pollutant transport (Xie and Castro, 2006). Their capability for producing reasonable predictions and acceptable results, as well as their short computational time, have been emphasized by many authors (Lien *et al.*, 2004; Xie and Castro, 2006; Zhai *et al.*, 2007). Despite the shortcomings of the standard $k-\epsilon$ model, it is robust and simple enough to be tractable numerically (Lien *et al.*, 2006), and is still commonly used in pollutant transport applications (Yassin *et al.*, 2008; Tominaga and Stathopoulos, 2009; Gousseau *et al.*, 2011a; Salim *et al.*, 2011). For these reasons, standard $k-\epsilon$ model testing was planned for a two-building configuration. Special attention was paid to the pollutant concentrations on the emitting building roof, as well as to those on the roof and leeward wall of the upwind tower. Simulation results were compared to wind tunnel experiments conducted by Stathopoulos *et al.* (2004) in a boundary layer wind tunnel.

2.2 Model description

The physical model used in this study consists of two lined up buildings, named the BE building and the Faubourg tower. The tower faces the wind and the BE building is located in the wake region of the tower. Although all buildings up to a distance of 50 m were included in the experimental model, only the upstream tower is judged to be the main obstacle capable to produce major effects on the overall behaviour of the wind flow and concentration fields around the BE building. Therefore, only these two buildings are considered in the study. The BE building and the tower dimensions are $L_{BE} \times W_{BE} \times H_{BE} = 48 \times 53 \times 12.5$ m^3 and $L_{Fb} \times W_{Fb} \times H_{Fb} = 32 \times 53 \times 45$ m^3, respectively. One structure is located at the roof centre of the tower, and its dimensions are $20 \times 37 \times 5$ m^3. The BE building has several structures on its roof, but only three of these were deemed of sufficient dimensions to disturb the flow on the roof. These three structures are a penthouse ($6.2 \times 18.4 \times 4$ m^3) an elevator shaft ($10 \times 4 \times 4$ m^3) and a skylight ($34.6 \times 6.8 \times 2.2$ m^3). The other details taken into account in the CFD modelling of the two buildings were the inclined north-west side, the back step at the south-east side for the BE building, and the staircase form of the leeward wall for the Faubourg tower. The stack on the BE roof, from which the pollutant is emitted, sits upstream and is 0.4 m in diameter; its height varies from 1 m to 7.2 m. Fig. 2.1 shows a general view of the buildings and shows details of all dimensions of the physical model under consideration. The origin of the reference frame was set at the centre base of the downstream wall of the BE building, and the positive x direction was opposite to the wind direction.

Elements not taken into account were the entry of the BE building, located on the windward wall, and a parapet 1 metre high, running along the perimeter of the roof. It was decided that the entry did not disturb the flow in the region of interest and, since the parapet had not been reproduced in the wind tunnel experiments, it would not be reproduced in this numerical study.

2.3 Mathematical model

2.3.1 Governing equations

The fundamental equations governing the motion of steady turbulent flows without body forces are the time-averaged Navier–Stokes and continuity equations. For an incompressible flow, they can be written as:

Continuity equation:

$$\frac{\partial U_i}{\partial x_i} = 0 \tag{2.1}$$

Momentum equation:

$$U_j \frac{\partial U_i}{\partial x_j} = \frac{1}{\rho} \frac{\partial}{\partial x_j} \left[-P\delta_{ij} + 2\nu S_{ij} - \overline{u_i' u_j'} \right] \tag{2.2}$$

where ρ is the density of air in [kg m^{-3}], ν the kinematic viscosity in [m^2 s^{-1}], P the mean pressure in [kg m^{-1} s^{-2}], S_{ij} is the velocity strain rate tensor expressed as $S_{ij} = 1/2\,(\partial U_i/\partial x_j + \partial U_j/\partial x_i)$ and δ_{ij} is the Kronecker delta. U_i and u_i' represent the mean and fluctuating velocity components in [m s^{-1}], respectively.

Through the Reynolds-averaging approach, more variables are introduced, which means that the two equations above are not closed. The Reynolds stress terms $-\overline{u_i' u_j'}$ appearing in Eq. (2.2) represent the diffusive transport of momentum by turbulent motion. These terms need to be determined by a turbulence model before the mean flow equations can be solved. For the various RANS $k-\epsilon$ models compared in this study, i.e. the standard $k-\epsilon$ model (Jones and Launder, 1972; hereafter SKE), the re-normalization group $k-\epsilon$ model (Yakhot *et al.*, 1992; hereafter RNG) and the realizable $k-\epsilon$ model (Shih *et al.*, 1995a; hereafter RLZ), turbulent Reynolds stresses and mean velocity gradients were related by turbulent viscosity using the Boussinesq assumption. The mathematical expression for this is:

$$-\overline{u_i' u_j'} = \nu_t \left(\frac{\partial U_i}{\partial x_j} + \frac{\partial U_j}{\partial x_i} \right) - \frac{2}{3} k \delta_{ij} \tag{2.3}$$

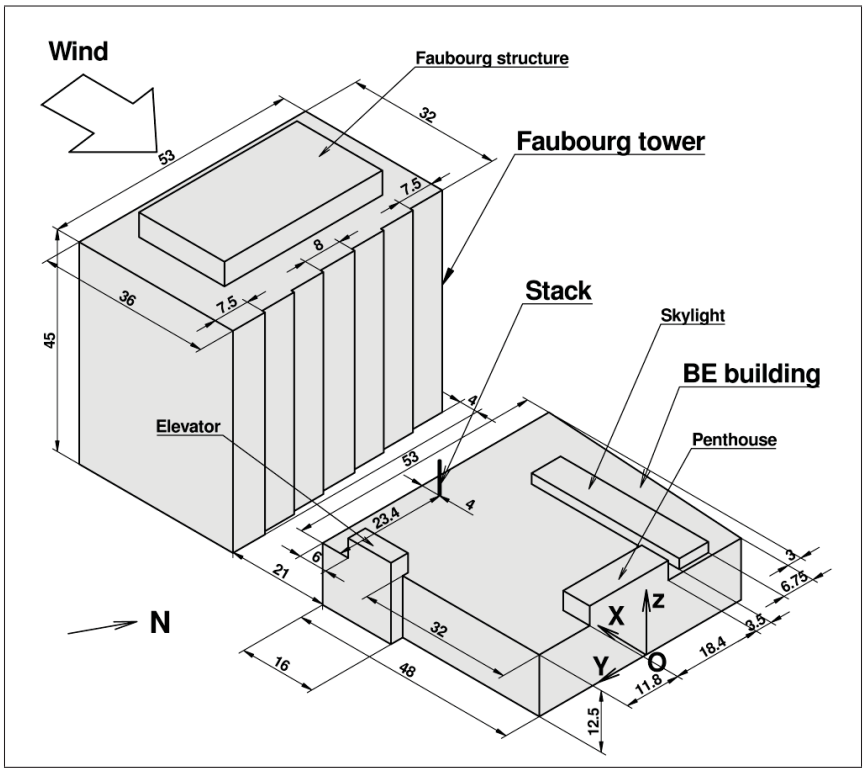

Figure 2.1 Geometry of the two-building configuration and dimensions in metres.

Turbulent kinetic energy k and turbulent dissipation rate ϵ characterizing the local state of turbulence are related to the turbulent viscosity in the so-called "two equations" model by the following equation:

$$\nu_t = C_\mu \frac{k^2}{\epsilon} \tag{2.4}$$

where C_μ is a parameter that depends upon the turbulence model; turbulent kinetic energy, k, is written as:

$$k = \frac{1}{2}\overline{u_i'^2} \tag{2.5}$$

with $\overline{u_i'^2}$ representing the Reynolds normal stresses in the streamwise x-, spanwise y- and vertical z- directions in [m^2 s^{-2}].

2.3.2 Turbulence models

To close the system of equations, one transport equation for turbulent kinetic energy, k, and another for turbulent dissipation rate, ϵ, were added. For the various $k-\epsilon$ turbulence models tested, only the turbulent dissipation rate equation differed. The transport equation for turbulent kinetic energy was the same, and was expressed as follows:
Transport equation of k:

$$U_j \frac{\partial k}{\partial x_j} = \frac{\partial}{\partial x_j}\left(\frac{\nu_t}{\sigma_k}\frac{\partial k}{\partial x_j}\right) + P_k - \epsilon \tag{2.6}$$

where P_k is the production of turbulent kinetic energy expressed by $P_k = \nu_t S^2$, S is defined by the velocity strain rate tensor as $S = \sqrt{2S_{ij}S_{ij}}$ and the constant σ_k is equal to 1.0.

In the following sections, the transport equation of the turbulent dissipation rate is detailed for each turbulence model.

2.3.2.1 Standard $k-\epsilon$ model

The turbulent dissipation rate of the SKE $k-\epsilon$ model is expressed by the following equation:

$$U_j \frac{\partial \epsilon}{\partial x_j} = \frac{\partial}{\partial x_j}\left(\frac{\nu_t}{\sigma_\epsilon}\frac{\partial \epsilon}{\partial x_j}\right) + \frac{\epsilon}{k}\left[C_{\epsilon 1}P_k - C_{\epsilon 2}\epsilon\right] \tag{2.7}$$

The model constants are $\sigma_\epsilon = 1.3$, $C_{\epsilon 1} = 1.44$ and $C_{\epsilon 2} = 1.92$, and the constant C_μ appearing in Eq. (2.4) is equal to 0.09.

2.3.2.2 RNG $k-\epsilon$ model

It is well known that applying a SKE model to complex flows yields poor performance, which in turn limits its scope of applicability (e.g. limitation to high Reynolds numbers, overestimation of k in the impinging regions (Lien *et al.*, 2006)). The RNG model introduces an additional term into the turbulent dissipation rate, ϵ, equation which makes the model more accurate and reliable for a wider class of flows than is the SKE turbulence model (for example, for rapidly strained or swirling flows).

RNG transport equation for ϵ:

$$U_j \frac{\partial \epsilon}{\partial x_j} = \frac{\partial}{\partial x_j}\left(\frac{\nu_t}{\sigma_\epsilon}\frac{\partial \epsilon}{\partial x_j}\right) + \frac{\epsilon}{k}\left[C^*_{\epsilon 1} P_k - C_{\epsilon 2}\epsilon\right] \tag{2.8}$$

The turbulent eddy viscosity constant C_μ was set to 0.0845. The other constants were $\sigma_\epsilon = 0.719$ and $C_{\epsilon 2} = 1.68$, and $C^*_{\epsilon 1}$ was expressed by $C^*_{\epsilon 1} = 1.42 - \eta(1 - \eta/4.38)/(1 + 0.012\eta^3)$ with:

$$\eta = \frac{k}{\epsilon} S \tag{2.9}$$

2.3.2.3 Realizable $k - \epsilon$ model

This $k - \epsilon$ model consisted of a new model dissipation rate equation and a new realizable eddy viscosity formulation. The realizability effect was achieved by the constant C_μ of the turbulent eddy viscosity, which was no longer a constant but a function of the turbulent fields, mean strain and rotation rates. This model has been extensively validated for a wide range of flows, including boundary layer flows and separated flows (Shih *et al.*, 1995a).

RLZ transport equation for ϵ:

$$U_j \frac{\partial \epsilon}{\partial x_j} = \frac{\partial}{\partial x_j}\left(\frac{\nu_t}{\sigma_\epsilon}\frac{\partial \epsilon}{\partial x_j}\right) + C_1 S\epsilon - C_2 \frac{\epsilon^2}{k + \sqrt{\nu\epsilon}} \tag{2.10}$$

where $\sigma_\epsilon = 1.2$, $C_2 = 1.9$, $C_1 = \max[0.43, \eta/(\eta + 5)]$ with η defined as in Eq. (2.9), and $C_\mu = 1/(4.04 + \frac{A_s k U^*}{\epsilon})$ for which $A_s = \sqrt{6}\cos\phi$, $\phi = (1/3)\cos^{-1}\sqrt{6}W$, $W = S_{ij}S_{jk}S_{ki}/\check{S}^3$, $\check{S} = \sqrt{S_{ij}S_{ij}}$, $U^* = \sqrt{S_{ij}S_{ij} + \widetilde{\Omega}_{ij}\widetilde{\Omega}_{ij}}$, and $\widetilde{\Omega}_{ij} = \Omega_{ij} - 2\epsilon_{ij}\omega_k$.

2.3.3 Dispersion equation

For the dispersal of a non-buoyant passive scalar contaminant without a source generation rate, the transport equation is:

$$U_j \frac{\partial C}{\partial x_j} = \frac{\partial}{\partial x_i}\left(-\overline{u_i' c'}\right) \tag{2.11}$$

The term $-\overline{u_i'c'}$ appearing in this equation represents the diffusive transport of the concentration by turbulent motion, where c' indicates fluctuations of concentration. The turbulent concentration fluxes and the mean concentration gradients are related, using the same analogy as the one used for the Reynolds stress terms, by the following expression:

$$-\overline{u_i'c'} = \frac{\nu_t}{Sc_t}\frac{\partial C}{\partial x_i} \tag{2.12}$$

where Sc_t is the turbulent Schmidt number equal to 0.7 a value commonly used (Tominaga and Stathopoulos, 2007) and further justified in this paper.

2.4 Numerical method

2.4.1 Domain size and computational grid

A staggered rectangular grid system was adopted for this study. The construction of the domain was done according to the instructions recommended by Franke *et al.* (2007) and Tominaga *et al.* (2008), and special care was taken in arranging the computational grid cells, as advised by Hefny and Ooka (2009).

Following Celik *et al.* (2008), three grids were used in order to estimate uncertainty due to discretization: Grid 1, Grid 2 and Grid 3. These had 1.59, 1.99 and 2.29 million cells, respectively. Since the computed concentration obtained for the two successive refined grids were so close (the average error was found to be less than 2%), it was determined that further grid refinement would significantly increase processing time with only a negligible increase in accuracy. For this reason, only the results from the calculations using Grid 3 have been included in this paper (for the grid refinement study – see Lateb *et al.* (2010a)). The computational domain was extended $20.1H_{Fb}$ (streamwise) $\times$ $10H_{Fb}$ (spanwise) $\times$ $6.1H_{Fb}$ (height), as shown in Fig. 2.2, and was divided into 187 $\times$ 126 $\times$ 102 grid points, along the x, y and z axes, respectively. The mesh details in the neighbourhood of the two buildings of interest are illustrated in Fig. 2.3. Note that the grid configuration was created using a stretching ratio of about 1.2 except near the base of the Faubourg tower where the ratio is greater. The choice of this grid

was made following several configuration tests carried out in order to obtain the best numerical data as compared with the experimental results. The exhaust cross-section of the stack was divided into 24 cells.

2.4.2 Boundary conditions

Enhanced wall treatment was used for near-wall modelling; according to Wang (2006), it is a better approach for predicting the recirculation zones near the windward edge and in the wake of the building. This wall treatment is called the low-Reynolds number approach; it resolves the viscous sublayer and computes the wall shear stress from the local velocity gradient normal to the wall. It requires a very fine mesh resolution in wall-normal direction. The Y^+ values obtained close to the walls were within a range of 2 to 5, which demonstrates the suitability of the grid selected here. At all building walls, the no-slip condition was used assuming smooth wall. Horizontal homogeneity was assured and tested previously in an empty domain by using a specified wall shear stress ($\tau_w = 1.15$ Pa) at ground level, as suggested by Blocken *et al.* (2007).

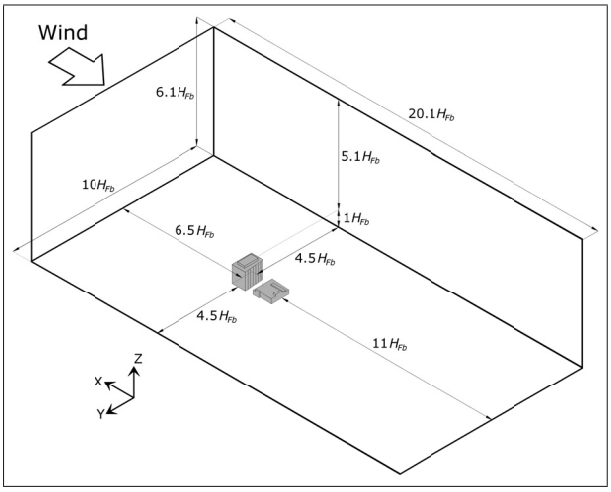

Figure 2.2 Dimensions of the domain grid.

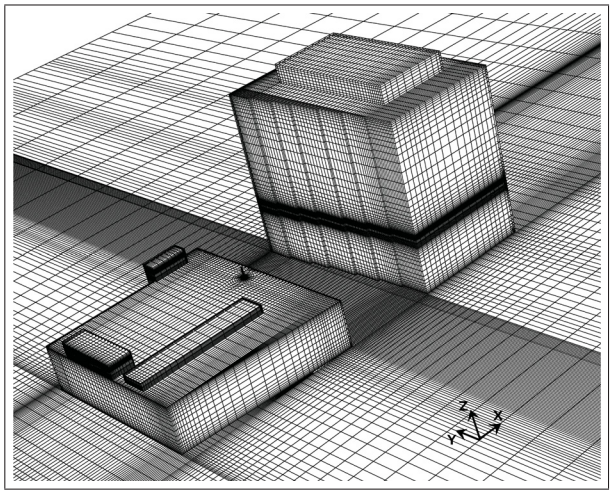

Figure 2.3 Mesh on the two-building configuration.

At the domain entry, all flow properties were assigned. The different profiles used on this part of the domain are shown in Table 2.1. The velocity profile $U(z)$ and the turbulent intensity $TI(z)$ at the inlet were derived from curves proposed by Saathoff *et al.* (1995). Turbulent kinetic energy and rate of dissipation profiles were deduced from equations (2.13) to (2.15)

$$k(z) = \frac{3}{2}\left[U(z)TI(z)\right]^2 \tag{2.13}$$

$$\epsilon(z) = \frac{u^{*3}}{\kappa z} \tag{2.14}$$

$$\frac{U(z)}{u^*} = \frac{1}{\kappa}\ln\left(\frac{z}{z_o}\right) \tag{2.15}$$

where κ is the Von Karman constant ($= 0.42$), u^* the friction velocity ($= 0.97$ m s^{-1}) and z_o the roughness length at the model scale ($z_o = 0.0033$ m) evaluated by Stathopoulos *et al.* (2004) in the wind tunnel experiments.

Fully developed flow was assumed at the domain exit. The exit plane was located far downstream from the two buildings, so that all parameters in that plane had negligible influence on the velocity and concentration fields calculated in the vicinity of the two buildings. The stack exit conditions were matched as closely as possible to the wind tunnel experiments. The mass flow rates, as well as the concentration and momentum fluxes at the stack exit plane, were those measured experimentally. The pollutant exhaust velocity, w_e, and its concentration, C_e, were prescribed as uniform, whereas the turbulence intensity, TI_s, was specified using the following equation (Zhou and Kim, 2010):

$$TI_s = 0.16(Re_s)^{-1/8} \tag{2.16}$$

where $Re_s = (w_e d_s \rho_e)/\mu_e$ is the stack Reynolds number, d_s refers to the internal diameter of the stack and ρ_e and μ_e are the density and dynamic viscosity of the pollutant, respectively.

The stack Reynolds number for the lowest pollutant velocity value, w_e, was approximately 1940. This value was under the recommended threshold value for reaching the turbulence criterion in the stack. Since all criteria for modelling non-buoyant plume exhaust had been satisfied,

Stathopoulos *et al.* (2004) do not recommend an increase in pollutant exhaust velocity in order to reach the threshold value ($Re_s > 2000$). The wind tunnel results for the concentration measurements were provided in a non-dimensional form; therefore, all the numerical concentrations, C, were normalized in the same way and were expressed by the following equation:

$$K = \frac{CU_H H_{BE}^2 10^{-6}}{Q_e} \tag{2.17}$$

where C is the mean concentration measured in [ppb], U_H is the mean wind velocity at the roof height of the BE building in [m s^{-1}], H_{BE} is the height of the BE building in [m] and Q_e is the volumetric flow rate of the pollutant in [m^3 s^{-1}].

The simulation parameters used in this study are listed in Table 2.1, where M is the momentum ratio (the ratio between the exhaust velocity of the pollutant, w_e, and the wind velocity at height H_{BE} of the BE building). The different profiles at the inlet as well as the pollutant exit parameters are detailed for the various stack heights considered, i.e. 1 m, 3 m, 4 m and 7.2 m. The mean pollutant concentration at the stack exit, C_e, is equal to 1.

Table 2.1 Simulation test cases and their parameters.

Stack height $200h_s$ [m]	Momentum ratio M $(= w_e/U_H)$	Exhaust velocity w_e [m/s]	Turbulent intensity TI_s [%]	Profiles at the entry of the domain			
				Profile $U(z)$	Profile $k(z)$	Profile $\epsilon(z)$	Profile $TI(z)$
1	2.2	13.88	6.20	$14.5\times z^{0.3}$	$1.25/z^{0.4}$	$2.17/z$	$0.063/z^{0.5}$
	5	31.55	5.60				
3	2.2	13.88	6.20				
	4.5	28.40	5.70				
4	2.2	13.88	6.20				
7.2	2.2	13.88	6.20				

2.4.3 Numerical schemes

The QUICK scheme was used in the discretized momentum equations, and a second-order discretization scheme in other governing equations. The SIMPLE (Semi-Implicit Method for Pressure-Linked Equations) algorithm (Patankar and Spalding, 1972) was used for introducing

pressure into the continuity, and pressure discretization was taken care of by the Standard scheme. In order to reduce the round-off error, a double precision solver was used. Franke *et al.* (2007) recommend a reduction of the residuals at least four orders of magnitude; hence, the iterative convergence criteria used for reaching the solution was 10^{-5}.

2.5 Results

In this section, a comparison between the measured and simulated concentrations obtained using the turbulence models tested will be described. The objective was to compare the performance of various turbulence models. This comparison made it possible to produce the concentration distribution of the pollutant operating in the wake region of the two-building configuration of interest. Since no velocity and pressure measurements were available, in the following sections, only the numerical concentration values will be compared to the wind tunnel measurements.

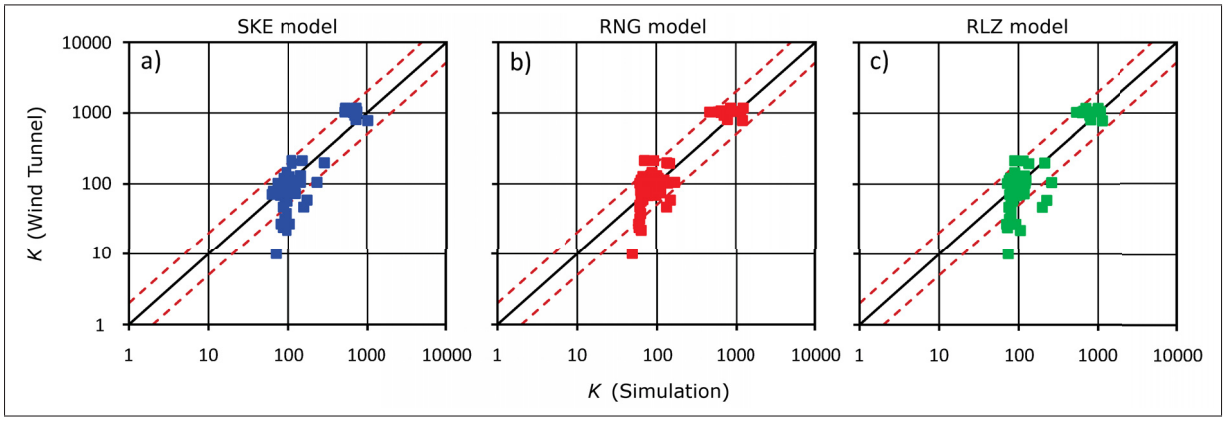

Figure 2.4 Scatter plots of simulation and wind tunnel K data for stack heights of 1 and 3 m and momentum ratios of 2.2, 4.5 and 5 obtained with (a) SKE turbulence model, (b) RNG turbulence model and (c) RLZ turbulence model.

2.5.1 Average error of sampler concentrations

Fig. 2.4 shows the scatter plots for the non-dimensional concentration K values from the wind tunnel measurement and numerical simulations with both stack heights (h_s = 1 and 3 m) and various momentum ratios (M = 2.2, 4.5 and 5) for each turbulence model. Eighty percent

(80%) of concentration values were located within a range factor of 2, as can be seen through points situated between the dashed lines on each side of the median line in Fig. 2.4a and c, for the SKE and RLZ turbulence models, respectively, whereas in Fig. 2.4b, the RNG model shows 83% of K values within this range. The average error, e_a, for simulated and experimental concentrations obtained with stack heights of 1 and 3 m (both are momentum ratios for each stack height) and the SKE turbulence model were approximately 50% and 92%, respectively. Note that the average error was calculated as defined in Lateb *et al.* (2010a). The corresponding average errors for the RLZ model were smaller than those for the SKE model, i.e. 45% and 88%. The RNG model remained the best approach for evaluating concentrations with average errors of 38% and 56% for stack heights of 1 m and 3 m, respectively. For the lowest stack height ($h_s = 1$ m) and the lowest momentum ratio ($M = 2.2$), the RLZ turbulence model displayed the smallest average error of about 36%. This value was slightly under the values of 37% and 38% obtained with the SKE and RNG turbulence models, respectively. In the case of a stack height of 1 m and a momentum ratio of 5, the RNG model showed better capability to approach the experimental results, with an average error of 38% compared to the RLZ and SKE models, which provided 54% and 63%, respectively. Note that the corresponding correlation coefficients, R, of the concentration dispersion values in Fig. 2.4, are 0.93, 0.92 and 0.93 for SKE, RNG and RLZ models, respectively.

2.5.2 Concentrations on the BE building roof and the top of the Faubourg tower leeward wall

Figs. 2.5 and 2.6 show the concentration values obtained using CFD simulations and wind tunnel experiments for the lower stack height ($h_s = 1$ m) and the higher stack height ($h_s = 3$ m), respectively. Two momentum ratios are shown in each figure. The non-dimensional concentration K values obtained using numerical simulations and wind tunnel experiments are displayed for each sampler location. The analysis of these results will be discussed separately for the BE building roof and the Faubourg tower leeward wall. Afterwards, a general tendency will be expressed.

2.5.2.1 On the BE building roof

The SKE turbulence model showed an underestimation of the concentration in the central and south-east part of the roof for both stack heights using the lower momentum ratio ($M = 2.2$). The increase in momentum ratio revealed an opposite tendency (an overestimation) in the centre, while the same tendency (an underestimation) was still roughly observed in the south-east part of the roof. Major overestimations were noted at samplers located in the windward and north-west parts of the BE building roof for all the cases studied.

The RNG model also underestimated concentrations in nearly all parts of the roof for both stack heights with the lower momentum ratio. Only a few samplers located near the perimeter of the roof were overestimated (R_5, R_6, R_{14}, and R_{25}). The tendency was reversed for a few samplers in the centre with the increase of momentum ratio: numerical values overestimated the experimental ones. The underestimation persisted in the central and upwind parts of the roof for the case using $h_s = 1$ m and $M = 5$. For higher stack heights and momentum ratios ($h_s = 3$ m and $M = 4.5$), the simulations agreed relatively well with the experimental results in the centre of the roof. Underestimation was observed, however, for all cases at sampler R_4, near the stack. The overestimation observed in the side parts with $h_s = 1$ m and $M = 5$ were still noticeable at the highest stack ($h_s = 3$ m).

The RLZ turbulence model showed under- and overestimation on the BE building roof for both stack heights ($h_s = 1$ and 3 m) using the lowest momentum ratio ($M = 2.2$). For the smaller stack height, an overestimation was observed at many samplers located along the perimeter of the roof. At the roof centre, an underestimation of concentrations was observed and only a few samplers saw their concentration tendencies reversed along with increasing stack height ($h_s = 3$ m). For higher pollutant exhaust velocities, the concentrations of the roof samplers increased surpassing the experimental values. Only two of the three samplers located near the upwind edge of the roof remained underestimated: $h_s = 1$ m and $M = 5$. At the farthest sampler towards the south-east side, R_6, an overestimation of K remained.

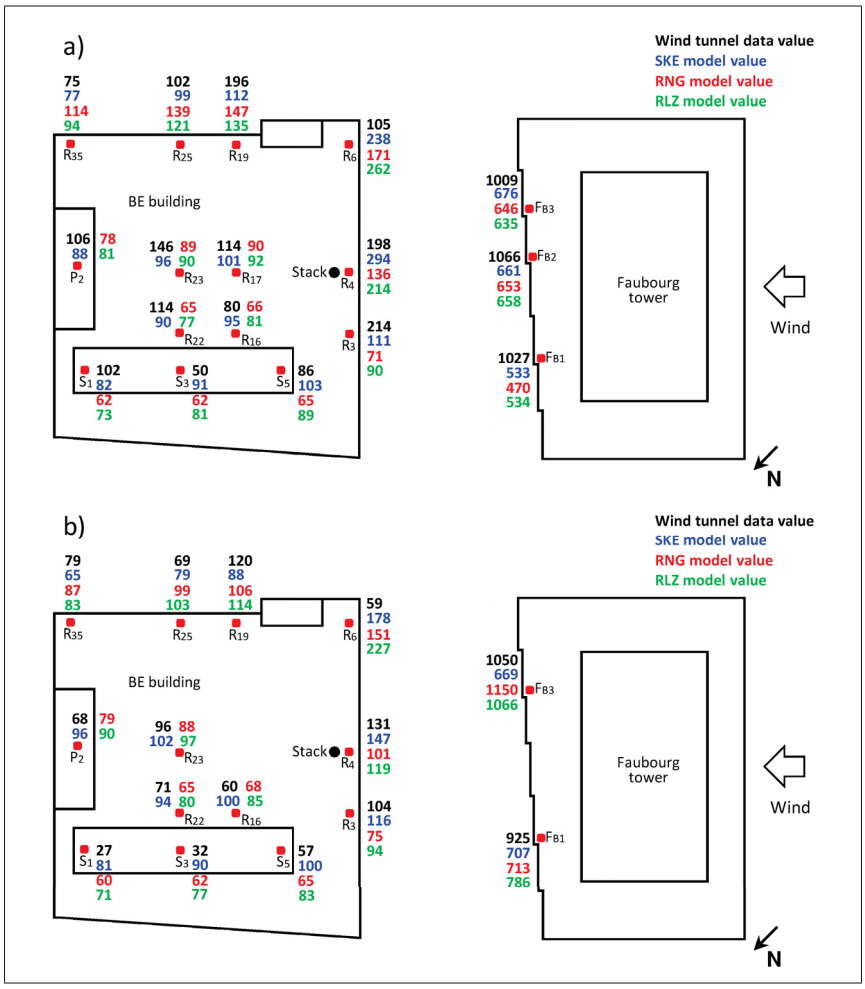

Figure 2.5 Simulation and wind tunnel values of K for a stack height, h_s, of 1 metre with (a) $M = 2.2$ and (b) $M = 5$.

2.5.2.2 On the top of the Faubourg tower leeward wall

The results obtained for all the turbulence models underestimated the concentration K on the Faubourg tower leeward wall, with a lower momentum ratio for both stack heights. Increasing the exhaust velocity did not significantly change the SKE turbulence model: the underestimation remained, except at the sampler in the centre, F_{B2}, and for the highest stack ($h_s = 3$ m). For the RNG model, the computed concentration was greater than the experimental value for the higher pollutant velocity at sampler F_{B3}, whereas an underestimation was observed at sampler F_{B1}. All K values obtained using the RLZ model underestimated the experimental results for $M = 2.2$ and both stack heights, whereas with the highest pollutant velocities, the RLZ

model showed an overestimation at almost all samplers except for F_{B1} and F_{B3}, where K was underestimated for h_s of 1 and 3 m, respectively.

2.5.3 Variation of K along the stack axis on the BE building roof

Fig. 2.7a and b shows the evolution of concentrations K for momentum ratios of 2.2 and 5, respectively, with a stack height of 1 metre at samplers R_4, R_{23} and P_2 located at the stack axis on the BE building roof. For both momentum ratios, the RLZ model provided the best concentration value at sampler R_4 near the stack, compared to those obtained with SKE and RNG models. All models showed slight differences between their results for the higher momentum ratio. For the lower value of M, however, discrepancies were clearly noticeable at sampler, R_4, near the stack. The RNG model underestimated the K value within 30%, while the SKE model provided an overestimation of 48%. Far downstream of the stack, agreement between the simulated concentration values and experimental values was better. The RLZ model seemed to provide more accurate concentration values at samplers close to the stack, as compared to the SKE and RNG models.

2.5.4 Concentrations along the Faubourg tower leeward wall

Fig. 2.8 shows the vertical evolution of the measured and simulated concentrations along the leeward wall of the Faubourg tower. All the turbulence models used overestimated the experimental values and displayed approximately the same concentration values at the samplers located at the higher level of the tower leeward wall and at the BE building roof level. Discrepancies between the numerical and experimental values were greater at the building roof level. At mid-height on the Faubourg tower, the SKE model predicted a more accurate K value, whereas the RLZ model showed an inadequate result. Although none of the turbulence models tested reproduced the concentration trend in the upper region between the two buildings, the RLZ model remained the only one to reproduce the trend slope in the lower region. This seems to indicate that the RLZ model correctly reproduced pollutant distribution in that lower region.

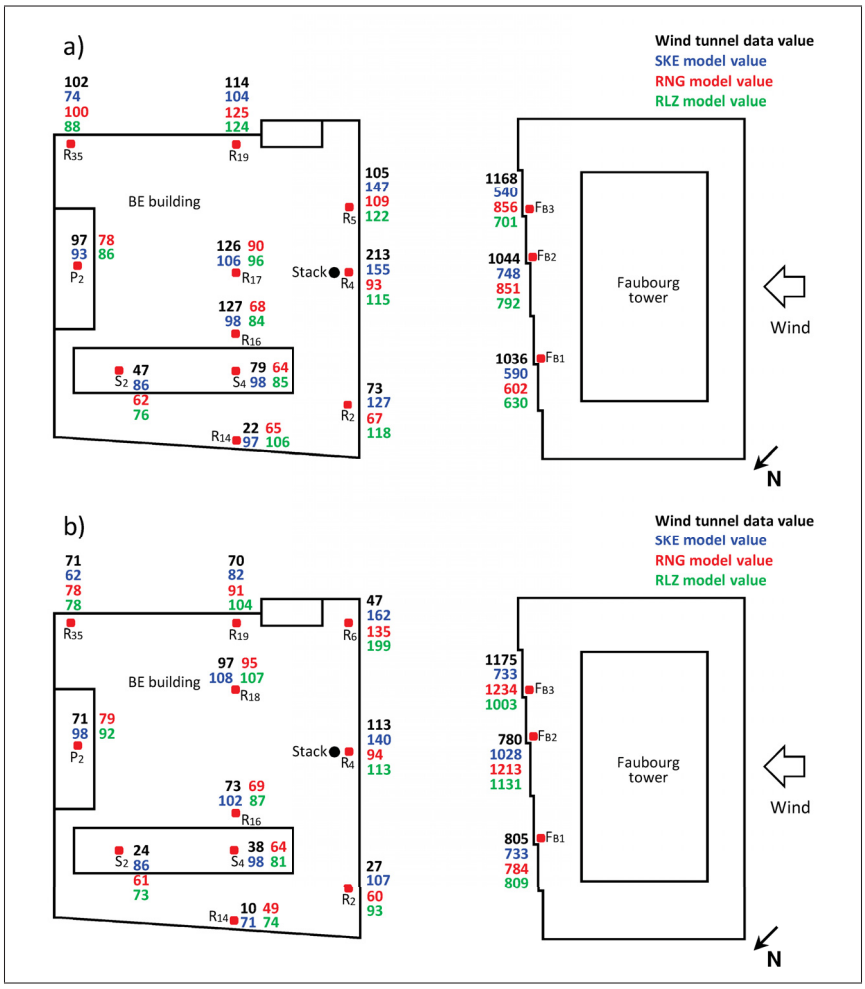

Figure 2.6 Simulation and wind tunnel values of K for a stack height, h_s, of 3 metres with (a) $M = 2.2$ and (b) $M = 4.5$.

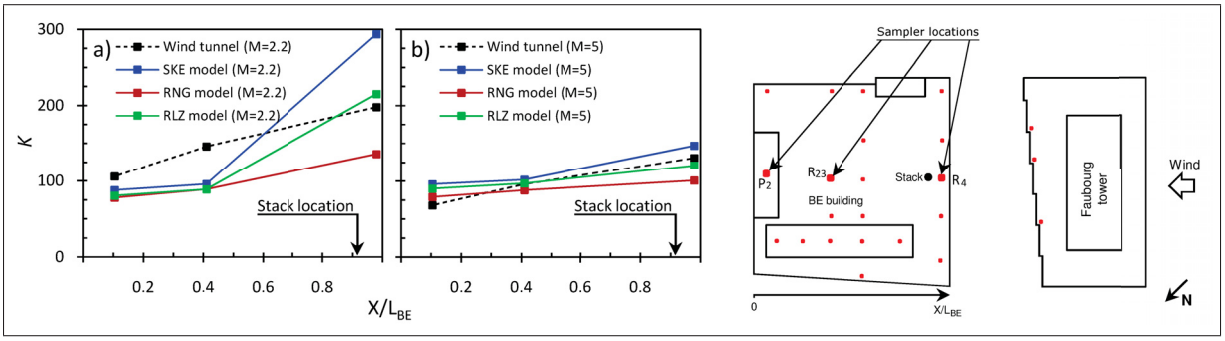

Figure 2.7 Measured and calculated variation of K at samplers R_4, R_{23} and P_2 along x axis on BE roof with $h_s = 1$ m and for momentum ratios of (a) $M = 2.2$ and (b) $M = 5$.

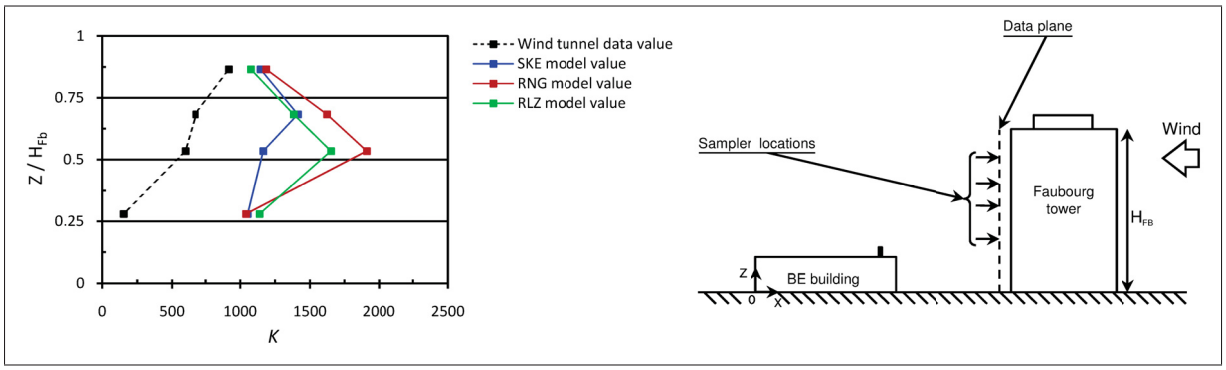

Figure 2.8 Vertical profiles of K on the leeward wall of the Faubourg tower (Wind tunnel and simulation 1:200 scale values, $M = 4.5$ and $h_s = 3$ m).

2.5.5 Variation of K at specified samplers for different stack heights

Fig. 2.9 shows the dependence of concentration on stack height at different samplers located on the BE building roof and on the Faubourg tower leeward wall. For the BE building roof, the samplers are those located along the stack axis, i.e. R_4, R_{17} and P_2, and those on the tower leeward wall are F_{B1}, F_{B2} and F_{B3}. At sampler R_4, near the stack, the RLZ model provided the best overall agreement with the wind tunnel results: a slight overestimation of K was noted for the lower stack height ($h_s = 1$ m), whereas for higher stack heights ($h_s = 4$ and 7.2 m), very good agreement was observed. For a stack height of 3 m, the SKE model provided the best approach. The RNG model underestimated K values for all stack heights, with less discrepancy for h_s of 4 and 7.2 m. In the central and the leeward parts of the roof, represented by samplers R_{17} and P_2 shown in Fig. 2.9b and c, respectively, all models provided roughly the same results and the same trend. The concentrations obtained remained constant with increasing stack height, whereas a decrease of K was noted in the experimental values.

On the Faubourg tower leeward wall, the trend of the experimental concentrations was the same for all three samplers. K concentration increased between stack heights of 1 and 3 m, except at sampler F_{B2}, where a constant trend was noted; afterwards, K decreased for the remaining stack heights, with an abrupt decrease between stack heights of 3 and 5 metres. The simulated concentration trend was showed a slight increase for all models tested at samplers F_{B1} and F_{B2}, with a strong underestimation of K at the lowest stack height ($h_s = 1$ m), and an overestimation

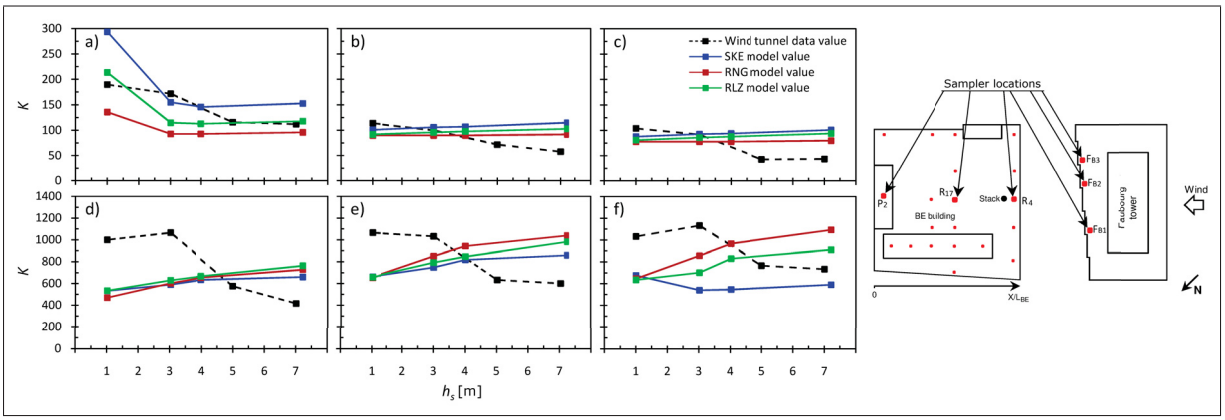

Figure 2.9 Measured and calculated concentrations K for $M = 2.2$ and for different stack heights, h_s, at samplers (a) R_4, (b) R_{17}, (c) P_2, (d) F_{B1}, (e) F_{B2} and (f) F_{B3}.

for the highest stack height ($h_s = 7.2$ m). All the models provided roughly the same results at sampler F_{B1}, and better agreement between the numerical and the experimental values of K was found at the 4-metre stack. At sampler F_{B3}, the RLZ and RNG turbulence models showed the same evolution as for samplers F_{B1} and F_{B2}, while the SKE model systematically underestimated K for all stack heights. The SKE model seemed to be the best model for $h_s = 7.2$ m at sampler F_{B3}, whereas the RNG and RLZ models displayed improved prediction using a stack height of 4 m.

2.6 Discussion

The average errors for the numerical concentrations as compared to the experimental measurements indicate that the RNG turbulence model reproduced better concentration for stack heights of 1 and 3 m, with greater momentum ratios ($M = 5$ and 4.5). The RLZ model showed the best agreement with experimental results for the smallest stack ($h_s = 1$ m) using the lower momentum ratio ($M = 2.2$). For this case ($h_s = 1$ m and $M = 2.2$), the RNG and SKE models showed similar levels in averaged error (e_a) values, compared to the RLZ model. Significant discrepancies in e_a values were observed mainly for higher stack heights, and greater momentum ratios for the three turbulence models tested, and the largest e_a values were observed with the SKE model. Given the well-known problems of SKE models in reproducing the basic flow structure around a building, and since the prediction accuracy of dispersion is strongly related

to the simulated flow field, as stated by Tominaga and Stathopoulos (2009), the inaccuracy of the SKE model was expected, even more so with higher pollutant velocities, where strong interactions occurred above the stack, between the wind flow and the exhausted pollutant.

The behaviour of the flow field in the vertical cross-section at the stack position ($y = 0.0155$ m) is shown in Fig. 2.10 for two momentum ratios with stack heights of 1 and 3 m. The significant underestimation obtained at most samplers on the BE building roof and the tower leeward wall, for both stack heights ($h_s = 1$ and 3 m) and the lowest momentum ratio ($M = 2.2$), was due to the pollutant, which was directed at the lower region between the two buildings, as shown in Fig. 2.10a and c for all the turbulence models used. This behaviour also explains the underestimated concentrations obtained at samplers located at higher levels, i.e. F_{B1}, F_{B2} and F_{B3}. For higher exhaust velocities, the pollutant rose towards the upper region between the two buildings and reached the tower roof, as shown in Fig. 2.10b and d; consequently, an overestimation of the concentration was observed at sampler F_{B2}, as shown in Fig. 2.6b, and at samplers located along the tower leeward wall, as indicated in Fig. 2.8. This was predictable, since none of the turbulence models tested was able to reproduce the upper region between the two buildings, as stated previously in Fig. 2.8.

The well-established airflow pattern around a building, as reported by authors such as Rodi (1997); Blocken *et al.* (2011); and ASHRAE (2009), induces a horseshoe vortex system at the ground level of a building upwind facade. This phenomenon seems to be better represented by the RNG turbulence model, as compared to the SKE and RLZ models, each of which displays a very small vortex at the tower upwind wall, as shown in Fig. 2.10. The flow structure in the horizontal plane (x-y) at different levels from the ground (i.e. height levels of 1/2H_{BE}, 3/2H_{BE} and 3H_{BE}) for the three turbulence models is depicted in Fig. 2.11. The flow field shows strong curvatures and recirculation zones around the two-building configuration, particularly at the lower region, as shown in Fig. 2.11a. This lower region shows a complex separated flow for the RLZ turbulence model, whereas the SKE model shows a configuration with a clear generation of two main vortices spread out over each side, between the tower and the building. For the RNG model, the recirculation fluxes seem to occur mainly in the vertical plane. In the

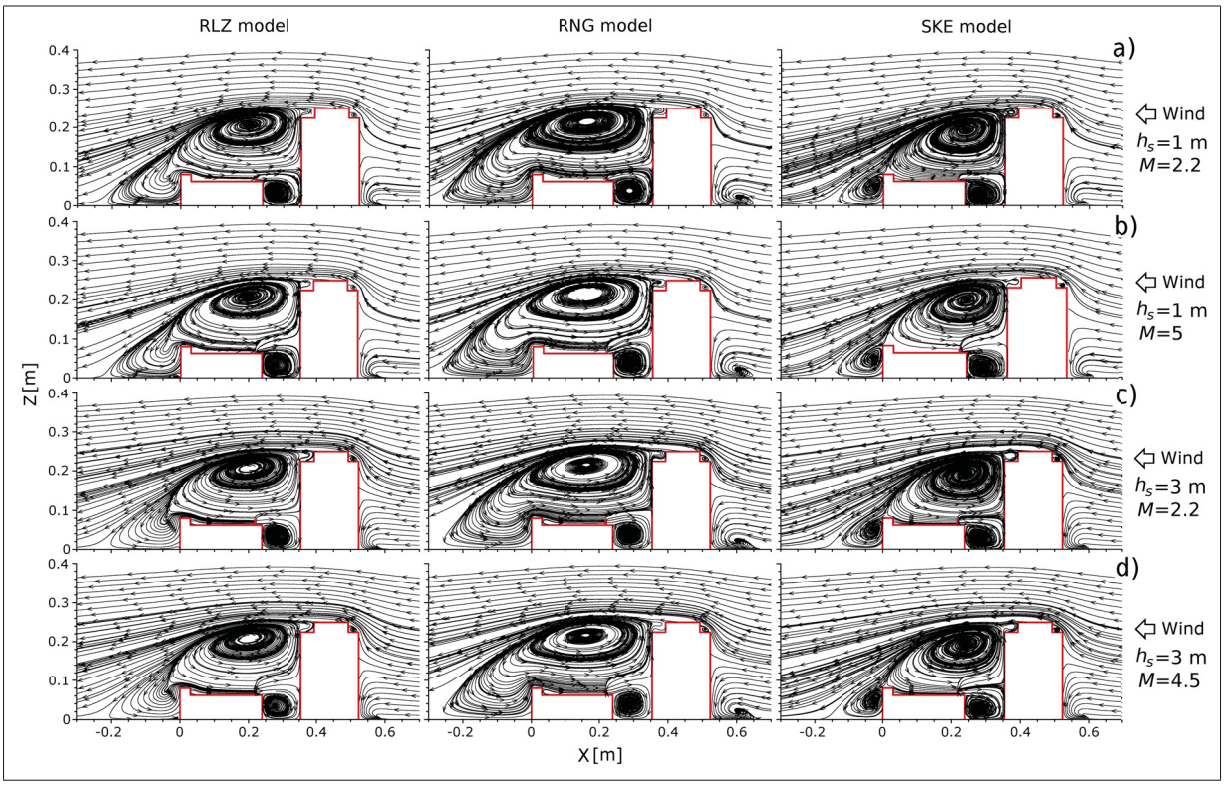

Figure 2.10 Streamlines on the vertical (x-z) plane through stack position ($y = 0.0155$ m) for (a) $h_s = 1$ m and $M = 2.2$, (b) $h_s = 1$ m and $M = 5$, (c) $h_s = 3$ m and $M = 2.2$ and (d) $h_s = 3$ m and $M = 4.5$. Columns from left to right represent results for RLZ, RNG and SKE models, respectively.

BE building wake, two horizontal vortices occur with the RLZ and RNG turbulence models; however, the only vortex displayed by the SKE model seems to be occurring in the vertical plane. For higher levels, as indicated in Fig. 2.11b, the streamlines skirt the tower along its sides and display two wide main recirculation zones in the tower wake. These zones, which are less significant for the SKE model when compared to RLZ and RNG models, become even smaller as one moves towards the upper levels, as shown in Fig. 2.11c.

Fig. 2.12 shows the ways in which turbulent kinetic energy k is distributed over the vertical cross-section at the centre of the domain ($y = 0$ m), obtained using the turbulence models tested for $h_s = 1$ m and $M = 5$. As can be seen at the Faubourg tower upstream corner, the highest turbulent kinetic energy iso-contour value is obtained with the SKE turbulence model.

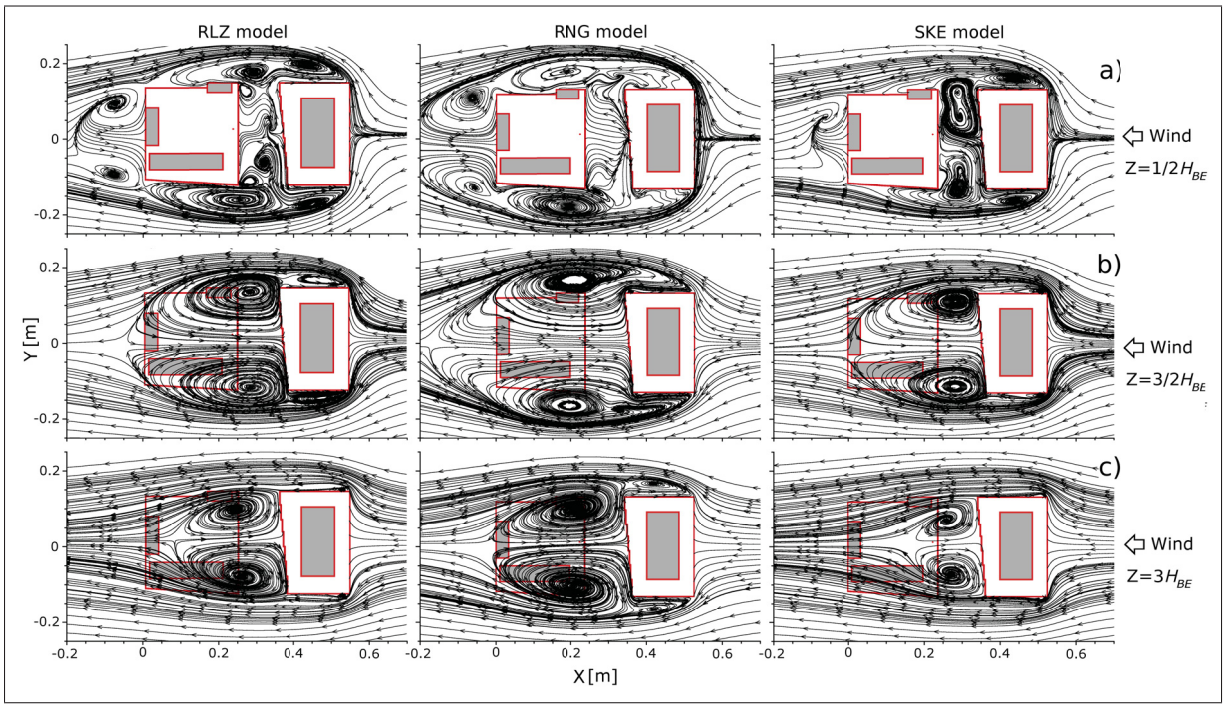

Figure 2.11 Streamlines on the horizontal (x-y) plane at different vertical positions for case $h_s = 1$ m and $M = 5$. Columns from left to right represent the results of RLZ, RNG and SKE models, respectively, at height (a) 1/2H_{BE}, (b) 3/2H_{BE} and (c) 3H_{BE} from the ground.

The maximum values for k produced by the SKE model are 13% and 46% higher, compared to those obtained with RLZ and RNG models, respectively.

This high production of k, as stated by several authors (e.g. Murakami, 1993; Rodi, 1997; Murakami, 1998; Wright and Easom, 2003; Tominaga *et al.*, 2008), is a well-known shortcoming of the SKE model, which induces inaccurate wind-flow patterns. According to some of these authors (Murakami, 1993; Rodi, 1997; Wright and Easom, 2003), this excessive k-production takes its origin from isotropic turbulent viscosity formulation.

According to Wright and Easom (2003), the wake region exhibits strong turbulence anisotropy where the lateral Reynolds stress component, $\overline{u_2' u_2'}$, dominates; the inability of the isotropic turbulent viscosity models to simulate correctly the difference between Reynolds normal stresses produces an underprediction of the lateral Reynolds stresses. Moreover, Nallasamy (1987) has stressed the assumption of isotropic turbulent viscosity as the main practical limitation of the

two equation models; Pope (2000) has noted that the assumption of the turbulent viscosity hypothesis is more reasonable in cases where the mean velocity gradients and turbulence characteristics evolve slowly, following the mean flow. For this reason, since the distribution of the mean velocity gradients varies significantly; since it is dependent upon its relative position over the configuration (Murakami, 1993), and since it is directly related to the Reynolds stress components, the complex flow field around this two-building configuration may be poorly reproduced using two equation $k-\epsilon$ models. In addition, the flow field around the configuration under study is characterized by vortex shedding from the tower leeward sides and roof, which generate a strong degree of unsteadiness and periodic fluctuation. On the one hand, turbulence dispersion is the dominant mechanism for particle spread (Canepa, 2004) and cannot be predicted accurately by assuming a steady-state process (Chang and Meroney, 2003). On the other hand, when using steady-state models, Rodi (1997) has emphasized a severe underprediction of turbulence fluctuations in the wake region, and Shirasawa *et al.* (2008) have found that turbulent diffusion flux was insufficiently spread in lateral directions. Consequently, the steady state of the tested models is probably an additional weakness that contributes to inaccuracy regarding the flow and dispersion fields.

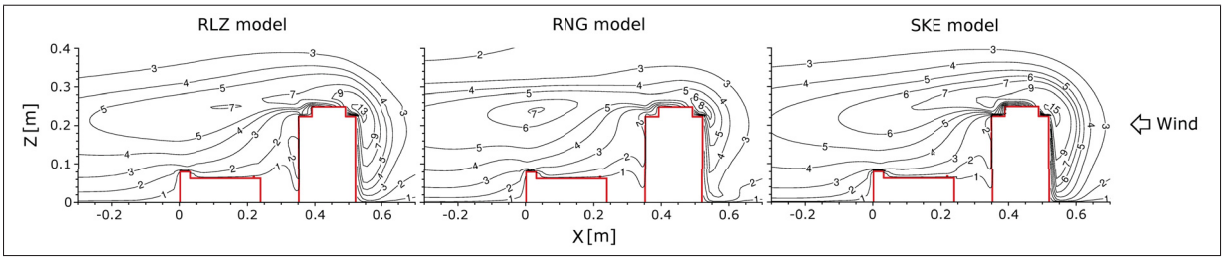

Figure 2.12 Distribution of turbulent kinetic energy k in [m^2 s^{-2}], on the vertical (x-z) plane through the centre of the domain ($y = 0$ m), obtained with RLZ, RNG and SKE turbulence models for case $h_s = 1$ m and $M = 5$.

Fig. 2.13 shows the distribution of the non-dimensional Reynolds stress components (i.e. $\overline{u_1'^2}/2k$, $\overline{u_2'^2}/2k$, $\overline{u_3'^2}/2k$ and $\left|\overline{u_1'u_3'}/2k\right|$) and the turbulent viscosity, ν_t, in the vertical cross-section ($y = 0$ m) for $h_s = 1$ m and $M = 5$. According to Shih *et al.* (1995b), the "realizability" condition imposes as requirement (i) the non-negativity of each Reynolds normal stress ($0 \leq \overline{u_\alpha'^2}$),

and (ii) Schwarz's inequality ($\overline{u'_\alpha u'_\beta}^2 / \overline{u'^2_\alpha}\ \overline{u'^2_\beta} \leq 1$) between any fluctuating quantities in the entire computational domain, to prevent the flow field from reproducing non-physical results. Using the turbulent kinetic energy expression Eq. (2.5), both requirements can be written in non-dimensional form as $0 \leq \overline{u'^2_\alpha}/2k \leq 1$ (non-negativity condition) and $0 \leq \left|\overline{u'_\alpha u'_\beta}/2k\right| \leq 1$ (Schwarz's inequality condition). Throughout Fig. 2.13, only the SKE model fails to respect the realizability criterion, due to the negative values found at the upper region of the tower windward wall, as shown in Fig. 2.13c. The region of concern is located in the upper region of the stagnation point, which occurs on the tower windward facade and whence the wind flow is deviated and accelerated to the upward, downward and sideward zones, inducing strong velocity gradients along the vertical and lateral directions. Therefore, the negative values of vertical Reynolds normal stress are mainly due to the great local mean velocity gradients, $\partial U_3/\partial z$, in the vertical direction, since the displayed values of turbulent viscosity ν_t, in that region are not very significant, as illustrated in Fig. 2.13e of the SKE model. However, Schwarz's inequality condition is rigorously respected by all the tested models, as shown in Fig. 2.13d.

To ensure that the requirement of realizability is respected throughout the computational domain, other critical planes were analyzed. These included the horizontal plane at the stagnation point and the vertical plane passing by the stack position, since strong interactions occurred between the emitted pollutant and the wind flow above the stack exit. The same anomaly was observed with the SKE model: negative values of vertical Reynolds normal stress, in the vertical plane passing by the stack, due to strong velocity gradients. The SKE turbulence model was the only model to produce non-physical values in the computed results, whereas the other models, i.e. RLZ and RNG models, appear to have rigorously respected the physical principle of the realizability requirement.

The significant underestimation of concentration K obtained at most sampler locations on the BE building roof and at the top of the Faubourg tower leeward wall, with lowest momentum ratio ($M = 2.2$) and both stack heights ($h_s = 1$ and 3 m), as stated previously in Figs. 2.5a and 2.6a, is probably due to a lack of lateral dispersion. To promote the plume dispersion artificially, various turbulent Schmidt numbers representing the ratio of turbulent viscosity to

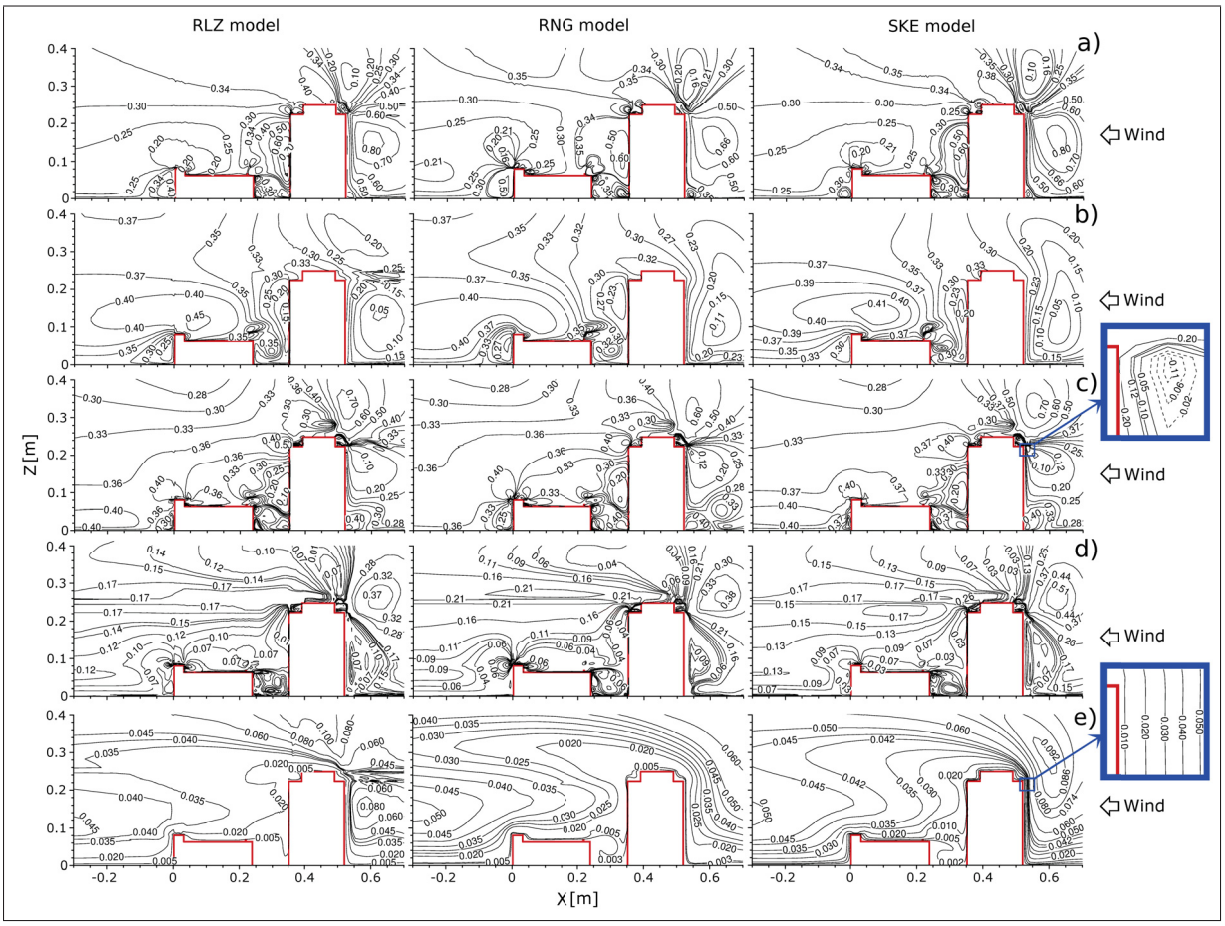

Figure 2.13 Distribution on the vertical (x-z) plane through the centre of the domain ($y = 0$ m) for case $h_s = 1$ m and $M = 5$ of the non-dimensional Reynolds stress components (a) $\overline{u_1^2}/2k$, (b) $\overline{u_2'^2}/2k$, (c) $\overline{u_3'^2}/2k$, (d) $\left|\overline{u_1' u_3'}/2k\right|$ and (e) turbulent viscosity ν_t in [m^2 s^{-1}]. Columns from left to right represent the results of RLZ, RNG and SKE models, respectively. Dashed lines indicate negative values.

turbulent mass diffusivity ($Sc_t = \nu_t / D_t$) were tested, as suggested by Lateb *et al.* (2010b). Various low Sc_t values (0.1, 0.3 and 0.5), compared to the commonly used number 0.7, were tested in order to favour turbulent mass diffusivity, D_t, against turbulent viscosity ν_t (not reported here, for the sake of brevity). Only the SKE and RLZ models were tested, since the RNG model does not allow a modification in the Sc_t value when using Fluent. Surprisingly, the results obtained showed no significant changes in concentration values, in contrast to some previous studies (Tominaga and Stathopoulos, 2007; Blocken *et al.*, 2008; Gousseau *et al.*, 2011a; Chavez *et al.*, 2011), which showed an influence of Sc_t on the concentration distributions when

it is question of a single building. Notwithstanding, Chavez *et al.* (2011) concluded that the changes in Sc_t do not have a major impact on pollutant dispersion in the presence of adjacent buildings, which is the case in this study. In addition, Sc_t varies with different dispersion problems and flow structures (Hang *et al.*, 2012) and a change of turbulent Schmidt number influences only the diffusion mechanism and not the fluid dynamics (Di-Sabatino *et al.*, 2007). Finally, the dispersion process is probably dominated by the advection transport phenomenon since it cannot be compensated by promoting the dispersion through low Sc_t values in this case of a complex flow field where strong separation/recirculation zones occur. Therefore, the turbulent diffusion mechanism which seems insignificant – in the wake region where most of all samplers are located – can be a consequence of a high underestimation of Reynolds normal stress components and the steady-state methodology.

2.7 Summary and conclusions

Pollutant dispersion in a two-building configuration was investigated using various RANS turbulence $k-\epsilon$ models (a standard $k-\epsilon$ model, a RNG $k-\epsilon$ model and a realizable $k-\epsilon$ model) in order to determine the best turbulence model to reproduce pollutant plume dispersion. It was found that the realizable turbulent $k-\epsilon$ model yielded the best agreement with wind tunnel experimental data for the lower stack height and momentum ratio, while the RNG turbulence model performed best for the higher stack height and both momentum ratios. Despite an overestimation of K using the RLZ model for higher momentum ratios, this model is the only one that provided the correct trend for concentration distribution in the lower region between the two buildings. Given the well-known problems of the SKE model in reproducing flow-field structures around buildings, this model was generally found to be inadequate for reproducing vertical concentration distribution, and was the only turbulence model that failed to satisfy the realizability requirement, consequently producing non-physical results. For the simulated complex flow fields where strong separation/recirculation zones occur, the dispersion process is probably dominated by the advection transport phenomenon and cannot be compensated by promoting the turbulent diffusion process through low turbulent Schmidt number values: the incorrect estimation of the Reynolds normal stresses and the steady-state assumption of

the turbulence models tested are thought to be the main sources of the insignificant turbulent diffusivity stated in the wake region, therefore the origin of the lack of lateral dispersion previously observed. It is recommended that an attempt be made to use unsteady turbulence models in order to shed light on the effects of steadiness on both the dispersion process and flow-field structure.

CHAPTER 3

NUMERICAL SIMULATION OF POLLUTANT DISPERSION AROUND A BUILDING COMPLEX

Mohamed Lateb[1], Christian Masson[1], Ted Stathopoulos[2] and Claude Bédard[1]

[1]Department of Mechanical Engineering, École de technologie supérieure,

1100 Notre-Dame West, Montreal, Qc, Canada H3C 1K3

[2]Department of Building, Civil and Environmental Engineering, Concordia University,

1455 de Maisonneuve Blvd. West, Montreal, Qc, Canada H3G 1M8

Portions of this chapter were presented at the *4th International Conference on Advances in Wind and Structures* (AWAS'08) – May 2008, Jeju, Korea – and the entire chapter is published August 2010 by Elsevier in *Building and Environment*, vol. 45, no. 8, p. 1788−1798.

Abstract

The dispersion of exhausted pollutants from a building roof stack situated in the wake of a neighbouring tower has been studied using the realizable $k-\epsilon$ turbulence model and computational fluid dynamics (CFD). Two scales are considered in this work, full scale (1:1) and wind tunnel scale (1:200). Of primary interest are the distributions of the plume and of the pollutant concentrations on the building roof as well as on the leeward wall of the tower. Two stack heights and pollutant exhaust velocities have been considered to study the distribution of pollutant concentrations in the neighbourhood of the building from which the pollutant is emitted. Results are compared with measurements from field and wind tunnel experiments to estimate the accuracy of simulations.

Keywords: Numerical simulation, computational fluid dynamics, (CFD) pollutant dispersion, atmospheric boundary layer (ABL), realizable $k-\epsilon$ turbulence model.

3.1 Introduction

Increasing levels of pollution in urban environments has motivated the development of new techniques to model the dispersion of pollutants in the atmosphere. This topic is of special significance in urban areas as it is one of the significant sources of poor indoor air quality due to contamination of fresh-air intakes. In the present study, the particular interest is in pollutant emissions from rooftop stacks and how the presence of the tower upstream the emitting building affects the distribution of pollutant concentrations around buildings.

Current standards for building ventilation systems recommend that rooftop stacks be designed such that their emissions do not contaminate the fresh-air intakes of the emitting or any nearby buildings. Several studies have been carried out on the dispersion of pollutants in urban environments, most of which considering a single building without neighbours. Of note are the works of Mavroidis *et al.* (2003) who was interested in pollutant distributions around a cubic building with a transmitting continuous source of tracer gas, from different lateral and vertical positions; the research by Li and Meroney (1983a,b), who studied the concentration of exhausted pollutants from a building roof for different wind directions and stack positions; other works taking into account neighbouring structures have been carried out at wind tunnel scale. For instance, Stathopoulos *et al.* (2002) studied pollutant concentration, on the roof and windward wall of a building, caused by a small roof stack emitting pollutants at various speeds. Yassin *et al.* (2005) has reproduced a built-up area within a 500 m radius to study dispersion under various weather conditions.

Some works have been directed at improving model parameters, such as the prescription of boundary conditions or wall functions, in order to better reproduce field measurements. Among them, the work of Liu *et al.* (2003) focussed on the use of two important parameters, namely roughness height and friction velocity, in establishing velocity and turbulence intensity profiles at the inlet of the domain. The work of Wang and Stathopoulos (2007) considered the impact of roughness height upstream of the site and on the velocity profile at the domain inlet for homogeneous and inhomogeneous terrains. Finally, Wagaman *et al.* (2002) carried out flow visualizations in the recirculation zones for two different building heights.

The present study considers a building in the wake of another higher building located upstream. This research complements previous experimental works completed at Concordia University in the wind tunnel and at full-scale by applying numerical modelling techniques (Computational Fluid Dynamics – CFD). The aim is to numerically reproduce experimental works of Stathopoulos *et al.* (2004), particularly the field experiments of August 12th and 26th, 2002. These experiments are simulated using the software Gambit 2.4.6 for the domain and mesh design, and Fluent 6.3.26 for the solution of the system of partial differential equations. Special attention is given to the analysis of the distribution of pollutant concentrations at various locations on the roof of the building compared to the site of the stack, while taking into account the influence of momentum ratio. The current study also provides an evaluation of the numerical approach for reproducing controlled and non-controlled experiments.

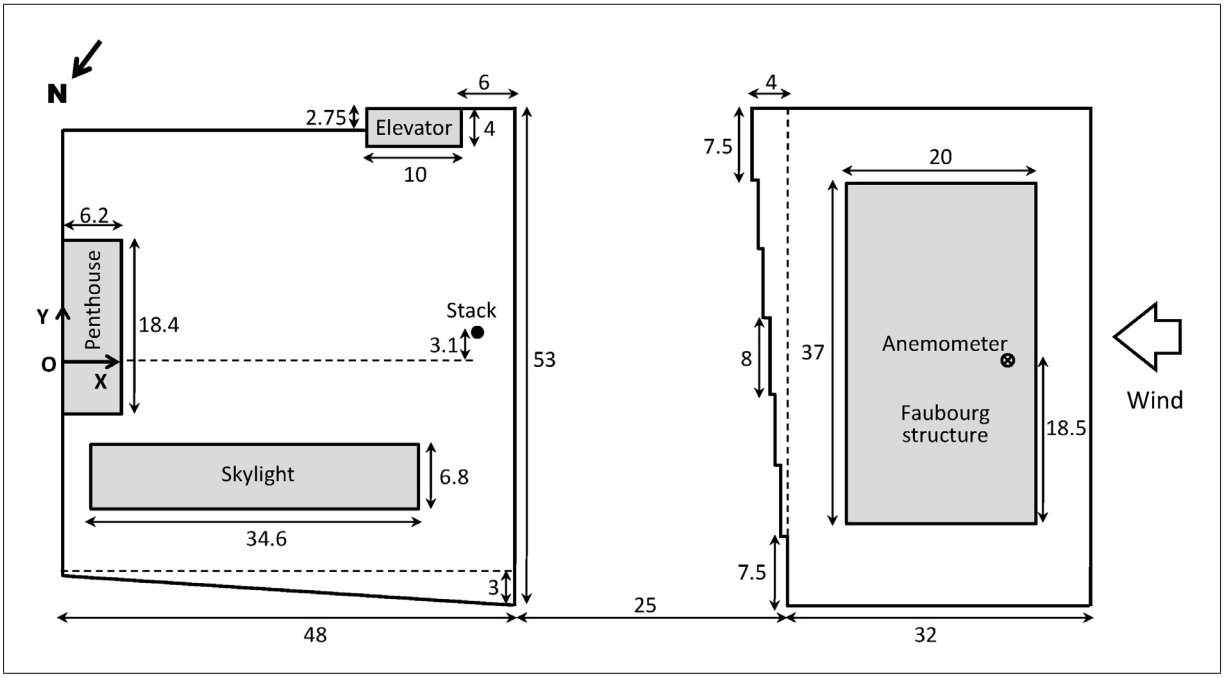

Figure 3.1 Plan view of the BE building and Faubourg tower. All dimensions in [m].

3.2 Numerical simulations

3.2.1 Model description

3.2.1.1 Geometric model

The geometric model consists of a building, referred to as BE, and the Faubourg tower which has the same width and four times the height of BE. The wind arrives perpendicular to the windward wall of the Faubourg tower which places the BE building in its wake. The dimensions of the BE building are $L_{BE} \times W_{BE} \times H_{BE} = 48$ m $\times$ 53 m $\times$ 12.5 m and those of the Faubourg tower are thus $L_{Fb} \times W_{Fb} \times H_{Fb} = 32$ m $\times$ 53 m $\times$ 45 m. Three structures are situated on the roof of the BE building. A penthouse is located at the back of the roof, along the downstream wall, with dimensions 6.2 m $\times$ 18.4 m $\times$ 4 m. There is also a skylight, with dimensions 34.6 m $\times$ 6.8 m $\times$ 2.2 m, and an elevator shaft with dimensions are 10 m $\times$ 4 m $\times$ 4 m. The stack, from which the pollutant is exhausted, is at the upstream edge of the roof near the windward wall of the building. Its diameter is 0.4 m and its height varies from 1 m to 3 m. Only one structure exists at the centre of the Faubourg tower roof with dimensions 20 m $\times$ 37 m $\times$ 5 m. Figs. 3.1 and 3.2 show the layout of these structures in plan view and elevation view, respectively. The origin of the reference frame is located at the base of the wall downstream of the BE building at its centre. Note that the wind blows in the negative x direction. Not taken into account in this geometric model are the entry of the building, located on the windward wall, and a small wall of height 1 m (parapet) that runs along the perimeter of the BE roof.

3.2.1.2 Mathematical model

The realizable $k - \epsilon$ turbulence model is used for closure of the system of equations composed of the continuity equation, the Reynolds-averaged Navier–Stokes equations and an equation modelling dispersion. This choice is made following the work of Blocken *et al.* (2008) who studied the dispersion of pollutants around the BE building without the Faubourg tower by numerical simulation. The study concluded that the realizable $k - \epsilon$ turbulence model with enhanced wall treatment better predict the recirculation zones near the windward edge and in

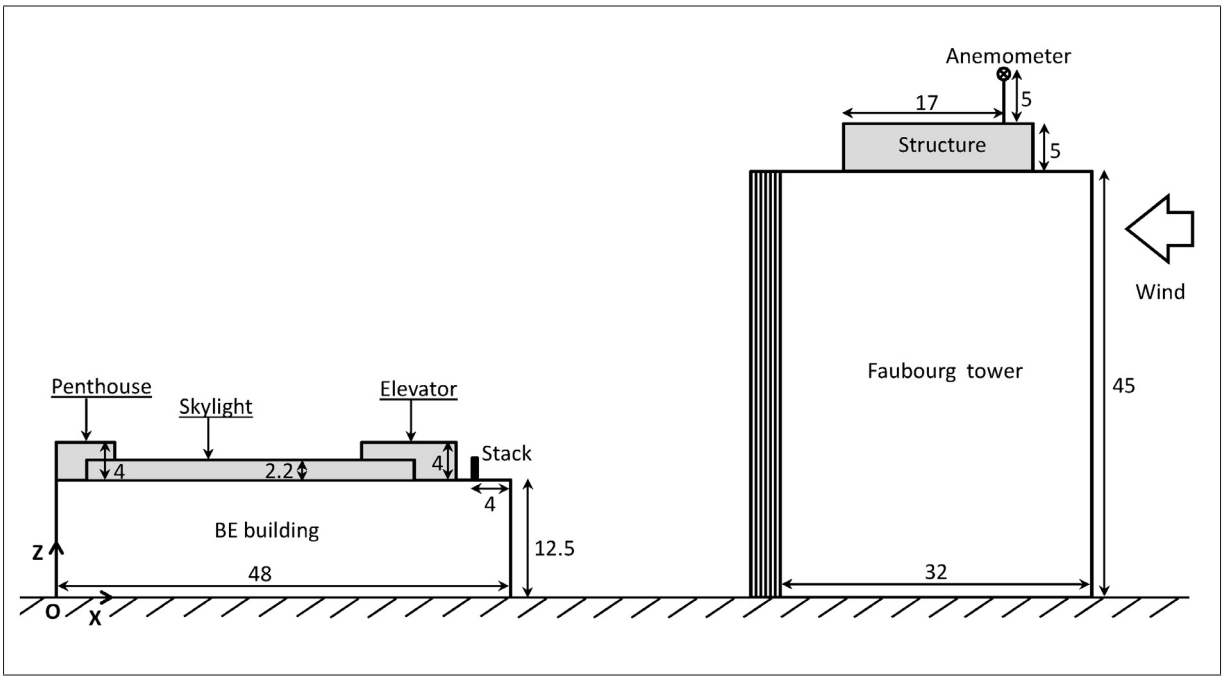

Figure 3.2 Elevation view of the BE building and Faubourg tower. All dimensions in [m].

the wake of the building than the standard $k-\epsilon$ model. The set of equations in steady-state form are summarized below:

Equation of continuity:

$$\frac{\partial U_i}{\partial x_i} = 0 \tag{3.1}$$

Equation of momentum:

$$U_j \frac{\partial U_i}{\partial x_j} = -\frac{\partial}{\partial x_i}\left(\frac{P}{\rho} + \frac{2}{3}k\right) + \frac{\partial}{\partial x_j}\left(\nu_t \frac{\partial U_i}{\partial x_j}\right) + \frac{\partial \nu_t}{\partial x_j}\frac{\partial U_j}{\partial x_i} \tag{3.2}$$

Equation of transport of k:

$$U_i \frac{\partial k}{\partial x_i} = \frac{\partial}{\partial x_i}\left(\frac{\nu_t}{\sigma_k}\frac{\partial k}{\partial x_i}\right) + P_k - \epsilon \tag{3.3}$$

Equation of transport of ϵ:

$$U_i \frac{\partial \epsilon}{\partial x_i} = \frac{\partial}{\partial x_i}\left(\frac{\nu_t}{\sigma_\epsilon}\frac{\partial \epsilon}{\partial x_i}\right) + C_1 S\epsilon - C_2 \frac{\epsilon^2}{k + \sqrt{\nu\epsilon}} \tag{3.4}$$

Equation of dispersion:

$$U_i \frac{\partial C}{\partial x_i} = \frac{\partial}{\partial x_i}\left(\frac{\nu_t}{Sc_t}\frac{\partial C}{\partial x_i}\right) + S' \tag{3.5}$$

with:

$$\nu_t = C_\mu \frac{k^2}{\epsilon} \tag{3.6}$$

and: $C_\mu = 1/(A_o + \frac{A_s k U^*}{\epsilon})$; $C_1 = \max[0.43, \eta/(\eta+5)]$; $P_k = \nu_t S^2$; $\eta = (k/\epsilon)S$; $S = \sqrt{2S_{ij}S_{ij}}$; $A_s = \sqrt{6}\cos\phi$; $\phi = (1/3)\cos^{-1}\sqrt{6}W$; $W = S_{ij}S_{jk}S_{ki}/\check{S}^3$; $\check{S} = \sqrt{S_{ij}S_{ij}}$; $S_{ij} = 1/2(\partial U_i/\partial x_j + \partial U_j/\partial x_i)$.

P: Mean pressure [kg m^{-1} s^{-2}];

U_i: Mean velocity components along the three directions x, y and z [m s^{-1}];

C: Mean concentration of pollutant;

k: Turbulent kinetic energy [m^2 s^{-2}];

ϵ: Isotropic dissipation of turbulent kinetic energy [m^2 s^{-3}];

ν_t: Turbulent eddy viscosity [m^2 s^{-1}];

ρ: Air density [kg m^{-3}];

Sc_t: Turbulent Schmidt number;

S': Mean volume contaminant source generation rate.

The model constants are the same as those defined in Fluent (2005): $\sigma_k = 1.0$; $\sigma_\epsilon = 1.3$; $A_o = 4.04$; $C_2 = 1.9$; $Sc_t = 0.7$.

The pollutant concentration K is deduced after calculation by the following non-dimensional expression:

$$K = \frac{C U_H H_{BE}^2 10^{-6}}{Q_e} \tag{3.7}$$

with:

$$Q_e = \frac{\pi d_s^2 w_e}{4} \tag{3.8}$$

Q_e: Emission rate of the pollutant [m^3 s^{-1}];

C: Mean concentration of pollutant [ppb];

H_{BE}: Height of the BE building [m];

d_s: Diameter of the stack [m];

U_H: Mean velocity of the wind at the roof height of the BE building [m s^{-1}];

w_e: Exhaust velocity [m s^{-1}].

3.2.1.3 Numerical model

All distances were estimated taking into account the recommendations made by Tominaga *et al.* (2008) and Franke *et al.* (2007) who have proposed a set of guidelines for the CFD simulation of flows using in urban environments. The calculation domain is defined by an inlet at a distance $6.5H_{Fb}$ upstream of the Faubourg tower. This configuration was chosen to avoid perturbation of the velocity and pressure profiles in the upwind fetch due to the presence of the Faubourg tower. The domain outlet is at $11H_{Fb}$ downstream of the BE building. The lateral limits of the domain are $4.5H_{Fb}$ from each building. This choice has been made not to disturb the lateral recirculation zones caused by the Faubourg tower. The top of the domain is located at $5H_{Fb}$ from the top of the Faubourg tower.

Fig. 3.3 gives a global view of the grid around the building, the Faubourg tower and the structures on their roofs. A detailed grid around the stack is shown in Fig. 3.4. Twenty four cells are contained in the exhaust cross-section. The domain blockage ratio is 1.7%, thus it does not exceed 3% as recommended by Tominaga *et al.* (2008). A structured mesh was generated with a total number of around 2.29 million cells. At the edges and the walls of the two buildings the grid is more refined as advised by several authors. Murakami and Mochida (1988, 1989) have worked particularly on 3D simulations of flow around a cube with the standard $k-\epsilon$ turbulence model. They have researched the influence of the mesh on the velocity and pressure distributions. Riddle *et al.* (2004) compared CFD simulations using the software Fluent and ADMS (Atmospheric Dispersion Modelling System) for atmospheric dispersion modelling. All these authors have concluded that a refined grid is able to reproduce, with good agreement, the recirculation and separation zones at edges and walls. Recently, Hefny and Ooka (2009) have investigated the effect of cell geometry on CFD results for the pollutant dispersion problem around buildings. The study compared the computational solutions of hexahedral-based and tetrahedral-based meshes at various resolutions and has concluded that the hexahedral-based

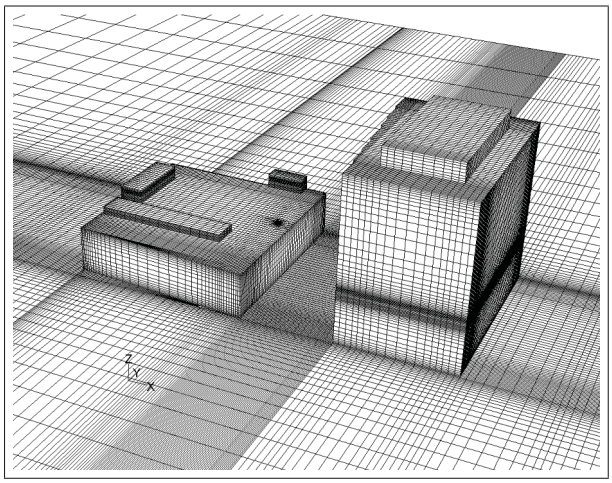

Figure 3.3 Plan view of the BE building and Faubourg tower. All dimensions in [m].

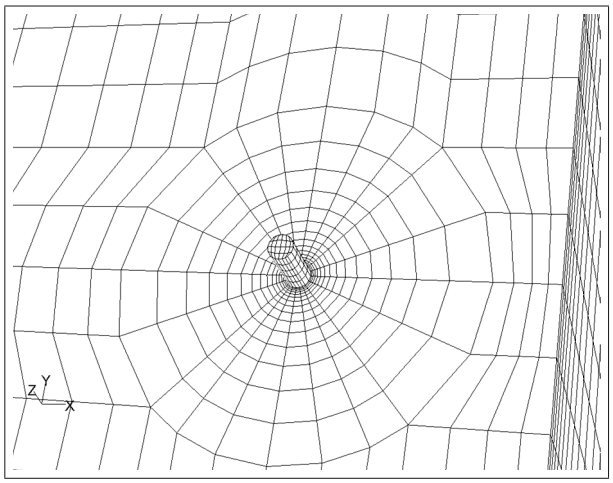

Figure 3.4 View of the detailed grid around the stack using the software Fluent.

mesh style provides the best computational solutions. Although meshes that employ tetrahedral elements can be constructed much faster in complex geometries, they can also increase the level of numerical diffusion. Factors that may be considered responsible for the deterioration of grid convergence in tetrahedral-based meshes are poor mesh quality, cell non-orthogonality, skewness, and non-alignment with the predominant flow direction.

In the present study, the grid is generated using software Gambit, whereas simulations are carried out with Fluent. The exit of the grid is defined as an outflow, the entry as a velocity inlet, the domain sides and top as symmetry. The segregated solver is used for getting the solution equations. The SIMPLE (Semi-Implicit Method for Pressure-Linked Equations) algorithm is used for introducing pressure into the continuity equation and QUICK scheme is used for discretizing the convection terms of momentum equation. Pressure discretization is taken care by Standard scheme. For both convection and viscous terms of the other governing equations, a second-order discretization scheme is used. The pollutant is considered a passive gas without thermal effects. As the purpose of this project is to compare results against two reports, we have chosen to take the same simulation characteristics.

2.1.3.1. Full-scale simulations. Inlet profiles are deduced from in situ measurements. The tests reproduced herein are those of Stathopoulos *et al.* (2004) carried out on the 12th and 26th of August, 2002. The wind data collected by the anemometer placed on top of the Faubourg tower (see Fig. 3.2) provide reference velocities U_{ref} and reference turbulence intensities TI_{ref} measured at the reference height z_{ref}.

The profiles $U(z)$ and $k(z)$ are varied at the entry until U_{ref} and TI_{ref} are obtained at the reference point. The velocity profile $U(z)$ is estimated using the power law in urban environment ($\alpha = 0.3$):

$$\frac{U(z)}{U_{ref}} = \left(\frac{z}{z_{ref}}\right)^{\alpha} \tag{3.9}$$

The turbulence intensity $TI(z)$ is deduced from the equation below which relates $U(z)$ and the turbulent kinetic energy $k(z)$:

$$k(z) = \frac{3}{2}\left[U(z)TI(z)\right]^2 \tag{3.10}$$

The rate of dissipation of turbulent energy $\epsilon(z)$ is given by the equation:

$$\epsilon(z) = \frac{u^{*3}}{\kappa z} \tag{3.11}$$

with u^* obtained from the reference point situated at z_{ref} by the following equation:

$$\frac{U(z)}{u^*} = \frac{1}{\kappa} ln\left(\frac{z}{z_o}\right) \tag{3.12}$$

where

κ: Von Karman constant $= 0.42$;

z_o: Roughness length of the model (for field $z_o = 0.66$ m and wind tunnel $z_o = 0.0033$ m – see Stathopoulos *et al.* (2004)).

2.1.3.2. Wind tunnel scale simulations. For the reproduction of wind tunnel tests (1:200 scale), boundary conditions are derived from curves presented by Dobrescu (1994), which give the profiles of velocity and turbulence intensity at the inlet. Turbulent kinetic energy and rate of dissipation profiles have been deduced from equations (3.10) to (3.12).

The turbulence intensity TI_s of the pollutant, at its exit from the stack, is calculated from the following relation:

$$TI_s = 0.16\,(Re_s)^{-1/8} \tag{3.13}$$

where $Re_s = (w_e d_s \rho_e)/\mu_e$ is the stack Reynolds number and ρ_e and μ_e are the density and dynamic viscosity of the pollutant, respectively.

Tables 3.1 and 3.2 list the simulation parameters used at the field and wind tunnel scales, respectively, where M is the momentum ratio, which is equal to the ratio between the exhaust velocity of the pollutant and wind velocity at height H_{BE} of the BE building. Details of vertical profiles of wind speed $U(z)$, turbulent kinetic energy $k(z)$, turbulence dissipation rate $\epsilon(z)$ and turbulence intensity $TI(z)$ specified at the domain entry for stack heights of 1 and 3 m are shown in the tables.

Table 3.1 Simulation parameters used at field scale (1:1).

Stack height h_s [m]	Momentum ratio M $(= w_e/U_H)$	Emission rate Q_e [m^3/s]	Turbulent intensity TI_s [%]	Profiles at the entry of the domain			
				Profile $U(z)$	Profile $k(z)$	Profile $\epsilon(z)$	Profile $TI(z)$
1	2.3	0.96	3.45	$1.56\times z^{0.3}$	$0.47/z^{0.4}$	$0.391/z$	$0.3588/z^{0.5}$
	4.9	1.98	3.16	$1.51\times z^{0.3}$	$0.39/z^{0.4}$	$0.352/z$	$0.3398/z^{0.5}$
3	1.7	0.86	3.50	$1.90\times z^{0.3}$	$0.62/z^{0.4}$	$0.716/z$	$0.3383/z^{0.5}$
	3.9	1.93	3.17	$1.85\times z^{0.3}$	$0.54/z^{0.4}$	$0.653/z$	$0.3236/z^{0.5}$

Table 3.2 Simulation parameters used at wind tunnel scale (1:200).

Stack height $200h_s$ [m]	Momentum ratio M $(= w_e/U_H)$	Emission rate $\times 10^{-5}$ Q_e [m^3/s]	Turbulent intensity TI_s [%]	Profiles at the entry of the domain			
				Profile $U(z)$	Profile $k(z)$	Profile $\epsilon(z)$	Profile $TI(z)$
1	2.2	4.36	6.20	$14.5\times z^{0.3}$	$1.25/z^{0.4}$	$2.17/z$	$0.063/z^{0.5}$
	5	9.91	5.60				
3	2.2	4.36	6.20				
	4.5	8.92	5.70				

3.2.2 Error evaluation

In the present study, two different types of errors have been evaluated. The first kind concerns inlet profile inhomogeneity and the second discretization errors due to cell sizes. To analyse inhomogeneity, the streamwise evolution of inlet profiles in an empty domain (mean wind speed U, turbulent kinetic energy k, turbulence dissipation rate ϵ and turbulence intensity TI) have been plotted at 200 m intervals starting from the inlet. For the other case, the influence of the number of cells on the simulation results has been evaluated.

3.2.2.1 Inhomogeneity error

Recently, many researchers have studied the presence of inhomogeneity in the simulated atmospheric boundary layer. Yang *et al.* (2005) concluded that it is important as a precondition for numerical simulation to evaluate the quality of the simulated equilibrium boundary layer. Blocken *et al.* (2007) also suggested that it is advisable to assess the effects of horizontal inhomogeneity by performing a simulation in an empty computational domain. In this work, the error related to inhomogeneity is evaluated as suggested by Blocken *et al.* (2007) and the results obtained are comparable to that work.

3.2.2.2 Grid refinement error

Celik *et al.* (2008) detailed a procedure for the estimation of uncertainty due to discretization in CFD applications. The study recommended a 5-step process: define a representative cell, select three significantly different sets of grids, calculate the apparent order, determine the extrapolated values and evaluate the estimated errors. The fine grid convergence index (GCI) has been calculated with the averaged relative error of the parameter of interest; in this case, the concentration K at several samplers. For the evaluation of the grid refinement error, three grids were selected with a total number of 1.59, 1.99 and 2.29 million cells, respectively. The process is detailed below.

The definition of a representative cell or mesh size l for three-dimensional problems is:

$$l = \left[\frac{1}{N} \sum_{i=1}^{N} \Delta v_i \right]^{\frac{1}{3}} \tag{3.14}$$

where Δv_i is the volume of the ith cell and N is the total number of cells used in the grid. The grid refinement factor r is defined as the ratio of representative coarse cell size to representative fine cell size, illustrated by the following equation:

$$r = \frac{l_{coarse}}{l_{fine}} \tag{3.15}$$

Many researchers recommend using a minimal value of this factor between 1.1 and 1.3; the smaller value being sufficient to differentiate the discretization error from the sources of error like iterative convergence error or computer round-off error.

The relative error in K, at each sampler, between the coarse and fine resolutions is given by:

$$e = \left| \frac{K_{i,coarse} - K_{i,fine}}{K_{i,fine}} \right| \tag{3.16}$$

and the average relative error e_a for all the concentrations K_i obtained at all samplers and for all simulations with the same grid is calculated as follows:

$$e_a = \frac{1}{J} \sum_{i=1}^{N} e_i \tag{3.17}$$

where J is the total number of concentrations collected from all samplers for the same grid resolution (with any height and momentum ratio). The grid convergence index (GCI) then indicates, as a percentage, how far the computed value is from the asymptotic value. This gives an idea of how the variables of interest would change with further grid refinement.

$$GCI = F \frac{e_a}{r^p - 1} \tag{3.18}$$

with F as a safety factor and p as the order of the discretization method (if the systems of interest are based on second-order discretization of all terms in space, then $p = 2$). The F value used is 1.25, as suggested by Celik *et al.* (2008). Table 3.3 gives the details of the computational cases used for this grid refinement study.

Through the current analysis of discretization error, it appears that the lowest values of e_a and GCI are obtained for the two successively finer grids at both simulation scales. At field scale the lowest average error and grid convergence index are about 0.64% and 7.78%, respectively, which are lower than those found at wind tunnel scale. This means that the two finer grids for the field scale simulations give concentration values relatively closer to each other than those obtained in the wind tunnel simulations, in the case of the average relative error. For the grid convergence index, the percentage value, at field scale, is again smaller than that found at wind tunnel scale. It can be concluded that for the field scale simulations, with the two successively more refined grids, the solution changes less in relative terms than it does at wind tunnel scale. To obtain comparable values from the wind tunnel simulations, it would be necessary to further refine the grid. As the concentrations K obtained for the two successive

Table 3.3 Calculation details of the grid refinement error.

Scale simulation	Total number of cells [$\times 10^6$]	Grid refinement factor value r	Average relative error e_a [%]	Grid convergence index CGI [%]
1:1	1.99 vs 2.29	1.05	0.64	7.78
	1.59 vs 1.99	1.08	9.55	71.74
1:200	1.99 vs 2.29	1.05	1.06	12.92
	1.59 vs 1.99	1.08	8.72	65.49

refined grids are so close, the errors obtained are acceptable and further grid refinement would significantly increase processing time with only negligible increase in accuracy. Therefore, 2.29 million cells were used for the remainder of the study. Please note that the obtained Y^+ values near the walls are in the range of 2-5.

3.3 Numerical results and validation

The experiments of Stathopoulos *et al.* (2004) were used to validate the numerical model. These experiments were carried out, in full-scale, on the roof of a 3-storey building which used to house the Department of Building, Civil and Environmental Engineering at Concordia University in downtown Montreal. The building is situated 25 m away from a 12-storey tower located on its south-west side. The field tests were carried out in strong winds ($U_{Dorval} > 4$ m s^{-1}) according to measurements taken at Dorval airport provided by Environment Canada. The wind arrives from the south-west and places the BE building in the wake of the Faubourg tower. Wind speeds of this magnitude correspond, according to classes defined by Pasquill, to a neutral or slightly unstable atmosphere and lend themselves well to wind tunnel modelling according to Stathopoulos *et al.* (2004).

The wind tunnel tests were carried out at the boundary layer wind tunnel of Concordia University. The models of the BE building, Faubourg tower, and surroundings were reproduced at 1:200 scale. In the windward direction, the surroundings were reproduced up to a distance of 250 m. In the leeward direction, the neighbouring buildings were included up to a distance of 50 m.

The results of the field and wind tunnel experiments carried out by teams at IRSST (Institut de recherche Robert-Sauvé en santé et sécurité du travail) and at Concordia University, respectively, have allowed comparisons of concentrations obtained at different samplers located on the leeward wall of the Faubourg tower and on the emitting building roof, for configurations of interest with different stack heights and exhaust velocities of pollutant.

In the present study, numerical results obtained at each scale are presented and compared to their corresponding experimental values.

3.3.1 Full-scale simulations

Fig. 3.5 presents the K distribution on the BE roof and leeward wall of the Faubourg tower, for a stack height of 1 m and for a momentum ratio of 2.3. The majority of K values obtained

are overestimated at most sampler locations. Only those on the windward part of the roof and in close vicinity of the stack are underestimated. The underestimation average error is about 62%. On the leeward wall of the Faubourg tower, K is underestimated at sampler F_{B1} whereas at sampler F_{B3} it is overestimated. This is due to the staircase shape of the leeward facade which does not permit a symmetric dispersion of the pollutant in this part between the two buildings. The highest overestimation errors are found at samplers R_{35} and R_{25} located at the south-east corner of the BE roof.

Fig. 3.6 also presents the distribution of K, but for a momentum ratio of 4.9 with the same stack height. Again, almost all samplers on the BE roof overestimate K. Only in the close vicinity of the stack is K underestimated, as in the previous case. On the leeward wall of the Faubourg tower, overestimation is also observed. However, a reduction in the underestimation of K around the stack (R_3 and R_4) with increased exhaust velocity was noted. The highest average error of overestimation remains at sampler R_{25}. Overall, the increase in exhaust velocity produces a smaller zone around the stack where K is underestimated, and increases the overestimation of K at the centre of the south-east wall, particularly at samplers R_{25} and R_{19}. For sampler R_6, located at the south corner of BE building, the effect is completely reversed.

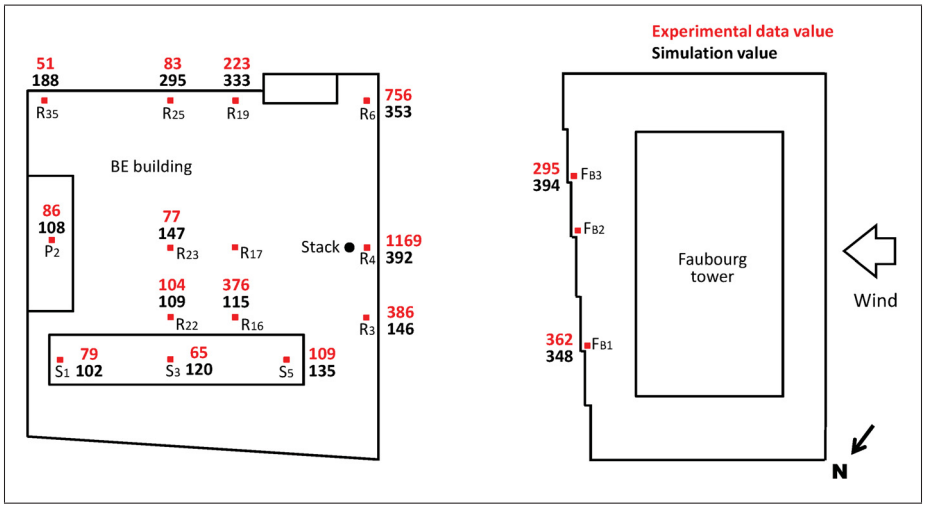

Figure 3.5 Simulation (1:1 scale) and field values for K ($M = 2.3$ and $h_s = 1$ m).

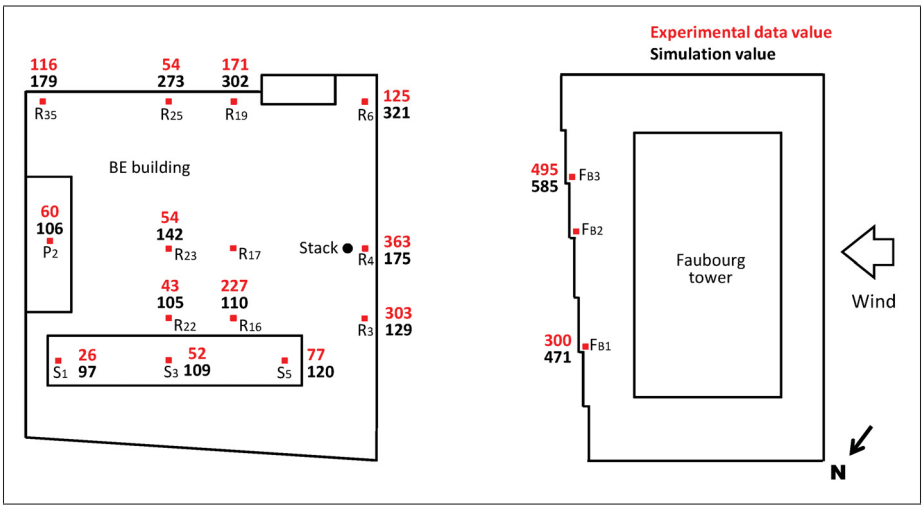

Figure 3.6 Simulation (1:1 scale) and field values for K ($M = 4.9$ and $h_s = 1$ m).

Fig. 3.7 presents a comparison of K values between field tests and full-scale simulations for three samplers (R_4, R_{23} and P_2) along the x (stack) axis and for two different exhaust velocities. The underestimation of the simulated K values noted before, in Fig. 3.5 at sampler R_4, is clearly shown on this figure. For $M = 2.3$, the measured concentration is three times higher than the calculated value at sampler R_4. But, for a momentum ratio twice greater ($M = 4.9$), the field value is just two times that of full-scale simulations. Better results for this case were expected: doubling the emission velocity should increase the turbulence intensity, the dispersion near the stack and consequently K at the sampler R_4. However the computed value at $M = 4.9$ is still lower than that obtained for $M = 2.3$. Clearly, the dispersion is not well reproduced despite the increase in velocity. The same observation has been made by Stathopoulos *et al.* (2004) in their work.

Fig. 3.8 presents the vertical distribution of K along the leeward wall of the Faubourg tower upwind of the stack. Here, simulations significantly overestimate K. The calculated distributions for the lower half of the Faubourg tower have the same form as their measured counterparts and the overestimation is roughly constant for this region although very significant. In contrast, the simulated K profile varies in reverse fashion with respect to the field profile for the upper half. The overestimation decreases to its smallest value at the top of the Faubourg tower.

The pollutant plume does not appear to be as well evacuated vertically as observed in the field experiment. Consequently, the major part of the pollutant is transported to the lower half and makes the K values overestimated. Since similar evolutions of K are observed in the lower half region for both measurements and simulations, flow recirculation occurring in the lower half region seems to be well reproduced.

The dispersion of K values between field tests and simulations at full-scale is given in Fig. 3.9a and b. On the BE roof (Fig. 3.9a), the majority of samplers have overestimated K, only 21% of them are underestimated. Forty percent (40%) of values are positioned within a range of factor 2, as indicated by points situated between the lines on each side of the median line. For the samplers located at the top of the Faubourg leeward wall (F_{B1}, F_{B2}, and F_{B3}) all values are within a factor of 2 and overestimation is still the dominant tendency (Fig. 3.9b).

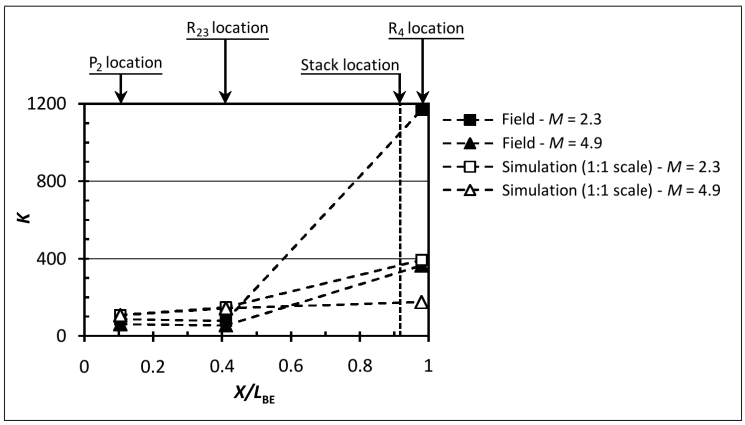

Figure 3.7 Measured and computed (1:1 scale) variation of K along x axis on BE roof ($h_s = 1$ m).

To summarize, simulation values overestimate, at most samplers, the concentrations compared to those recorded in the field. An underestimation on the windward part of the BE roof is observed and it is more important around the stack for low pollutant velocity. Doubling the pollutant exhaust velocity produces a significant decrease of the underestimation in this region. Far from the stack, at the roof centre, the variation with exhaust velocity is less important than around the stack. The pollutant plume is not sufficiently evacuated vertically and the flow seems to be correctly reproduced in the lower part between the two buildings, but not in the

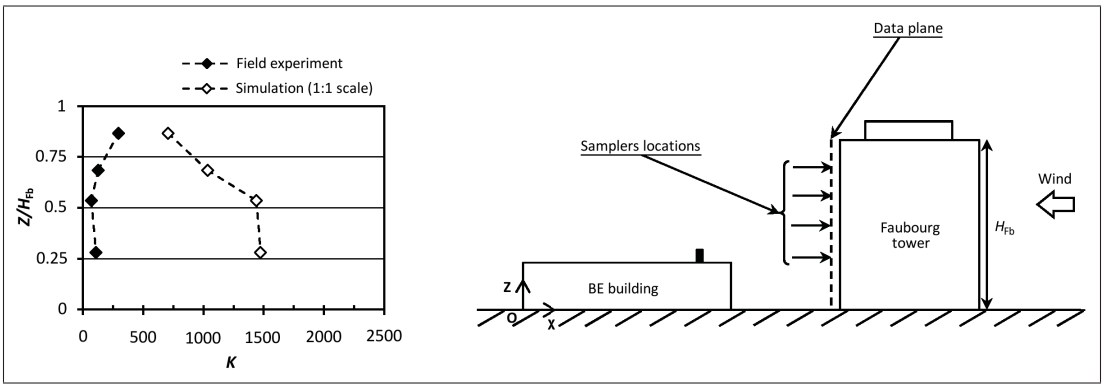

Figure 3.8 Vertical profiles of K on leeward wall of Faubourg tower (Field and simulation 1:1 scale values, $M = 3.9$ and $h_s = 3$ m).

upper part. The dispersion around the stack appears to be poorly predicted, even for the high exhaust velocity case. Probably, the existence of the parapet in the field experiments imprisons the pollutant at samplers located in the windward zone of the roof and particularly at sampler R_4. This parapet is not simulated in CFD, so it can be the origin of poor prediction in this area.

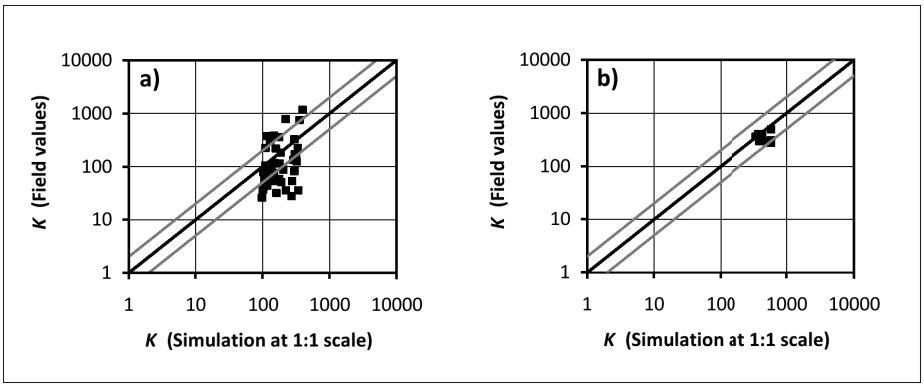

Figure 3.9 Scatter plots of simulation (1:1 scale) and field K data. (a) On the BE roof and (b) on the Faubourg leeward wall.

3.3.2 Wind tunnel scale simulations

Figs. 3.10 and 3.11 present experimental and simulation values of K at the wind tunnel scale for a stack height of 1 m and for $M = 2.2$ and 5, respectively. For moderate exhaust velocity (Fig. 3.10), almost half of samplers have overestimated K and the majority of them are situated

along the south-east wall of the BE roof and on the skylight structure. The sampler R_4 near the stack also overestimates K, but this is the only sampler located along the centre region of the roof which does so. Most of the others have underestimated K by a factor less than 2.

For higher pollutant velocities (Fig. 3.11), the calculated concentration at most samplers increases and surpasses those measured in the wind tunnel experiments. Only at samplers in close vicinity to the stack as well as F_{B1} and R_{19} K is still underestimated.

Comparing Fig. 3.12, at wind tunnel scale (1:200) with Fig. 3.7 at full-scale, it is clear that simulations at wind tunnel scale are in better agreement with measurements for samplers located near the stack and BE roof centre. As pollutant concentrations decrease away from the stack, the conclusions of Stathopoulos *et al.* (2004) that the leeward wall of the BE building, for this configuration, is the best side to install fresh-air intakes are confirmed.

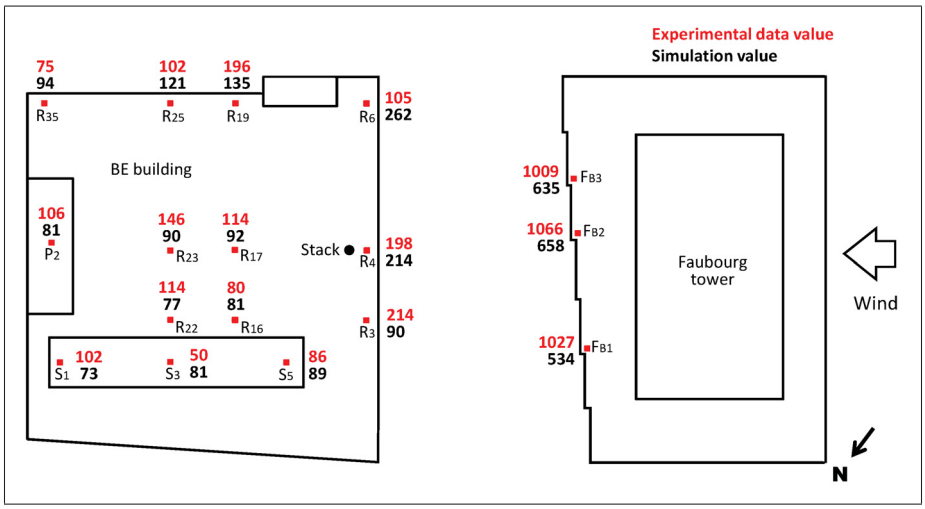

Figure 3.10 Simulation (1:200 scale) and wind tunnel values for K ($M = 2.2$ and $h_s = 1$ m).

Similar to Fig. 3.8, Fig. 3.13 presents the vertical distribution of concentrations along the leeward wall of the Faubourg tower. An overestimation is also noted for this simulation, but less significant than for the full-scale simulation. Distributions of K again have the same form in the lower half of the Faubourg tower but are reversed in the upper half. The closest values

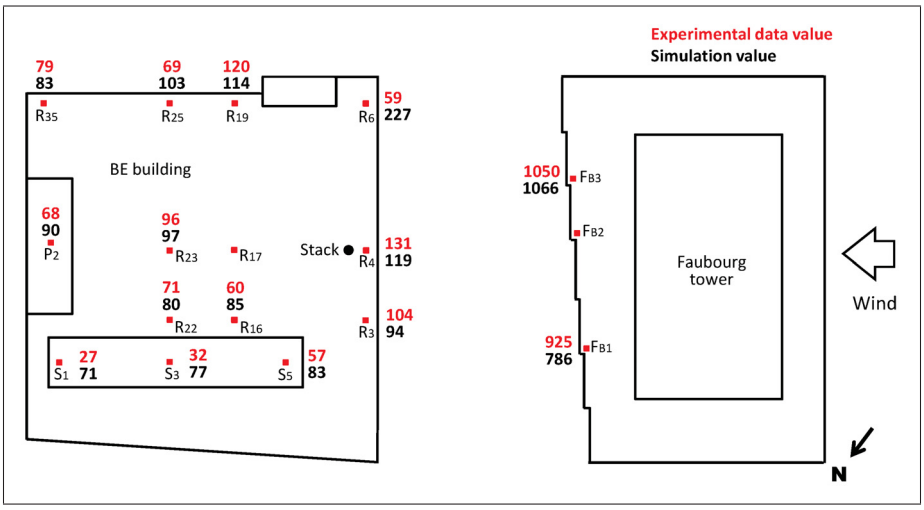

Figure 3.11 Simulation (1:200 scale) and wind tunnel values for K ($M = 5$ and $h_s = 1$ m).

are again reached at the top of the Faubourg tower. The results obtained at the two scales are comparable, but overestimation is larger at field scale.

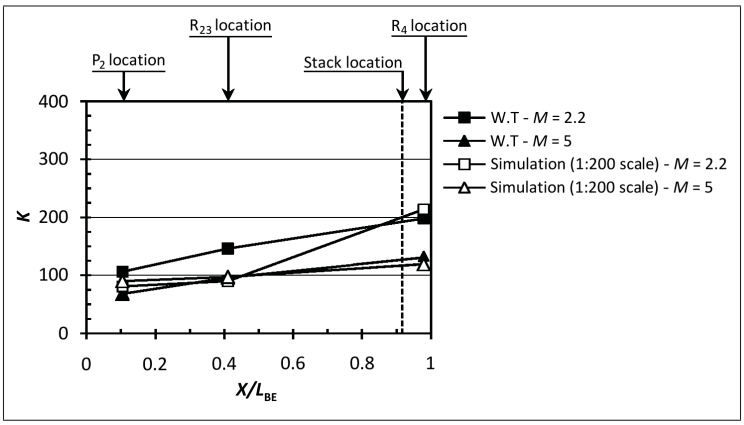

Figure 3.12 Measured and computed (1:200 scale) variation of K along x axis on BE roof ($h_s = 1$ m).

In the case of simulations at wind tunnel scale with $h_s = 3$ m and $M = 4.5$, the peak of K along the downstream wall of the Faubourg tower is at mid height. This is explained by the fact that the pollutant plume is evacuated upwards from the stack directly towards the leeward

wall of the Faubourg tower and it is separated thereafter in two directions: one ascending and one descending; as it moves away from the impact point, the concentration decreases.

As already observed in full-scale simulation, the pollutant plume does not appear to be as well evacuated vertically. Thus the general trends of pollutant concentration are well captured in the lower region, but not in the upper; and it is likely that recirculation has not been well reproduced above the mid height of the Faubourg tower.

Fig. 3.14a compares the dispersions of K values on the BE roof between wind tunnel experiments and CFD simulations at 1:200 scale. Eighty percent (80%) of concentration values are situated within a range factor of 2, with 30% of K values being underestimated. For results obtained on the leeward wall of the Faubourg, as shown in Fig. 3.14b, the same is observed and all K values are within a range factor of two. But in this case, 80% of results underestimate the measured K values contrary to field scale simulations where overestimation is the dominant tendency.

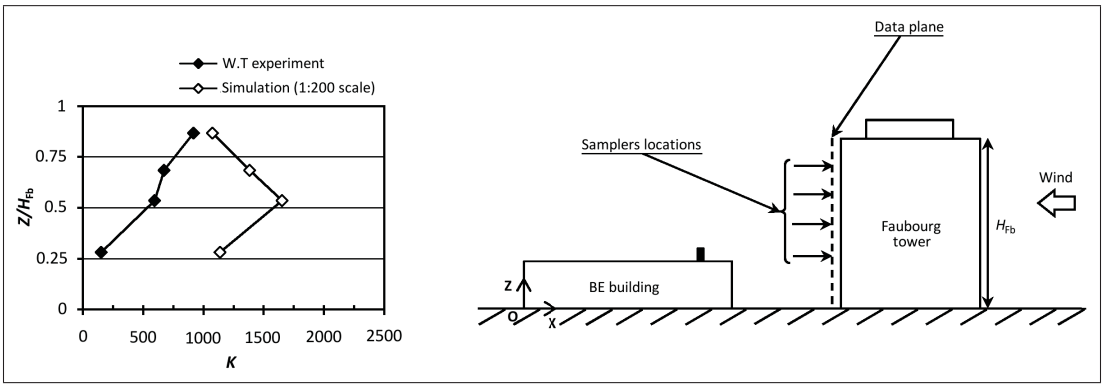

Figure 3.13 Vertical profiles of K on leeward wall of Faubourg tower (Wind tunnel and simulation 1:200 scale values, $M = 4.5$ and $h_s = 3$ m).

Wind tunnel simulation results show an overestimation of K values around the stack and in the south-east region of the BE roof. A small underestimation is noted at the other sampler locations on the roof. A more pronounced underestimation is observed on the leeward wall of the Faubourg tower. Increasing the pollutant exhaust velocity reduces the difference between experimental and simulated concentrations, except at sampler R_6. The flow field is better

reproduced in the lower part between the two buildings compared to the region above the mid height of the Faubourg tower.

3.3.3 Summary of simulation results

Differences between measured and calculated concentrations, at almost all sampler locations on the BE roof and Faubourg leeward wall, are more pronounced at field scale than at wind tunnel scale. At samplers located on the south-east wall (R_{35}, R_{25} and R_{19}), the variation of K with stack height and exhaust velocity is different than at other samplers on BE roof. The upstream flow coming around the Faubourg tower finds a broader opening on the side of sampler F_{B1}. This results in greater dilution on this side, thus driving a major part of the pollutants towards the south-east zone. Consequently, concentration at samplers located on that part of the BE roof increases. It is possible that the large differences in concentrations between simulations and experimental results are due to the presence of a neighbouring building which has not been included in the numerical model. Irrespective of this, overestimations are less pronounced at the wind tunnel scale.

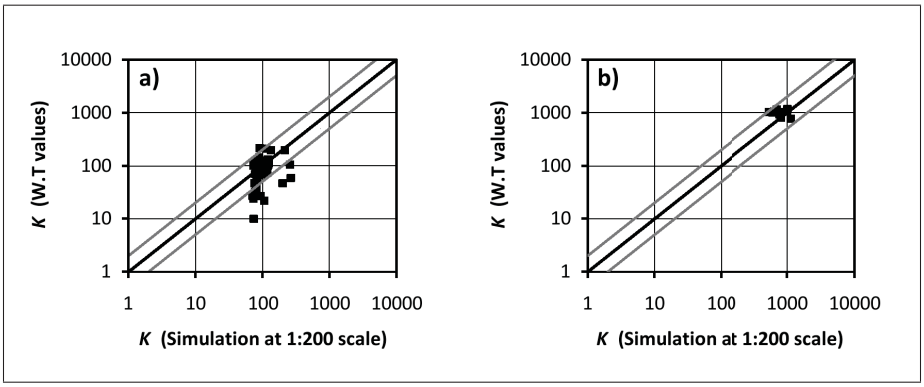

Figure 3.14 Scatter plots of simulation (1:200 scale) and wind tunnel K data. (a) On the BE roof and (b) on the Faubourg leeward wall.

At samplers located on the Faubourg tower leeward wall, simulation values of K overestimate field scale data, while for wind tunnel scale simulations, results underestimate experimental values. The pollutant plume is not sufficiently transported vertically in simulations than it has

been observed in experimental tests. For both scales, the vertical variation of concentration values shows that the flow between the two buildings has not been correctly reproduced in the upper half of the tower. However in the lower half, it seems to be correctly simulated.

Finally, simulations at wind tunnel scale have better reproduced the corresponding experimental values than at field scale. This is likely due to the highly controlled environment under which wind tunnel tests are performed.

3.4 Error analysis

The average error is calculated, using the equation below, over all samplers and for each stack height and exhaust velocity. Its variation as a function of momentum ratio for each stack height is shown in Fig. 3.15a and b for field and wind tunnel scales, respectively. The standard deviation is also included for each case.

$$e_a = \frac{1}{n}\sum_{i=1}^{n}\left|\frac{K_{i\ sampler,simulation(N\ cells)} - K_{i\ sampler,exp}}{K_{i\ sampler,stack\ exit}}\right| \tag{3.19}$$

with:

e_a: Average relative error of all samplers;

$K_{i\ sampler,exp}$: Concentration measured experimentally;

$K_{i\ sampler,stack\ exit}$: Concentration obtained numerically at the centre stack exit;

$K_{i\ sampler,simulation(N\ cells)}$: Concentration obtained numerically using a grid with N cells.

With respect to Fig. 3.15a, the average error and standard deviation are lowest for small exhaust velocities and tall stack heights at field scale. At wind tunnel scale, shown in Fig. 3.15b, the best results are obtained at high exhaust velocity and with the lowest stack height. Comparing the two figures, wind tunnel simulations better reproduce experimental results than field scale simulations, as already mentioned.

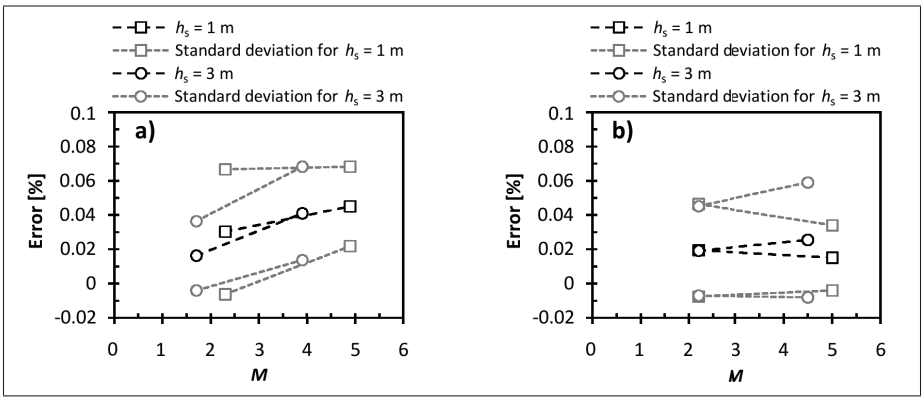

Figure 3.15 Average error between measured and calculated K for different M and h_s values. (a) Measured and calculated at (1:1 scale) and (b) at (1:200 scale).

3.5 Conclusion

This work investigates the dispersion of pollutants emitted from a roof stack in the wake of a tower in urban environment. Numerical simulations are carried out with the realizable $k-\epsilon$ turbulence model. Two scales are considered, namely full-scale (1:1) and wind tunnel scale (1:200). During this study, the primary interest is to reproduce field and wind tunnel experiments by calculating the distributions of pollutant concentrations in the vicinity of a building with a roof stack, for two different stack heights and exhaust velocities.

As a result of this work, conclusions can be summarized as follows:

- Simulation results at full-scale (1:1) underestimate pollutant concentrations at samplers located around the BE roof stack and overestimate them everywhere else. The increase in exhaust velocity produces a smaller zone around the stack in which K is underestimated and increases the overestimation of K in the south-east part of the roof.

- Wind tunnel scale (1:200) CFD simulations tend to underestimate the values measured in wind tunnel experiments (particularly along the centre region of the roof and at leeward samplers of the Faubourg tower) except around the stack and on the south-east side of the BE roof. Increasing the exhaust velocity generally reduces differences in K values; however, the

opposite tendency is observed around the stack and on the south-east part of the Faubourg leeward wall (due to the staircase shape of the leeward facade). The relative errors are rather low compared to those at field scale.

- The calculated average errors for all K values show that results of wind tunnel scale simulations are closer to experiment than those at field scale. This clearly brings light on the numerical approach capability to reproduce experiments in controlled and non-controlled environments.

- At both scales, CFD simulations did not well reproduce the wake zone observed in the experiments. The lower region between the two buildings seems to be correctly reproduced, resulting in the same trends of pollutant concentrations. However the upper half has not been correctly simulated resulting in a pollutant plume which is not sufficiently elevated vertically when compared to the experiment observations.

- The leeward wall of the BE building remains the best side to install fresh-air intakes for this building with the configuration considered.

CHAPTER 4

EFFECT OF STACK HEIGHT AND EXHAUST VELOCITY ON POLLUTANT DISPERSION IN THE WAKE OF A BUILDING

Mohamed Lateb[1], Christian Masson[1], Ted Stathopoulos[2] and Claude Bédard[1]

[1]Department of Mechanical Engineering, École de technologie supérieure,

1100 Notre-Dame West, Montreal, Qc, Canada H3C 1K3

[2]Department of Building, Civil and Environmental Engineering, Concordia University,

1455 de Maisonneuve Blvd. West, Montreal, Qc, Canada H3G 1M8

Portions of this chapter were presented at the *4th International Conference on Advances in Wind and Structures* (AWAS'08) – May 2008, Jeju, Korea – and the entire chapter is published September 2011 by Elsevier in *Atmospheric Environment*, vol. 45, no. 29, p. 5150−5163.

Abstract

The dispersion of pollutants exhausted from a building roof stack located in the wake of a tower is investigated by means of the realizable $k-\epsilon$ turbulence model. Variations in stack height and pollutant exhaust velocity are considered to assess their influence on the distribution of pollutant concentrations in the neighbourhood of the emitting building. In order to determine optimum locations for fresh-air intakes, the worst case is considered, namely when the wind originates directly upstream of the tower and places the emitting building in its wake. Special attention is given to the evolution of the plume and distribution of pollutant concentrations on the roof and windward wall of the emitting building, as well as on the leeward wall of the upwind tower. Simulation results are compared to wind tunnel experiments conducted in a boundary layer wind tunnel. For this particular configuration, the paper shows that increasing the stack height has an effect similar to that obtained by increasing the momentum ratio, but with some differences, depending upon which wall of the two buildings is considered. On the emitting building, the leeward wall has the lowest concentration values for all stack heights and momentum ratios considered; thus this is the best location for fresh-air intakes. However,

for the tower, fresh-air intakes should not be located on the leeward wall due to high pollutant concentrations. The results show completely different pollutant dispersion patterns from those for an isolated building. This highlights the importance of accounting for structures that lie in close proximity to the emitting building.

Keywords: Computational fluid dynamics (CFD), atmospheric boundary layer (ABL), pollutant dispersion, pollutant exhaust velocity, stack height, turbulence model.

4.1 Introduction

Nowadays, pollutant dispersion from roof stacks in urban areas is a factor that can seriously affect the quality of fresh-air at intakes of the surrounding buildings, potentially compromising the well-being of these buildings' occupants. Finding a way to eliminate this harmful and sometimes hazardous problem poses a challenge for the scientific and engineering community.

Many parameters affect the dispersion of pollutants from roof stacks, including wind speed and direction; stack exhaust velocity; the presence of surrounding buildings; topography; stack location and height; atmospheric stability, and initial pollutant concentration (White and Stein, 1990). Some of these parameters (e.g. stack location and height, fresh-air intake locations, and pollutant exhaust velocity) are easier to study than others in terms of respecting the air quality norms inside the surrounding and emitter buildings. Stack height and pollutant exhaust velocity are the parameters of interest for this study.

Pollutant dispersion studies are generally carried out using field measurements, wind tunnel testing and, more recently, by numerical simulation with Computational Fluid Dynamics (CFD). Those carried out at field and wind tunnel scales, as reviewed by Blocken and Stathopoulos (2008), provide concentration discrete-point data. CFD allows for easier control of each parameter and can be a powerful tool for parametric analysis of the factors influencing flow and dispersion processes. In this numerical study, the objective is to determine how stack height and pollutant exhaust velocity influence the emitted pollutant plume and dispersion, in order to find the fresh-air intake locations which best respect air quality norms. The results

are compared with experimental measurements carried out by Stathopoulos *et al.* (2004) in the boundary layer wind tunnel of Concordia University.

4.2 Review of previous dispersion studies

Several studies have been carried out previously to evaluate pollutant dispersion around buildings. Because incoming flow is complex and highly turbulent, most studies have been conducted on isolated buildings (sometimes on cubic buildings) in order to simplify not only the flow field (e.g. Meroney *et al.*, 1999; Blocken *et al.*, 2008; Tominaga and Stathopoulos, 2009; Santos *et al.*, 2009; Tominaga and Stathopoulos, 2010) but also the implications of certain parameters. As such, the features of the wind pattern around an isolated building are now well established in the wind engineering community, as mentioned by several authors (e.g. Meinders and Hanjalic, 1999; Blocken and Stathopoulos, 2008; ASHRAE, 2009; Blocken *et al.*, 2011). As stated by Blocken *et al.* (2011) these studies serve as generic basic situations and have proven quite suitable for validation, verification and sensitivity analyses. Although other studies have been conducted in complex sites (e.g. building groups, urban sites, building complexes), starting from the 1990s, fundamental studies focussing to multiple-building configurations have been increasingly performed. In these cases, the parameters generally studied are wind direction (e.g. Yassin *et al.*, 2005; Gousseau *et al.*, 2011a); wind speed (e.g. Stathopoulos, 2006); the influence of surrounding buildings on flow and diffusion fields (e.g. Murakami *et al.*, 1991; Chavez *et al.*, 2011), or one or more of the other parameters mentioned in the previous section.

Turbulent plumes exhausted from a building stack have been studied and compared with experimental data gathered by Onbasioglu (2001). These studies show that higher exhaust velocities affect the entrainment mechanism and that decreasing jet velocity not only limits the vertical rise of a buoyant plume, but also restricts dilution as compared to higher jet velocities. Although exit temperature does not affect the lateral and vertical coordinates of plume formation, it decreases the plume in size and its concentration also decreases more rapidly towards the inside of the stack.

Nakiboglu *et al.* (2009) have recently studied pollutant dispersion from a stack located in an atmospheric boundary layer. Concentration and velocity fields in a vertical plane were compared with wind tunnel measurements. The experimental concentration field was determined via two methods: Aspiration Probe (AP) measurements and Light Scattering Technique (LST). Large Scale-Particle Image Velocimetry (LS-PIV) was used to obtain the velocity field. Although good agreement was found between CFD and AP measurements when using a Schmidt number of 0.4, a correction function had to be applied for LST measurements in order to obtain close agreement.

An analysis of the Reynolds number effect on plume trajectories for pollutants emitted by a stack was carried out in wind tunnel experiments by Contini *et al.* (2009); the critical Reynolds number of stack emissions Re_s proved to be approximately 3000 for the particular case studied. The effect of having a lower Re_s than the indicated threshold led to an overestimation of the plume rise in wind tunnel measurements as compared to full-scale emission. This observation was due to the corresponding Re_s value in full scale, which is much higher, leading to the distortion of the emission velocity profile caused by an excess in the emitted momentum flux.

A wind tunnel study evaluating the influence of stack height was carried out by White and Stein (1990). Their aim was to determine the minimum stack height necessary in order to keep the stack outlet free of upstream wake effects. Several cases using various stack heights, stack locations and wind directions were studied. Within the same context, in order to determine laboratory exhaust stack height in order to avoid re-entry of exhaust and possible air quality problems, Ratcliff and Sandru (1999) used the dilution prediction equations from the ASHRAE (1997) handbook as well as the Halitsky dilution criterion to provide a method for specifying stack heights in future handbooks. The authors suggested using a comparison with wind tunnel data for the revised equations.

In previous cases, Blocken *et al.* (2008), Lateb *et al.* (2010a) and Gousseau *et al.* (2011a) have conducted their studies on the same site with the present study. All these works have a common point: to compare numerical simulation results with experimental results obtained at Concordia University wind tunnel. Gousseau *et al.* (2011a) have reproduced the whole site configuration

of the wind tunnel experiment using two different turbulence models, i.e. RANS (Reynolds-averaged Navier–Stokes) standard $k - \epsilon$ and LES (large-eddy simulation), and have validated their work for two different wind directions by comparison with wind tunnel measurements. Blocken *et al.* (2008) have simplified the computational grid including only the BE building, and the simulations were performed with the Reynolds Stress Model (RSM) and with enhanced wall treatment. Lateb *et al.* (2010a) have considered a two-building configuration for two different scales, i.e. full scale (1:1) and wind tunnel scale (1:200), using two stack heights and two exhaust pollutant velocities for each scale.

4.3 Problem description

As introduced in the previous section, this study refers to the same site, and uses the same mathematical and numerical models as those used in Lateb *et al.* (2010a). In the following sections, general information is given concerning the computational domain and governing equations.

4.3.1 Geometric model

The geometry considered in this study is comprised of two in line buildings (referred to as the BE building and the Faubourg tower), both located in an urban zone in downtown Montreal. Fig. 4.1 shows the site configuration alone with the dimensions of the two structures. The wind arrives perpendicular to the Faubourg tower from the south-west and places the BE building in its wake. For the BE building, only the three most prominent rooftop structures have been taken into account; an entry located on the windward wall and a one-metre-high parapet running along the roof perimeter have been omitted. It is worth noting that the leeward wall of the Faubourg tower takes the form of a horizontal staircase. Consequently, the spacing between the two buildings increases by 4 metres from the south-east to the north-west ends.

4.3.2 Computational domain

Calculations were carried out on a hexahedral grid in all parts of the domain composed of $187 \times 126 \times 102$ cells. The grid was fairly coarse near the boundaries of the domain, with cells concentrated near the stack and the building walls, as can be seen in Figs. 4.2 and 4.3.

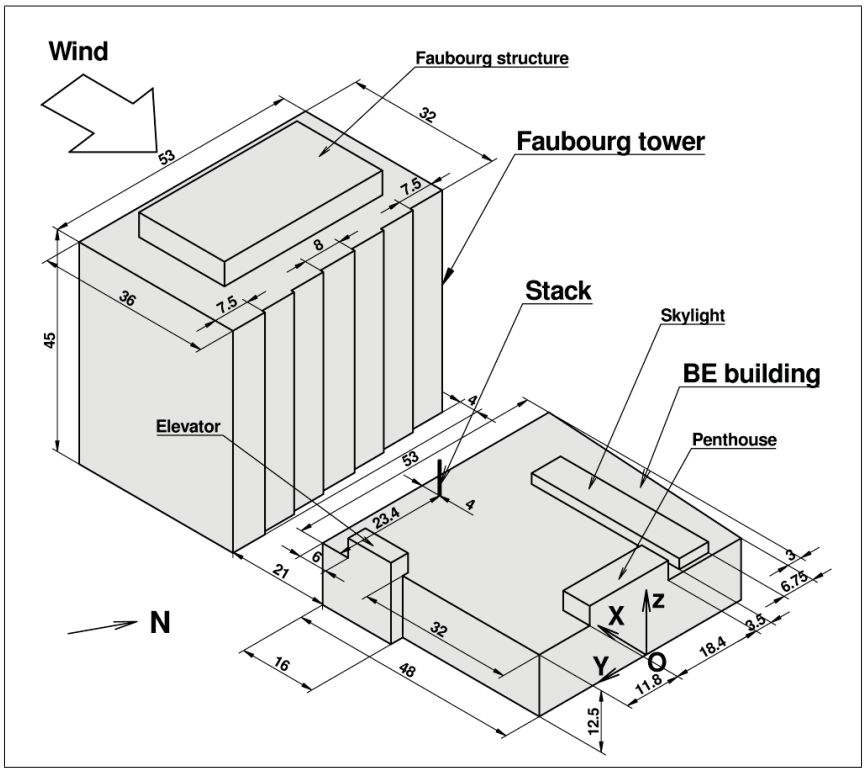

Figure 4.1 General view of the two buildings, their structures and their full-scale dimensions. All dimensions in [m].

The top of the domain is located $5H_{Fb}$ from the top of the Faubourg tower and the lateral boundaries are $4.5H_{Fb}$ distant from each building. A symmetry condition is imposed for all (i.e. top and lateral) sides of the domain. This condition implies that there is zero normal velocity and zero normal gradients for all variables on these planes. The domain entry is at a distance of $6.5H_{Fb}$ upstream of the Faubourg tower, and a velocity inlet is imposed as boundary condition. The profiles of velocity and turbulence properties, i.e. turbulent kinetic energy k and turbulent rate dissipation ϵ, are specified and listed in Table 4.1. The error related to horizontal inhomogeneity is evaluated by performing a simulation in an empty computational domain using a specified wall shear stress, at the bottom of the grid, as suggested by Blocken *et al.* (2007) and the results obtained are comparable to that work. The domain exit located at $11H_{Fb}$ downstream of the BE building has an outflow boundary condition. This means that the flow is assumed to be fully developed and there is no diffusion flux for any of the flow variables. An error analysis of the grid refinement was performed on three computational grids, i.e. 1.59, 1.99

and 2.29 million cells, following the recommendations of Celik *et al.* (2008). As the average relative error of concentrations K obtained for two successive refined grids was found to be less than 2%, the grid of 2.29 million cells was used for the remainder of the study. Note that the grid configuration shown in in Fig. 4.3 was created using the software Gambit 2.4.6 with a skewness angle less than 0.42 for all hexahedral cells. For near-wall modelling, the enhanced wall function is used; the grid distribution has been controlled by clustering the mesh towards the walls in such a way that this near-wall treatment can be applied. The obtained Y^+ values for near-wall cells are in the range of 2 to 5. A no-slip condition is used at all walls of the buildings with zero heat flux.

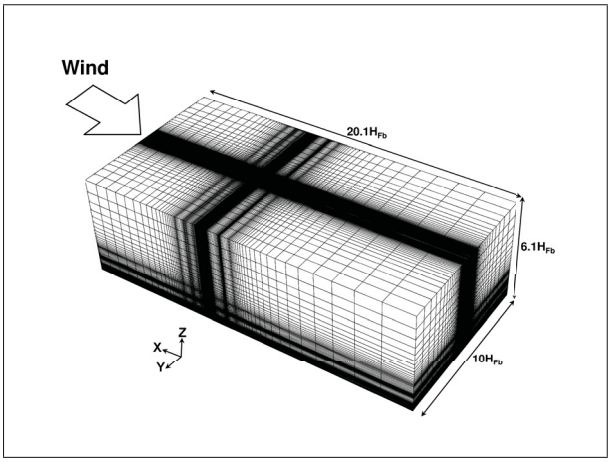

Figure 4.2 Dimensions of the grid.

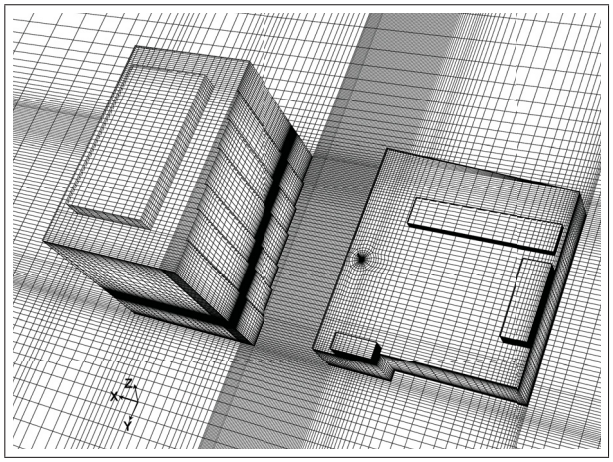

Figure 4.3 General view of the two buildings.

The wind within the simulated domain can be regarded as an incompressible, turbulent, inert flow. Air and pollutant densities are assumed to be constant and equal. According to Sini *et al.* (1996), this assumption holds for most environmental applications in the lower atmosphere. Stack discharge was considered to be a neutrally buoyant, passive gas without thermal effects. Table 4.1 shows a summary of the test cases for various stack heights. The first case, i.e. the case using $h_s = 1$ m and $M = 2.2$, was reproduced without the Faubourg tower upstream of the BE building. The parameters h_s and M represent stack height and momentum ratio, respectively, and TI_s is the pollutant turbulence intensity at stack exit.

Table 4.1 Summary of simulation test cases.

Stack height $200h_s$ [m]	Momentum ratio M $(= w_e/U_H)$	Exhaust velocity w_e [m/s]	Turbulent intensity TI_s [%]	Profiles at the entry of the domain			
				Profile $U(z)$	Profile $k(z)$	Profile $\epsilon(z)$	Profile $TI(z)$
1	2.2	13.88	6.20				
	5	31.55	5.60				
3	2.2	13.88	6.20				
	4.5	28.40	5.70				
	5	31.55	5.60	$14.5\times z^{0.3}$	$1.25/z^{0.4}$	$2.17/z$	$0.063/z^{0.5}$
4	2.2	13.88	6.20				
	5	31.55	5.60				
7.2	2.2	13.88	6.20				
	5	31.55	5.60				

4.3.3 Governing equations and turbulence model

The equations governing the flow field consist of the continuity and Reynolds-averaged Navier–Stokes equations which are an adequate representation of the wind tunnel's reality for a comparison with a wind tunnel experiments according to Franke *et al.* (2007). The realizable $k-\epsilon$ turbulence model was used, following the work of Wang (2006), to close the system, which requires the solution of two supplementary transport equations: one for k (turbulence kinetic energy) and another for ϵ (turbulence dissipation rate). The dispersion equation is given by the convection-diffusion equation for species transport. Full-model details are available in Lateb *et al.* (2010a).

Since the wind tunnel concentration measurements are provided in non-dimensional form, all calculated concentrations were normalized by:

$$K = \frac{4CU_H H_{BE}^2 10^{-6}}{\pi d_s^2 w_e} \tag{4.1}$$

where C is the mean pollutant concentration [ppb], U_H is the mean wind velocity at the roof height of the BE building [m s^{-1}]; H_{BE} is the BE building height [m]; d_s is the stack diameter [m], and w_e is the pollutant exhaust velocity from the stack [m s^{-1}]. Note that the pollutant source concentration, C_e, is equal to 1.

4.4 Model validation

The experimental data used to validate the numerical simulations were obtained from a detailed wind tunnel study by Stathopoulos *et al.* (2004). The surroundings were modelled up to points as far as 250 m upwind; buildings within 50 m were included in the downwind direction. In this paper, the study is limited to the two buildings concerned, i.e. the BE building and the Faubourg tower, as shown previously in Fig. 4.1. As explained by Blocken and Stathopoulos (2008), the wind tunnel experiment provides concentrations from samplers located at different locations on the BE roof and leeward wall of the Faubourg tower. The sampler locations in the wind tunnel experiment are shown in Figs. 4.4 and 4.5. Most of the measured concentrations were obtained for stack heights of 1 m and 3 m. The only measurements obtained for higher h_s are those collected at samplers R_4, R_{17} and P_2 located along the stack axis on the BE roof and at samplers F_{B1}, F_{B2} and F_{B3} on the Faubourg leeward wall, using a momentum ratio, M, equal to 2.2. The following figures provide a detailed comparison between the wind tunnel experiments and simulation results.

Figs. 4.4a and 4.4b show the non-dimensional concentrations at samplers on the BE building roof and on the Faubourg tower leeward wall for a stack height of 1 m, at two different momentum ratios of 2.2 and 5, respectively. At the majority of the samplers, the experimental concentrations are underestimated for the smaller momentum ratio. K is overestimated only upwind of the BE building (R_4 and R_6) and in the south-east corner. For the higher momentum ratio ($M = 5$), the opposite tendency is noted, and K is underestimated at only a few of the samplers; this tendency is also shown upwind of the BE building. On the leeward wall of the Faubourg tower, K is underestimated at all samplers by around 40%. By increasing the pollutant velocity, the differences become less pronounced (about 15%) at sampler F_{B1}. An overestimation of under 2% is noticed at sampler F_{B3}, however.

For a stack height of 3 m, as indicated in Fig. 4.5, the results for the lower momentum ratio show an underprediction at samplers located on the BE roof centre region and the Faubourg tower leeward wall. Increasing the pollutant exhaust velocity produces an overestimation of K for the majority of samplers, except at sampler F_{B3}, where the underestimation persists.

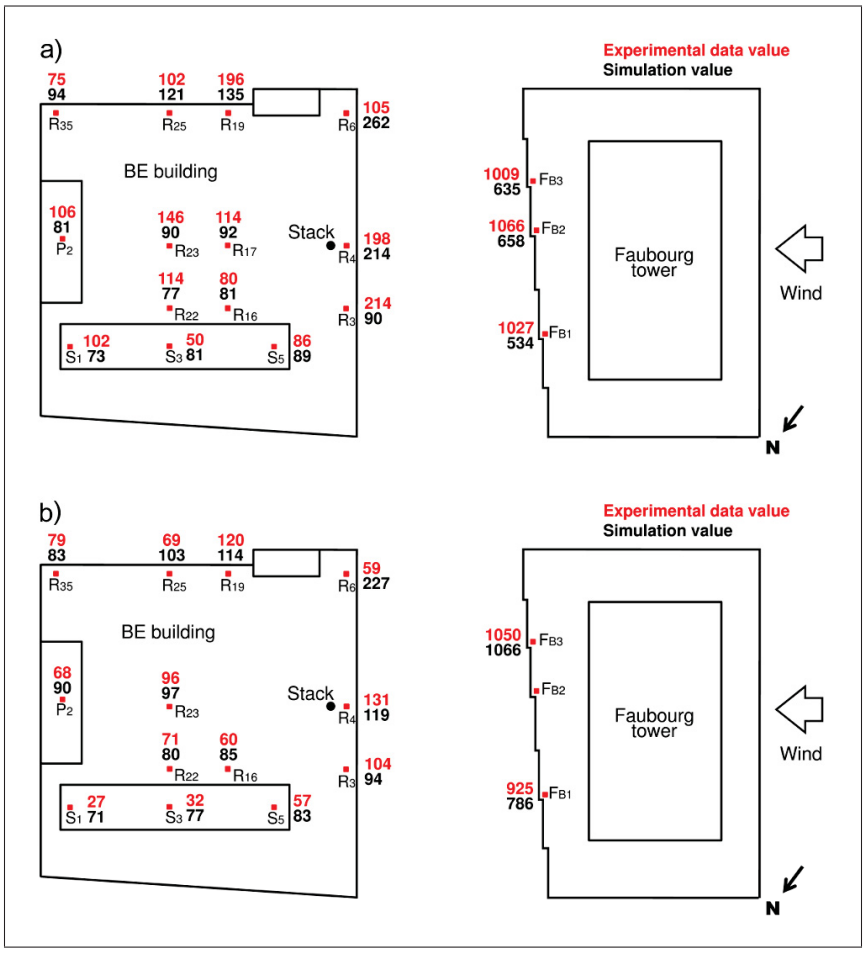

Figure 4.4 Simulation and wind tunnel values for K for stack height h_s of 1 m. For (a) $M = 2.2$ and (b) $M = 5$.

The differences between samplers F_{B1} and F_{B3} are probably due to the staircase form of the Faubourg leeward wall, which does not permit flow field symmetry between the buildings. At sampler R_4 near the stack and for both stack heights, a reduction in the difference between the wind tunnel and simulated values is noted with increasing pollutant velocity; for instance, the difference is smaller for the lower than for the higher stack height. However, K values at R_4 are identical for the higher momentum ratio, with $h_s = 3$ m.

Fig. 4.6 shows the scatter plots of the non-dimensional concentration K values for wind tunnel tests and CFD simulations for stack heights of 1 and 3 metres. The corresponding correlation coefficients, R, are 0.93 and 0.92, respectively. About 80% of the concentration values are positioned within a range of factor 2, as indicated by points situated between the dashed lines

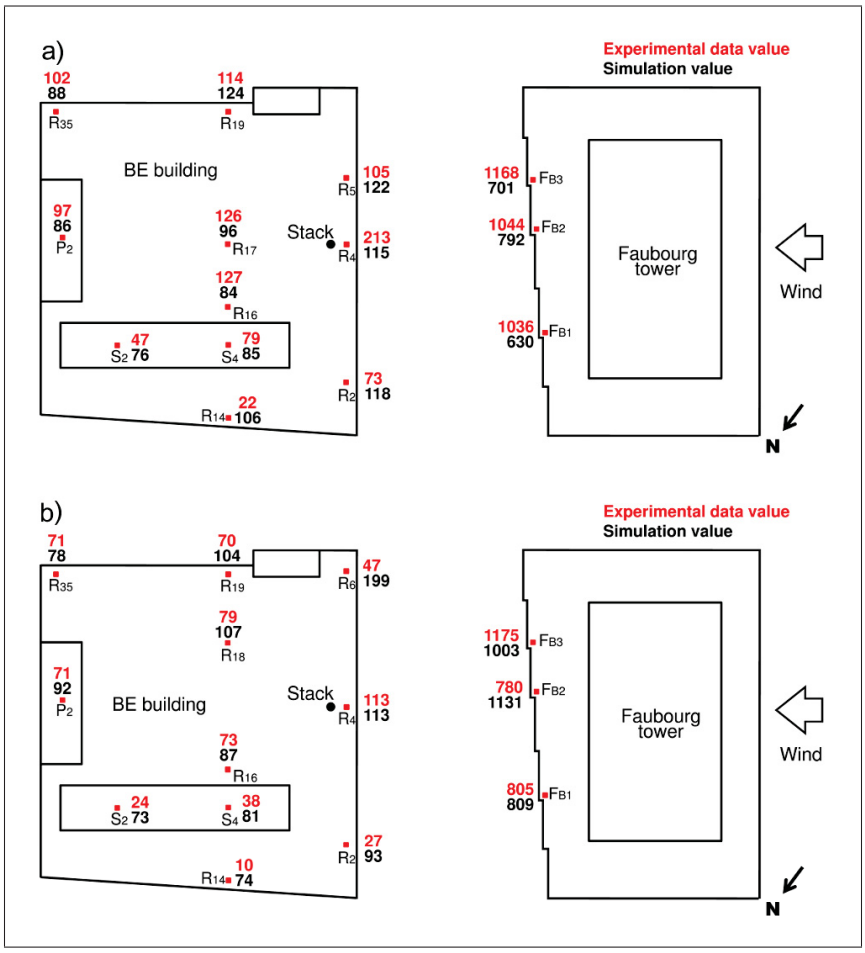

Figure 4.5 Simulation and wind tunnel values for K for stack height h_s of 3 m. For (a) $M = 2.2$ and (b) $M = 4.5$.

on each side of the median line. The averaged errors, e_a, for calculated and experimental values, are about 45% and 88% for stack heights of 1 m and 3 m, respectively.

Fig. 4.7 shows the distribution of K at samplers R_4, R_{17} and P_2 with increasing stack height for a momentum ratio of 2.2. For wind tunnel scale simulations, a small increase in K at all samplers is observed with increasing stack height. Only at sampler R_4 is there a clear decrease in K between 1 and 3 metres of stack height. For stack heights between 3 and 5 metres, however, this phenomenon is observed at all three samplers in the wind tunnel experiments. This may be explained by the fact that the pollutant plume reaches levels above the roof, where recirculation is present. The strong dilution recorded, which halves the concentration value,

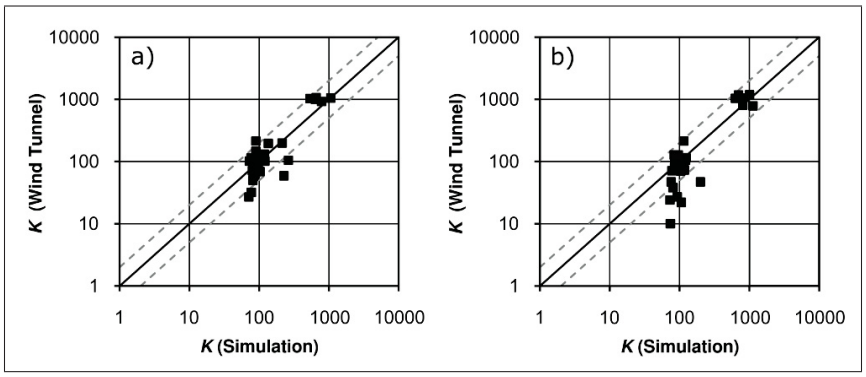

Figure 4.6 Scatter plots of simulation and wind tunnel K data for stack heights of (a) $h_s = 1$ m and (b) $h_s = 3$ m.

is observed at lower heights in the simulation results than in the wind tunnel experiments. The recirculating flow in the tower wake, particularly above the central roof portion of the BE building, seems to be situated at a lower level in the numerical simulations than in the wind tunnel experiments. Beyond this critical stack height (between 1 and 3 metres), concentrations still increase in the numerical simulations at all samplers, while they are observed to decrease slightly in wind tunnel experiments. However, the concentrations are still overestimated at samplers R_{17} and P_2 which are located far away downstream from the stack. At sampler R_4 near the stack, results are comparable. These overestimations are expected, since the pollutant plume is continually being drawn by the recirculating flow to a lower level than in the wind tunnel experiments.

For the samplers located at higher levels on the tower leeward wall, i.e. F_{B1}, F_{B2} and F_{B3}, as shown in Fig. 4.8, the same abrupt decrease in concentration levels is observed between 3- and 5-metre stack heights in wind tunnel results. Conversely, the numerical model predicts a slight increase. The higher altitude of the recirculation zones above the BE roof in the wind tunnel, as compared to the simulation experiments, remains the best explanation for these observations. The plume exhausted from the stack is transported higher in the wind tunnel than in the simulation, even for the lowest stacks, as can be seen through the values obtained for stacks of 1 and 3 metres. In the case of the higher stacks, the wind tunnel concentrations increase for the south-east direction from the sampler F_{B1} to F_{B3}. This is expected, since the wider opening

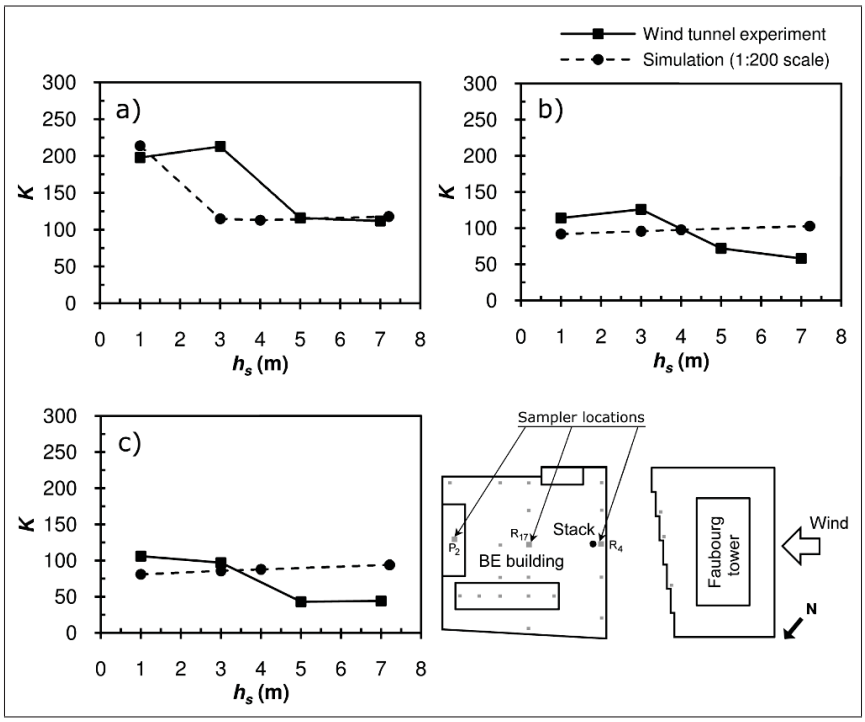

Figure 4.7 Measured and calculated concentrations K for $M = 2.2$ and various stack heights h_s, on the BE building roof at samplers (a) R_4, (b) R_{17} and (c) P_2.

at the lateral north-west side between the two buildings favours a strong stream dilution from that point, as compared to the opposite side. The concentration values in the simulation results remain comparable, in the case of higher stacks, between F_{B2} and F_{B3}. It is possible that even the lateral recirculation zones are poorly reproduced in the upper section, as previously found – see Lateb *et al.* (2010a).

The discrepancies found between CFD simulations and experimental results can be associated to limitations in the wind tunnel experiments or the numerical simulations. Since experimental tests were carried out respecting all the necessary criteria, as stated by Stathopoulos *et al.* (2004), and according to statements made by several authors (e.g. Blocken *et al.*, 2008; Tominaga and Stathopoulos, 2009, 2010; Lateb *et al.*, 2010b) concerning the capabilities of steady state RANS for unsteady flows, the most probable source of discrepancies seems to be related to the weakness of the steady state RANS approach. The differences observed in Fig. 4.8 suggest that steady state results in separated flow may be biased to high and/or low concentrations.

As mentioned by Blocken and Stathopoulos (2008), the flow pattern exhibits a strong degree of unsteadiness, while the separation and re-attachment points determined by the interaction of aerodynamic forces fluctuate with perturbations of the overall flow field. Since the wake is characterized by strong vortices shed from the tower leeward sides and roof, the steady state nature of a RANS approach remains the main suspected cause for poor resolution of the wake zone. Notwithstanding the above, the steady state model used in the present study provides comparable results with the wind tunnel experiments as can be seen through the scatter plots shown in Fig. 4.6.

4.5 Results and discussion

In this section, results are presented mainly in the form of non-dimensional iso-concentration contours obtained using numerical simulations for various cases studied on the roof and windward wall of the BE building, as well as on the Faubourg tower leeward wall. Concentrations on the BE building lateral walls are also assessed to obtain the best air intake locations for the BE building, in order to prevent exhausted pollutant from recycling. One case with a stack height of 1 m and a momentum ratio of 2.2 was studied without taking the tower upstream of the BE building into account; this was done to draw attention to the need to consider obstacles and buildings in the vicinity of the building of interest.

4.5.1 Concentrations on the BE building roof for various stack heights

Fig. 4.9 shows the non-dimensional iso-concentration contours on the BE building roof for various stack heights obtained using a momentum ratio of 2.2. Since the stack is located in the upstream part of the roof, the emitted plume is entirely swept along the upstream direction by the recirculation flow, particularly in the case of the lowest stack. Clearly, the most critical concentrations are observed for lower stack heights in that area of the roof. The concentrations become less significant further from the upstream edge: low concentrations are recorded further away, downstream of the roof. The iso-concentration contours are oblique with respect to the upstream edge, with a decrease in their values from the upstream edge towards the downstream area of the roof.

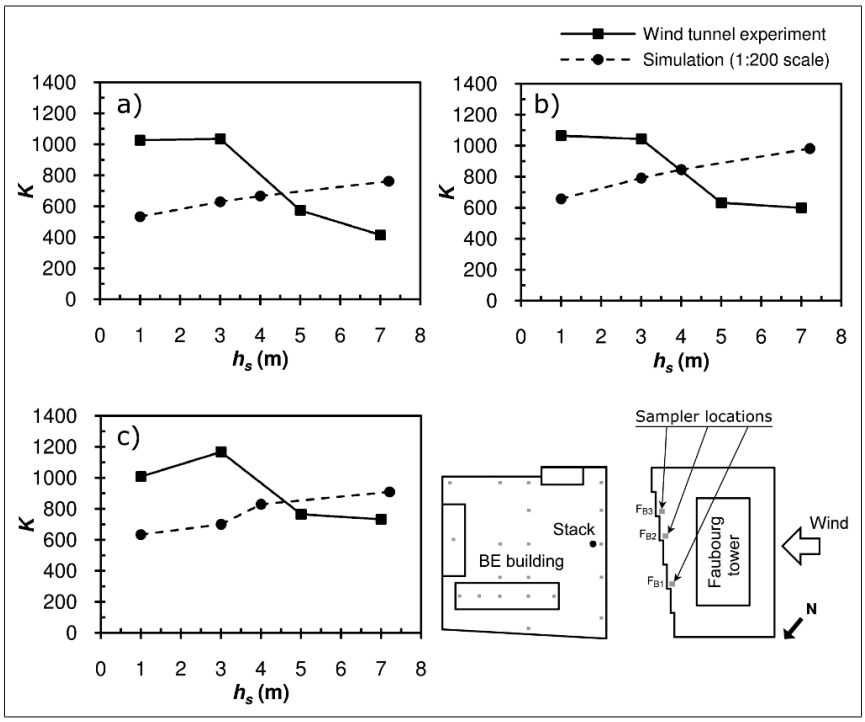

Figure 4.8 Measured and calculated concentrations K for $M = 2.2$ and various stack heights h_s, on the Faubourg tower leeward wall at samplers (a) F_{B1}, (b) F_{B2} and (c) F_{B3}.

Concentrations are higher along the upstream edge of the roof, with the strongest concentrations grouped at the extremities of that edge and in the direction upstream of the stack. On the roof, the iso-concentration contours appear arc-like, with peaks located in the upwind part of the penthouse structure. For $h_s = 1$ m and just upstream of the stack, the iso-concentration contours form half-circles, whose centres are located towards the upstream edge of the roof. The effect of stack height on the distribution of the iso-contours is such that the strongly concentrated pollutant zones, at the extremities of the upstream edge, gradually become diluted as stack height increases. The downstream regions of the roof remain at concentration levels that are comparable to levels observed at lower heights. For taller stacks, such as $h_s = 7.2$ m, the iso-concentration contours of the south-east part of the roof become curved in such a way as to form arcs with peaks directed towards the north-east, as shown in Fig. 4.9d.

Lastly, increasing the stack height significantly does not greatly change the concentration levels obtained over the roof, except in the upstream area. Indeed, the BE building roof is located

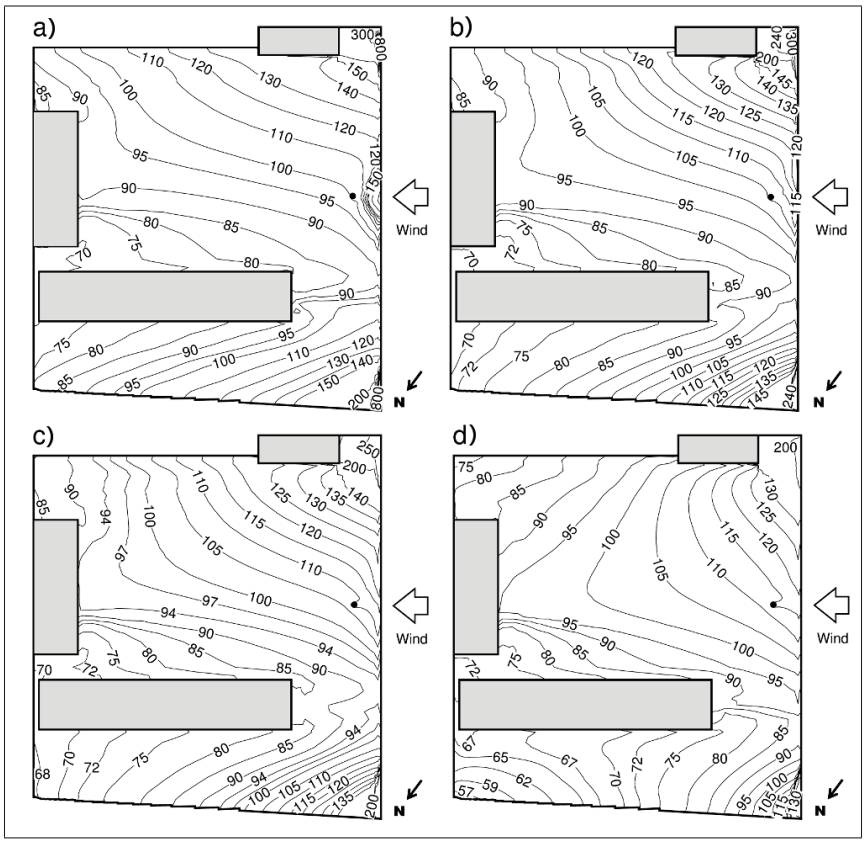

Figure 4.9 Simulation iso-concentration contours obtained on the roof of the BE building for various stack heights ($M = 2.2$), (a) $h_s = 1$ m, (b) $h_s = 3$ m, (c) $h_s = 4$ m and (d) $h_s = 7.2$ m.

entirely inside the wake region of the Faubourg tower, and K is smeared out uniformly on the roof, except at the upstream lateral sides, which are characterized by their particular forms (i.e. tilted and set back). The wind flow circumventing the tower modifies the distribution of K imposed by the wake of the upstream tower.

Fig. 4.10 shows the evolution of the iso-concentration contours for various stack heights when the momentum ratio is greater ($M = 5$). In these cases, the iso-concentration contours with half-circle form observed previously at the front of the stack on Fig. 4.9a do not exist, even for the lowest stack. The previous changes in the iso-concentration contour pattern observed on the south-east part of the roof for $h_s = 7.2$ m with $M = 2.2$, had already appeared for a stack height of 3 metres, as can be seen on Fig. 4.10b. Increasing the exhaust velocity has the same impact as does increasing stack height on the BE roof. Indeed, this is clearly illustrated when

the iso-concentration contour configurations of Figs. 4.9d and 4.10b are compared. These two figures correspond to the case where a stack height and an exhaust velocity increased by factors of 2.4 and 2.3, respectively, where $h_s = 3$ m and $M = 2.2$, as shown in Fig. 4.9b.

4.5.2 Concentrations on the BE building windward wall for various stack heights

As indicated in Fig. 4.11, the values for iso-concentration contours obtained on the windward wall of the BE building are higher than those observed on the BE roof. Most of the emitted pollutant is transported by the recirculation flow towards the region between the two buildings. This explains the strong concentrations displayed over the BE building windward wall. The iso-contours on this facade are arc-shaped and their peaks are flattened at the top level of the wall. The highest iso-concentration contours are clustered near the ground because the pollutant directed to this area is imprisoned by the vortices occurring there. The increase in stack height produces a displacement of these concentrated iso-contours towards the south-east direction, as shown in Figs. 4.11a to 4.11d.

For a low stack ($h_s = 1$ m) with a low momentum ratio ($M = 2.2$) as indicated in Fig. 4.11a, the higher iso-concentration contours are found below the stack. For the highest stack with the same momentum ratio, these contours move to the south-east part of the wall (the right side in this figure) as shown in Fig. 4.11d. For the larger momentum ratio ($M = 5$) shown in Fig. 4.12, the higher iso-concentration contours have already reached the south-east extremity of the wall with the low stack height ($h_s = 1$ m), as shown in Fig. 4.12a. These contours remain at the same location even for a taller stack ($h_s = 7.2$ m) as can be seen in Fig. 4.12d. It appears that the pollutant is trapped in that lower area between the two buildings. The lateral recirculation flow induced by the wind circumventing the upstream tower by the south-east side prevents the higher iso-concentration contour displacement from leaving the area between the two buildings.

The pollutant displacement observed on the windward wall of the BE building at $M = 2.2$ is probably due to the lack of symmetrical shape in the region between the two buildings caused by the "staircase" form of the tower leeward wall (see Fig. 4.4). Indeed, the particular form

of the leeward wall offers favourable access for the lateral wind flow from the north-west side because of its wider opening as compared to the south-east side. The lower region between the two buildings is continuously fed by a strong wind flow from the north-west: thus the pollutant is transported to the opposite side.

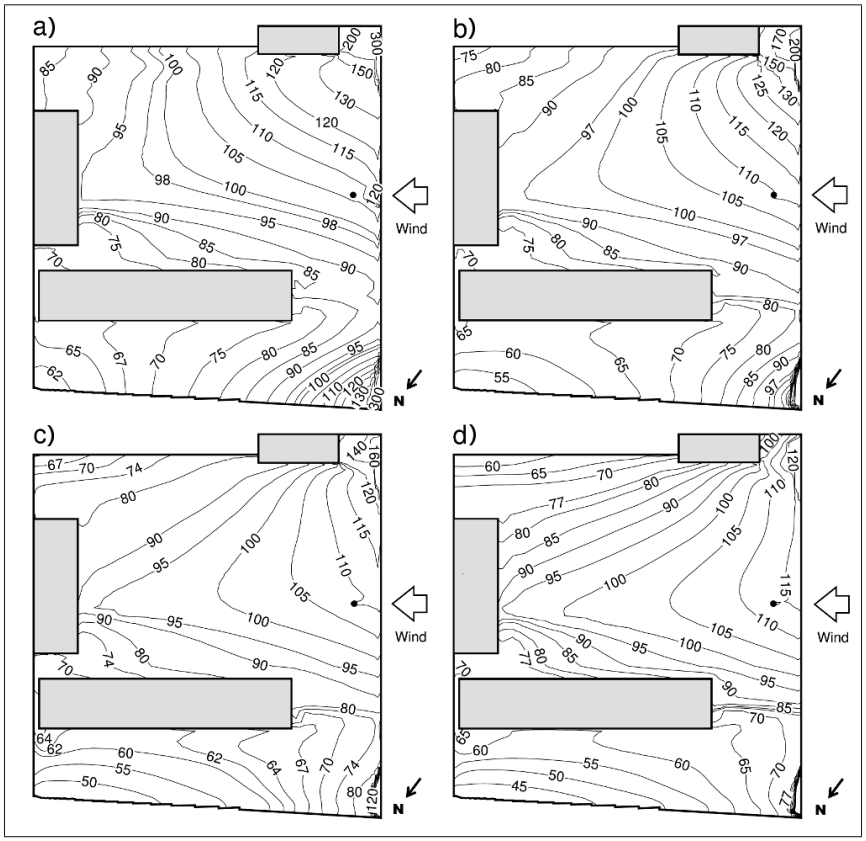

Figure 4.10 Simulation iso-concentration contours obtained on the roof of the BE building for various stack heights ($M = 5$), (a) $h_s = 1$ m, (b) $h_s = 3$ m, (c) $h_s = 4$ m and (d) $h_s = 7.2$ m.

Using the case with $h_s = 3$ m and $M = 2.2$ illustrated in Fig. 4.11b as a reference, increasing either the stack height by a factor of 2.4 (see Fig. 4.11d) or the momentum ratio by a factor of 2.3 (see Fig. 4.12b) reveals striking similarities in iso-concentration contour trends. The highest iso-concentration contour value is approximately 720 when stack height is increased (i.e. the reduction in highest K value is about 56% with respect to the reference case), whereas increasing the pollutant exhaust velocity provides a top iso-concentration contour value about

of 668 (i.e. the reduction in highest K value is about 59% with respect to the reference case). It appears that increasing the height by a factor of 2.4 would be approximately equivalent to doubling the pollutant exhaust velocity on the BE building windward wall for the reference case ($h_s = 3$ m and $M = 2.2$).

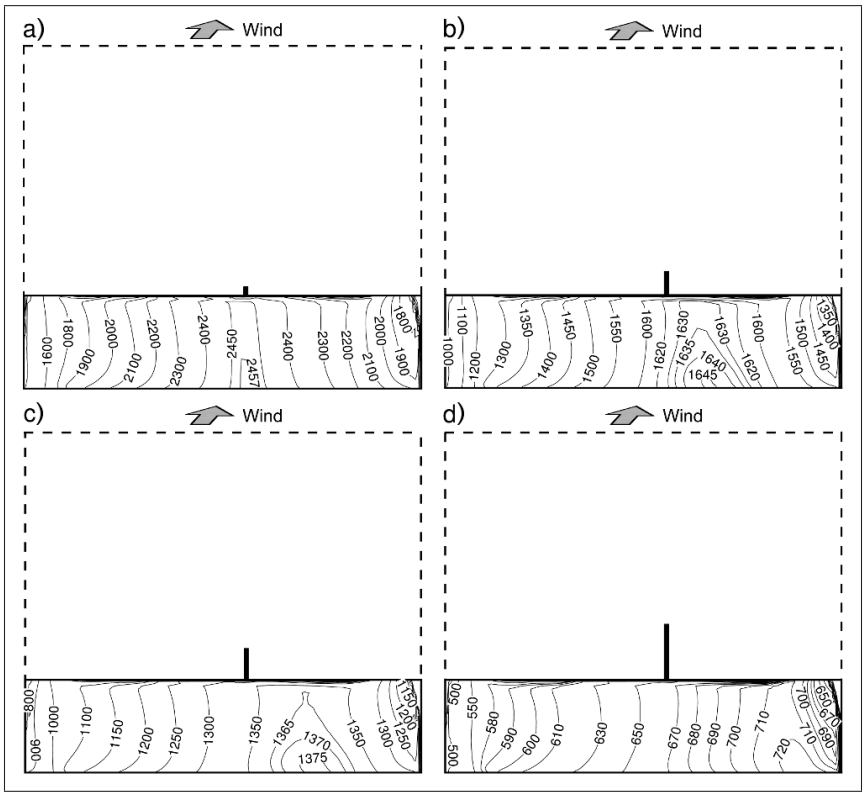

Figure 4.11 Simulation iso-concentration contours obtained on the windward wall of the BE building for various stack heights ($M = 2.2$), (a) $h_s = 1$ m, (b) $h_s = 3$ m, (c) $h_s = 4$ m and (d) $h_s = 7.2$ m.

4.5.3 Concentrations on the Faubourg tower leeward wall for various stack heights

Figs. 4.13 and 4.14 show the non-dimensional iso-concentration contours for various stack heights on the tower leeward wall, for momentum ratio values of 2.2 and 5, respectively. For the lower stack ($h_s = 1$ m) and lower momentum ratio ($M = 2.2$), the iso-contours display arc-like shapes. The highest iso-concentration contour is near the ground, located close to the vertical axis of the stack, as shown in Fig. 4.13a. The other iso-concentration contours

are smeared out around the iso-contour displaying the highest concentration. The contours concentration values decrease gradually as one moves away from the highest iso-concentration contour towards the upper section and sides of the wall. The peaks appearing on the contours may be attributed to the staircase form of the wall.

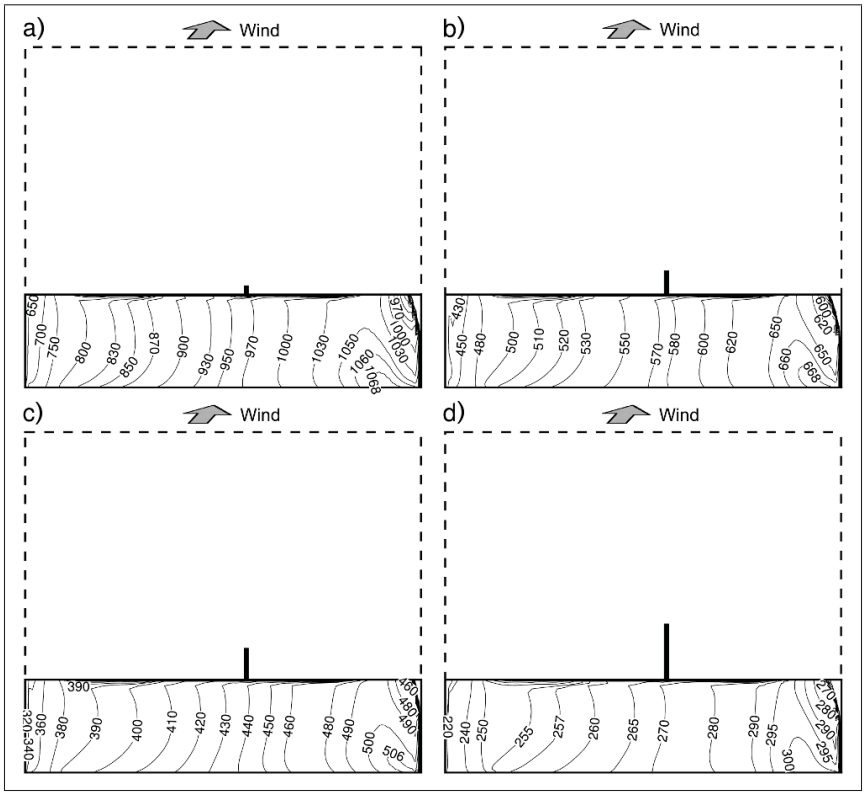

Figure 4.12 Simulation iso-concentration contours obtained on the windward wall of the BE building for various stack heights ($M = 5$), (a) $h_s = 1$ m, (b) $h_s = 3$ m, (c) $h_s = 4$ m and (d) $h_s = 7.2$ m.

The effects of increasing stack height are such that the highest iso-concentration contour decreases in value and moves upwards on the tower leeward wall. This vertical elevation is very likely due to the staircase form of the wall, which prevents displacement towards the south-east part, despite the wide opening on the north-west side between the two buildings. During its elevation, the highest iso-concentration contour remains at the same horizontal position while horizontal displacement was previously observed on the BE building windward

wall (see Fig. 4.11). For an increase of the stack height from 1 to 7.2 metres, a decrease in the highest iso-concentration contour value from 2200 to 1250 is noted as shown in Figs. 4.13a and 4.13d, respectively (i.e. the reduction in highest K value is about 43%).

For a significant momentum ratio ($M = 5$), similar observations are noted as shown in Fig. 4.14 (i.e. the elevation of the iso-contour displaying the highest concentration along the wall and a decrease in its value as stack height increases). For this momentum ratio ($M = 5$) and for a stack height of 4 metres and higher, the arc-like forms of the iso-concentration contours start to be inversed and become oriented towards the top of the tower leeward wall, as shown in Figs. 4.14c and 4.14d. For the stack height of 1 metre, the highest iso-concentration contour is located at the mid-height on the wall, as indicated in Fig. 4.14a, whereas as stack height increases to 7.2 m, the uppermost iso-contour reaches the upper region of the wall.

When stack height increases by a factor of 2.4, or when the momentum ratio is doubled with respect to the reference case of $h_s = 3$ m and $M = 2.2$, the behaviour noted previously on the BE building windward wall is also valid for the Faubourg tower leeward wall. Contour trend similarities are clearly shown in Figs. 4.13d and 4.14b. Increasing stack height by a factor of 2.4 induces a reduction in highest K value of 30% at the Faubourg tower leeward wall, while increasing the pollutant exhaust velocity by a factor of 2.3 results in a reduction of only 8%.

4.5.4 Concentrations on the BE building lateral walls for various stack heights

The evolution of the non-dimensional concentration K along the x direction of both the south-east and north-west lateral side walls of the BE building are shown in Figs. 4.15a and 4.15b, respectively, for various stack heights and two momentum ratios ($M = 2.2$ and 5). The curves show the distribution of K on the wall at a height of 3/4H_{BE} from the ground. This height was selected because here the air intakes are generally located at a rather high elevation from the ground, as recommended by ASHRAE (2007), to remain clear of wind-blown dust, debris and vehicle exhaust.

As shown in Figs. 4.15a and 4.15b, the strong concentrations are located in the upstream part of the BE building two lateral walls for all stack heights and both momentum ratios. The highest

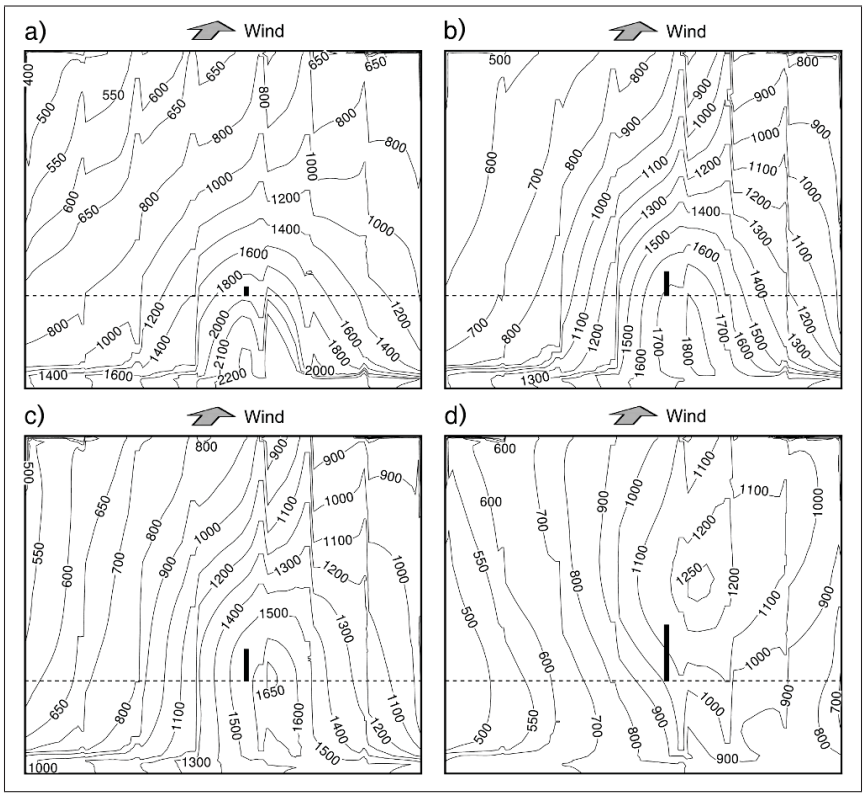

Figure 4.13 Simulation iso-concentration contours obtained on the leeward wall of the Faubourg tower for various stack heights ($M = 2.2$), (a) $h_s = 1$ m, (b) $h_s = 3$ m, (c) $h_s = 4$ m and (d) $h_s = 7.2$ m.

pollutant concentrations are recorded along the two sides for the lowest stack ($h_s = 1$ m) and for the lower momentum ratio ($M = 2.2$). Small K values are observed for the highest values of both h_s and M.

The evolution of K on the south-east lateral wall for $h_s = 7.2$ m and $M = 2.2$, shown in Fig. 4.15a, has similar behaviour to that obtained when increasing the momentum ratio by a factor of 2.3 ($M = 5$) and reducing stack height by a factor of 2.4 ($h_s = 3$ m). However, considering the north-west lateral wall (Fig. 4.15b), the stack height should be reduced by a factor slightly above 2.4 in order to obtain the same evolution when increasing the pollutant exhaust velocity by a factor of 2.3. In other words, the connecting factor between stack height and pollutant exhaust velocity must be selected with care and should take into account the surface of interest if one wishes to obtain absolute similarity between these two parameters.

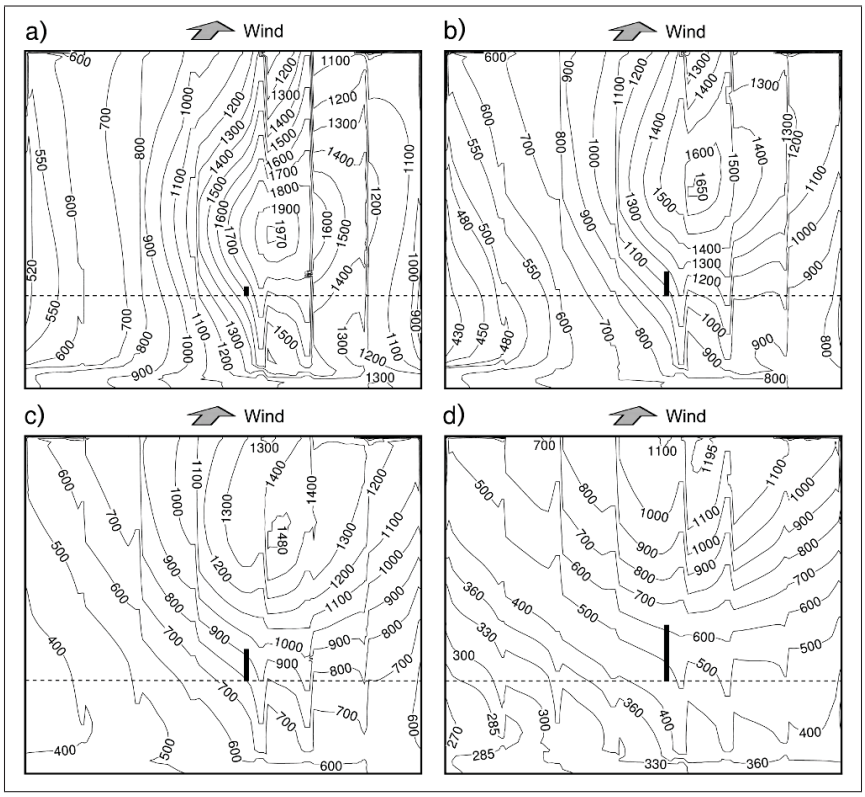

Figure 4.14 Simulation iso-concentration contours obtained on the leeward wall of the Faubourg tower for various stack heights ($M = 5$), (a) $h_s = 1$ m, (b) $h_s = 3$ m, (c) $h_s = 4$ m and (d) $h_s = 7.2$ m.

Lastly, if the circumstances impose air intakes on the BE building lateral sides, these should be located to the rear of each lateral side.

4.5.5 Concentrations around the hypothetically isolated BE building without the upstream Faubourg tower

This section sets out the case while intentionally excluding the Faubourg tower upstream of the BE building. The parameters considered are $h_s = 1$ m and $M = 2.2$. Figs. 4.16a and 4.16b show the computed non-dimensional iso-concentration contours on the roof and the windward wall of the BE building, respectively. The iso-concentration contours obtained without taking the upstream tower into account are completely different from those presented previously when including the presence of the tower.

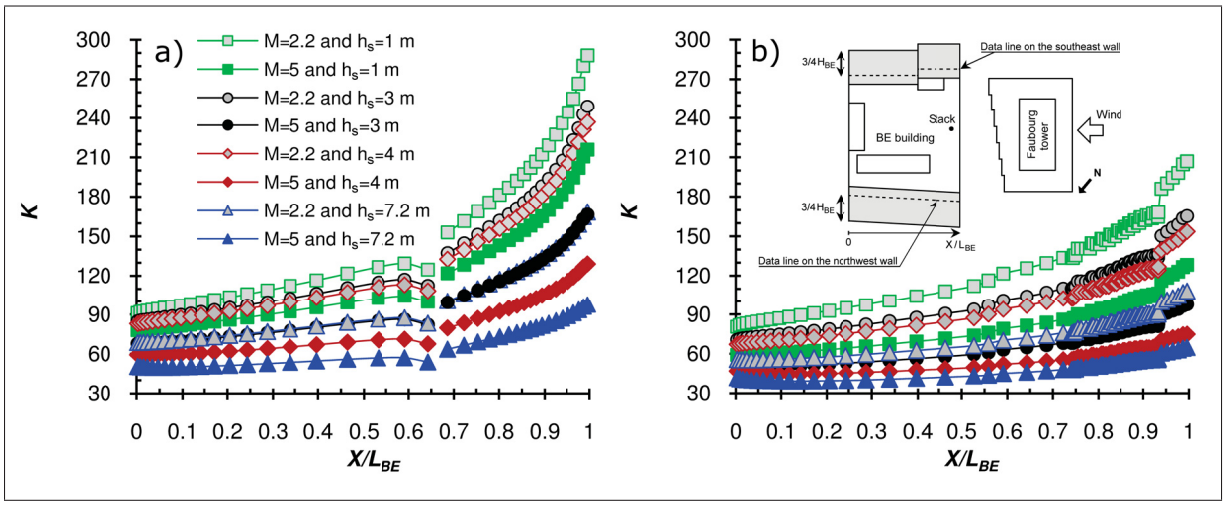

Figure 4.15 Simulation K profiles at 3/4H_{BE} height from the ground for various h_s and M on the (a) lateral south-east wall and (b) lateral north-west wall of the BE building.

Iso-concentration contour values are negligible on the BE building windward wall and much greater on the central part of the roof. Given the well-known (i) features of the wind pattern around an isolated building with a perpendicular wind to its windward facade, as described by ASHRAE (2009), and (ii) the dispersion evolution of roof stack pollutant emitted from the upwind part of a roof, as summarized by Blocken and Stathopoulos (2008), the vortices of the recirculation zone occurring at the upstream edge of the roof serve to trap the pollutant and increase the concentration values in this region, as indicated in Fig. 4.16a. However, far downstream, although the concentration values decrease in the central region, they remain significant.

At the lateral parts of the roof, concentrations are diluted by the wind flow circumventing the building, and this greatly lowers iso-concentration contour values. Locations that remain better adapted for fresh-air intakes are: the building windward wall, where concentrations are otherwise close to zero; or the lateral side walls, where the values are very low. Since most of the pollutant is led to the wake region, it is obvious that the building leeward wall must be avoided as a location for fresh-air intakes.

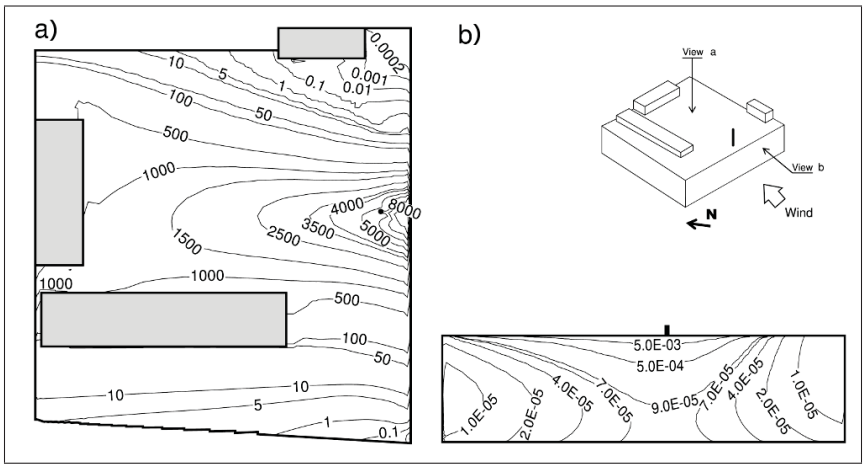

Figure 4.16 Simulation iso-concentration contours obtained without taking the Faubourg tower upstream into account, for $h_s = 1$ m and $M = 2.2$, (a) on the BE building roof and (b) on the BE building windward wall.

4.6 Conclusions

This paper has investigated the dispersion of a pollutant emitted from a roof stack in the wake of a tower, in a two-building configuration. It was carried out at wind tunnel scale (1:200) by numerical simulation (CFD) with the realizable $k - \epsilon$ turbulence model. This study examines the effect of stack height and pollutant exhaust velocity on the distribution of pollutant concentration on the emitting building walls as well as on the leeward wall of the tower, to determine the best locations for fresh-air intakes for the building. As a result of this study, conclusions for the configuration examined can be summarized as follows:

- Neglecting the impact of the Faubourg tower in the upstream of the building of interest leads to considerable errors in pollutant dispersion patterns. Clearly, omitting the upwind tower can lead to major design errors regarding the location of fresh-air intakes. For example, the presence of the tower induces a decrease in concentration values of about 95% on the emitting building roof centre.

- Increasing the stack height has an effect that is similar to increasing the pollutant exhaust velocity and the nature of this effect depends upon the wall of the building under consideration.

An example for the cases presented: a stack height of 3 metres with a momentum ratio of 2.2 will display approximately the same iso-concentration contour configuration on the emitting building roof when stack height and momentum ratio are increased by factors higher than 2.

- On the emitting building windward wall and the upstream tower leeward wall, distribution of the iso-concentration contours remains the same for the example quoted above ($h_s = 3$ m and $M = 2.2$) when increasing the two parameters h_s and M by factors higher than 2. However, the reduction in highest iso-concentration contour value obtained on the tower leeward wall is 22% less when increasing momentum ratio than when increasing stack height. On the emitting building windward wall, the opposite tendency is observed: increasing momentum ratio provides 3.2% higher value for the highest iso-concentration contour than does increasing stack height. Given this difference, it would be worthwhile to study which parameter should be modified in order to reduce pollution in certain places. However, the uncertainty of the concentration in the wind tunnel tests is about 5%, as mentioned by Stathopoulos *et al.* (2004).

- Varying these two parameters does not sufficiently alter the concentration displayed on the emitting building leeward wall. Their values remain the lower concentrations recorded on these building walls; this does appear to be the best location for the fresh-air intakes, however. On the other hand, for the upstream tower, fresh-air intake locations should not be placed on the leeward wall because of the high pollutant concentrations recorded there.

CHAPTER 5

SIMULATION OF NEAR-FIELD DISPERSION OF POLLUTANTS USING DETACHED-EDDY SIMULATION

Mohamed Lateb[1], Christian Masson[1], Ted Stathopoulos[2] and Claude Bédard[1]

[1]Department of Mechanical Engineering, École de technologie supérieure,
1100 Notre-Dame West, Montreal, Qc, Canada H3C 1K3

[2]Department of Building, Civil and Environmental Engineering, Concordia University,
1455 de Maisonneuve Blvd. West, Montreal, Qc, Canada H3G 1M8

A preliminary version of this chapter was presented at the *12th Americas Conference on Wind Engineering* (12ACWE) – June 2013, Seattle, WA, USA – and the entire chapter is submitted to *Journal of Fluid Mechanics* and presently undergoing first revision.

Abstract

A numerical simulation is developed using the unsteady-state detached-eddy simulation (DES) turbulence model on a structured highly refined grid to predict the wind-flow field and dispersion field of a pollutant emitted from a roof stack around a two-building configuration. The results obtained are compared with those of a steady-state re-normalization group (RNG) $k-\epsilon$ turbulence model, previously reported by the authors, as well as wind tunnel experiments. The pollutant concentrations are examined on the roof where the stack is located as well as on the leeward wall of an upstream tower to the emitting building in order to evaluate how the pollutant is dispersed by the DES model compared to RNG model. DES results are discussed against those from RNG $k-\epsilon$ approach and wind tunnel. The study emphasizes limits in reproducing correctly the wind flow and dispersion fields due to underestimation and/or overestimation of the Reynolds stress components and the steady-state methodology when using the RNG $k-\epsilon$ model. Despite such limits, the RNG model produces a similar average error, in terms of concentrations, to that obtained with the DES model. However, the DES model demonstrates that

the unsteady-state approach is clearly better suited to understand the flow-field development and the dispersion process.

Keywords: Dispersion modelling, detached-eddy simulation (DES), rooftop stack emissions, RNG $k-\epsilon$ turbulence model, two-building configuration.

5.1 Introduction

Pollution in the atmospheric boundary layer (ABL) is an important environmental problem which affects human health. Investigations of pollutant transport and dispersion have received a lot of attention in recent years, and become a focal point in environmental research because of the increasing interest for protecting air quality (Assimakopoulos *et al.*, 2003). Besides, this subject is of great concern especially in the urban environment when the crucial issues of well-being and human comfort are considered.

Turbulent wind flows have long presented a considerable obstacle to the accuracy and applicability of calculations in industrial applications (Mockett and Thiele, 2007). The types of flows encountered in the field of wind engineering are no exception, and consist of many complex flow features which may contain recirculation zones and stagnation points (Easom, 2000). Indeed, in the lower atmospheric boundary layer, specifically in cities around individual and/or groups of buildings, the superposition and interaction of the flow patterns induced by buildings and structures strongly affect the dispersion and govern the movement of pollutants (Chang and Meroney, 2001). Therefore, complicated and highly unpredictable dispersion phenomena are created. Clearly, understanding the process of pollution dispersion and its mechanisms still remains a great challenge for wind engineering researchers. Nonetheless, the scientific community has significantly contributed to daily life quality by controlling and maintaining air quality in buildings and offices within the acceptable norms typically established and authorised by governments and/or professional organizations (Sterling, 1988).

Substantial research projects have been carried out and are available in the literature on the topic of pollutant dispersion. They have used a wide range of different methods (e.g. field tests, laboratory modelling, semi-empirical methods and numerical approaches) to evaluate

pollutant dispersion, identifying their advantages and disadvantages (Blocken *et al.*, 2011). During the past years, especially in urban environments, pollutant dispersion has been studied extensively by means of both experimental and numerical approaches. Field measurements (e.g. Schatzmann *et al.*, 2000; Morris *et al.*, 2007), wind tunnel testing (e.g. Brown and Bilger, 1996; Vincont *et al.*, 2000), semi-empirical methods (e.g. ASHRAE, 2007; Hajra and Stathopoulos, 2012) and numerical modelling (e.g. Kang and Meneveau, 2001; Coceal *et al.*, 2007; Brethouwer and Lindborg, 2009; Philips *et al.*, 2013) have been performed, on the one hand to get an insight into the physical pollution processes, and on the other hand, to obtain a better comprehension of the coupled mechanisms occurring around buildings and/or cluster of buildings. Among these methods, numerical modelling with computational fluid dynamics (CFD) appears as one of the most accessible and largely spread approach to study wind environmental problems because of the lower costs, the advantages and reliability of such approach. However, CFD simulations are not straightforward to perform and their results still require validation to establish extended acceptability (Campos-Arriaga, 2009). Therefore, the need of validating numerical studies makes the experimental tests necessary.

Notwithstanding the widespread use of CFD studies, the quality of results depends mainly on many physical and numerical parameters which can compromise accuracy and reliability. From that point of view, many authors and organizations have developed practice guidelines (e.g. EPA, 1978; Snyder, 1981; Meroney, 1987; AIAA, 1998; Oberkampf and Trucano, 2002; Franke *et al.*, 2007; Tominaga *et al.*, 2008; AIAA, 2010; Franke *et al.*, 2011) to establish a common methodology for verification and validation of CFD simulations in certain cases, and/or to assist and support the users in making a better implementation of CFD in other cases. According to Franke *et al.* (2011), there are basically two types of difficulties that can produce erroneous results in CFD, (i) modelling errors (e.g. turbulence models and physical boundary conditions) and (ii) numerical approximation errors (e.g. grid design, discretization scheme and iterative convergence).

Regarding turbulence modelling errors, various turbulence models (i.e. steady Reynolds-averaged Navier-Stokes (RANS), unsteady RANS (URANS), large-eddy simulation (LES) and hybrid

URANS/LES) reported in the literature are well known to the computational wind engineering (CWE) community, as they have been listed by many authors (e.g. Franke *et al.*, 2007; Blocken *et al.*, 2011). Several studies have investigated and assessed the performance of such different turbulence models to predict the flow field around buildings (e.g. Rodi, 1997; Wright and Easom, 2003). However all studies agree on the difficulty of some models and the differences between the various approaches to reproduce the complex and random character of the flow field. In addition, the dispersion field is closely related to the overall behaviour of the wind flow as stated by Tominaga and Stathopoulos (2009). Therefore, the choice of the turbulence model is revealed crucial to reproduce an accurate dispersion process, and, consequently, essential to understand the pollutant transport mechanisms.

The present study follows previous work of Lateb *et al.* (2013) where various RANS $k-\epsilon$ turbulence models were compared (i.e. standard $k-\epsilon$, re-normalized group $k-\epsilon$ and realizable $k-\epsilon$ referred to as SKE, RNG and RLZ throughout, respectively). Previous work suggested that the limitations in RANS models to reproduce the experimental results are probably due to an incorrect estimation of Reynolds stress components and the steady-state methodology of the tested models. Thus, the purpose of this study is to emphasize the effects of the unsteadiness and the Reynolds stress component anisotropy in reproducing the flow and dispersion fields compared to the RANS approach using Fluent software. Therefore, the use of an unsteady turbulence model is clearly essential. The detached-eddy simulation (DES) model has been selected for the present study because of the well established limitations of the two following models in resolving the internally induced fluctuations of flow and concentration fields (Salim, 2011), i.e. the high computational cost of LES and the low accuracy of URANS.

According to Franke *et al.* (2007), the DES model approach is the most widely known hybrid URANS/LES. To the knowledge of the authors, the DES model was initially proposed by Spalart *et al.* (1997) and mainly developed and improved by the aerospace community (e.g. Travin *et al.*, 1999; Spalart, 2001; Caruelle and Ducros, 2003; Squires, 2004; Spalart and Squires, 2004; Spalart *et al.*, 2006; Spalart, 2009; Deck, 2012). The approach however has been less reported in CWE applications (e.g. Hasama *et al.*, 2008; Bechmann and Sørensen,

2010; Haupt *et al.*, 2011), and even less in pollutant dispersion problems (Wang *et al.*, 2011). The DES model presents the advantage of having been implemented in a wide range of existing RANS models in commercial CFD codes (Bunge *et al.*, 2007). The aim of this hybrid URANS/LES model is to combine the most favourable aspects of the URANS and LES techniques (Squires, 2004). Indeed, DES treats the boundary layer regions as URANS model and can be adjusted to predict these regions and their separation well (Spalart, 2009), while the regions massively separated are predicted with LES. Otherwise, the DES concept allows (i) the eviction of an excessively refined grid near walls by modelling the isotropic small structures and thus resulting in considerable savings in terms of central processing unit (CPU) time, and (ii) the use of LES approach to resolve the large eddies and unsteady structures in the separated regions.

In this work, one case is considered because of the long time required by DES modelling. Regarding the objectives of this work cited above, the most critical case is selected, namely when the pollutant is emitted at high speed from the stack (i.e. $h_s = 1$ m and $M = 5$, where h_s is the stack height and M the momentum ratio which represents the ratio between the exhaust velocity of the pollutant w_e and the wind velocity U_H at the height of the BE building). Such case induces complex pollutant/flow-field interactions above the stack. Consequently, the capability of the DES model to reproduce the dispersion process is severely tested. It is worth noting that among the various RANS $k-\epsilon$ models tested by Lateb *et al.* (2013), the RNG $k-\epsilon$ approach showed the best results compared to wind tunnel experiments obtained by Stathopoulos *et al.* (2004) for the current case ($h_s = 1$ m and $M = 5$). DES results are thus compared with those from the RNG approach and wind tunnel experiments.

The paper is organized as follows. Section 2 summarizes the computational details including the DES concept, the grid generation, the boundary conditions and the solution strategy. Section 3 demonstrates the consistency of both constructed grid and statistical averaging period. The results are described and compared to those of the RNG $k-\epsilon$ model and experimental data in section 4. The analysis and discussion of results are presented in section 5. Finally, the main findings of the study are summarized in section 6.

5.2 Computational details

5.2.1 Detached-eddy simulation model

The strategy of DES model is such that switching from URANS to LES models is realised according to mesh definition and not to the local turbulent properties of the flow (Caruelle and Ducros, 2003). Thus the turbulent viscosity obtained depends on the local grid spacing, Δx_i, and the sub-grid scale (SGS) stresses are parameterized using a turbulent viscosity model. The RLZ turbulence model is selected to calculate the turbulent viscosity for both strategies (i.e. as URANS model in boundary layer regions and LES sub-grid scale model in massive separated regions) since the RLZ model is the only model available in Fluent among the various RANS $k-\epsilon$ models tested by Lateb *et al.* (2013).

In addition to the continuity and momentum equations, two others are added to estimate the turbulent viscosity, ν_t, at each cell. One equation for the turbulent kinetic energy, k, another for the turbulent dissipation rate, ϵ, and their expressions are as follows.

Transport equation of k:

$$\frac{\partial k}{\partial t} + u_j \frac{\partial k}{\partial x_j} = \frac{\partial}{\partial x_j}\left(\frac{\nu_t}{\sigma_k}\frac{\partial k}{\partial x_j}\right) + P_k - Y_k \tag{5.1}$$

where P_k is the production term due to the mean velocity gradient, Y_k the dissipation term which depends on the local spacing cell Δx_i, and the constant σ_k equal to 1.

Transport equation of ϵ:

$$\frac{\partial \epsilon}{\partial t} + u_j \frac{\partial \epsilon}{\partial x_j} = \frac{\partial}{\partial x_j}\left(\frac{\nu_t}{\sigma_\epsilon}\frac{\partial \epsilon}{\partial x_j}\right) + C_1 S\epsilon - C_2 \frac{\epsilon^2}{k+\sqrt{\nu\epsilon}} \tag{5.2}$$

where the constants are $\sigma_\epsilon = 1.2$ and $C_2 = 1.9$, and C_1 is expressed by $C_1 = \max[0.43, \eta/(\eta+5)]$ with $\eta = (k/\epsilon)S$ and S as the strain rate tensor.

The local turbulence parameters k and ϵ are related by the turbulent viscosity, ν_t, as follows:

$$\nu_t = C_\mu \frac{k^2}{\epsilon} \tag{5.3}$$

where C_μ expression writes as $C_\mu = 1/(4.04 + \frac{A_s k U^*}{\epsilon})$ with $A_s = \sqrt{6}\cos\phi$, $\phi = (1/3)\cos^{-1}\sqrt{6}W$, $W = S_{ij}S_{jk}S_{ki}/\check{S}^3$, $\check{S} = \sqrt{S_{ij}S_{ij}}$, $U^* = \sqrt{S_{ij}S_{ij} + \widetilde{\Omega}_{ij}\widetilde{\Omega}_{ij}}$, and $\widetilde{\Omega}_{ij} = \Omega_{ij} - 2\epsilon_{ij}\omega_k$.

The dissipation term, Y_k, appearing in the turbulent kinetic energy equation is expressed as:

$$Y_k = \frac{k^{3/2}}{l_{des}} \tag{5.4}$$

where $l_{des} = \min(l_{rke}, l_{les})$ with $l_{rke} = k^{3/2}/\epsilon$ and $l_{les} = C_{des}\Delta x_{i_{\max}}$. The additional constant of the calibration, C_{des}, is set to 0.61 as suggested in the case of homogeneous turbulence (Basu *et al.*, 2005), and $\Delta x_{i_{\max}} = \max(\Delta x, \Delta y, \Delta z)$ is the maximum local length of the cell in the three directions. Note that a constant C_{des} of 0.65, calibrated by means of isotropic turbulence (Shur *et al.*, 1999), is commonly used by the aerospace community (Fröhlich and von Terzi, 2008). While this value remains open to revisions, sometimes lower values are used presumably to compensate for numerical diffusion (Spalart, 2001). However, Bunge *et al.* (2007) recommend to calibrate the C_{des} constant for each RANS model to be used in DES.

The expression of l_{des} compares the turbulence length scale (l_{rke}) and the spacing cell (l_{les}). Near walls in the boundary layer regions, the turbulence length scale remains smaller than the spacing cells, ($l_{rke} \ll l_{les}$) due to the high dissipation occurring there, hence $l_{des} = l_{rke}$ and the regions are supported by the RLZ model which performs as an unsteady RANS model. The dissipation term, Y_k, in Eq. (5.4) becomes similar as for RANS simulations and equal to ϵ. In the regions far from the solid walls, where the flow is fully developed, the turbulence length scale becomes larger than the spacing cells, ($l_{rke} \gg l_{les}$), therefore $l_{des} = l_{les}$ and the RLZ model works as a sub-grid scale. Consequently, the DES approach provides a LES solution.

5.2.2 Grid generation

Since the present research is complementary to Lateb *et al.* (2013) work, the same site is used. Therefore, the reader can refer to that work for more details about the configuration and the dimensions of the two buildings. The main difference in the grid generation of these two studies is the grid refinement required by this unsteady three-dimensional approach particularly in the separated flow regions where the LES model is used. The "wall function" is used as near wall treatment for the present study since it is the only approach available when using DES model. Basically, there are two overlapping layers over walls: an inner layer where viscous processes dominate, and an outer layer far from these effects (Coceal *et al.*, 2007). The near wall treatment used bridges the viscosity-affected region between the wall and the fully turbulent region; therefore, on the one hand a substantial refinement of grid meshing is saved, and on the other hand the attached boundary layer regions are assured to be modelled by the URANS model.

The process of refining the grid deals with three criteria. The spacing cells, Δx_i, should (i) be fine enough near wall regions to capture the high gradients which occur within the turbulent boundary layer, and to reach the slope -5/3, associated with the range of frequencies in which the energy cascade is dominated by the inertial transfer, (ii) be smaller than the turbulence length scales, defined previously as $l_{rke} = k^{3/2}/\epsilon$, to make sure that the separated flow regions will be treated by the LES approach out of the turbulent boundary layer, and (iii) keep the spacing length perpendicular to each wall at least equal or larger than the two other spacing directions to eliminate the gray zone and thus avoiding a modelled-stress depletion (MSD) defined and noticed by Spalart *et al.* (2006).

Starting from the grid used in Lateb *et al.* (2013) and the results obtained with the steady RLZ model solution, Taylor microscale $l_\lambda = (10\nu k/\epsilon)^{1/2}$ is evaluated using the k and ϵ parameters in several planes along x, y and z directions (Liao and Cowen, 2010). Note that l_λ is always much smaller than l_{rke} (Tennekes and Lumley, 1972). As a grid refinement study was already conducted for that grid (see Lateb *et al.* (2010a)), the l_λ values evaluated remain approximately the same at each cell even with a further refined grid. Afterwards the smallest l_λ value found

is taken as a benchmark for the spacing grid near solid walls in the three directions, and the stretching ratio is kept equal to 1 in the entire regions near walls, above the BE building roof and between the two buildings to respect the criterion (iii). It is worth noting that the grid is composed by hexahedral cells, hence only one refining is required for each direction. The spacing cells in these regions is set under the turbulence length scale benchmark to make sure that, out of the boundary layer regions, the inequality $l_{rke} \gg l_{les}$ is respected so that the switch to LES approach can occur. Therefore, the criteria (i) and (ii) are taken into account. Elsewhere, far from the near walls and between the two buildings, the stretching ratio is extended to 1.1 to respect the commonly recommended value of 1.3 (Tominaga *et al.*, 2008). Finally, the grid obtained for the unsteady DES simulations is composed of about 11 million cells spread over $321 \times 177 \times 194$ cells in x, y and z directions, respectively. Fig. 5.1 shows the neighbourhood of the two buildings of concern as a general view of the highly refined new grid, and the various positions of the vertical and horizontal lines evoked in the following sections.

5.2.3 Boundary conditions

After the converged solution obtained on the new grid (i.e. 11 million of cells) using the steady-state RLZ $k - \epsilon$ turbulence model with the same boundary conditions as those used by Lateb *et al.* (2013), a spectral synthesizer method, based on the random flow generation technique originally proposed by Kraichnan (1970) and modified by Smirnov *et al.* (2001), is imposed at the domain inlet to generate fluctuating velocity components with a Fourier harmonics number set to 100. The number of 100 is considered as the minimum threshold of large numbers (Fung *et al.*, 1992), and it is desirable to use the minimum number of harmonics since large numbers increase the computational cost (Maple, 2002). The exit of the domain is referred as an outflow boundary condition, which assumes no velocity gradient in the exit direction, since the exit plane is sufficiently far from the two buildings wake region. Symmetry condition, which implies zero normal velocity and zero normal gradients for all variables, is used at the top of the domain. For the side boundaries, periodic conditions are imposed to capture correctly the vortex shedding which can occur on these planes. The equations are discretized in time by using a second-order fully implicit scheme, and then iteratively solved using the seg-

regated solver, for which the SIMPLE (Semi-Implicit Method for Pressure-Linked Equations) algorithm (Patankar and Spalding, 1972) is used to derive the pressure-correction equations. The convection terms are discretized using a second-order upwind scheme, whereas for the momentum equations a second-order central difference scheme is used. All walls of the two buildings are assumed to be smooth by using no-slip condition.

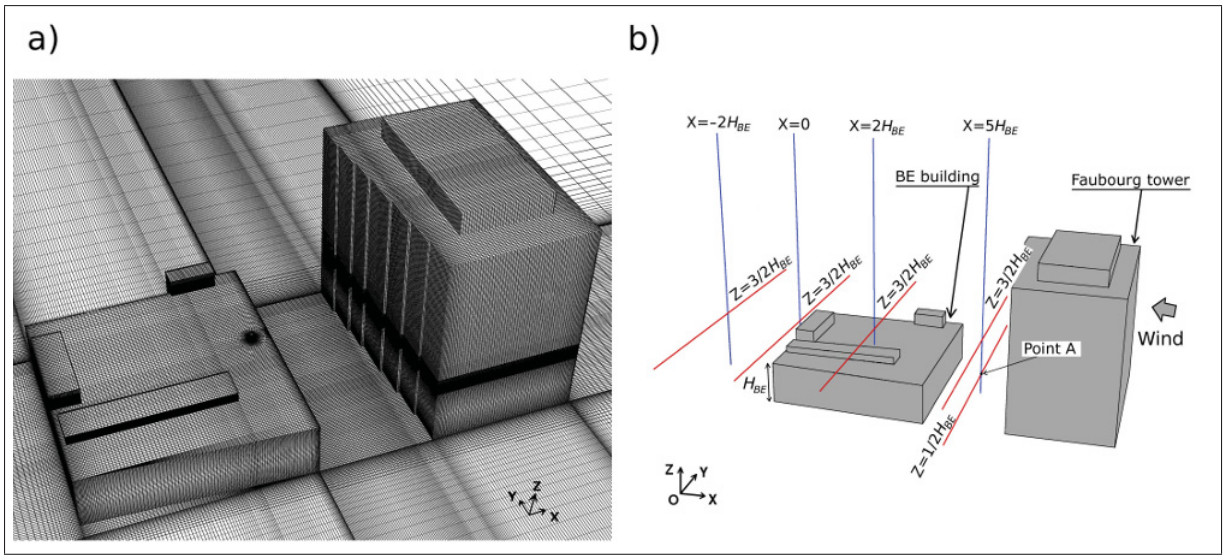

Figure 5.1 The two-building configuration showing (a) the highly refined meshing and (b) various positions of horizontal and vertical lines evoked in the present study.

5.2.4 Solution strategy

Primary circulation is carried out to reach the establishment of the flow field to remove the influence of the initial conditions before averaging to get statistically-steady values. Time scale of these first simulations is evaluated by the residence time of a single particle crossing through the whole computational domain. This time scale, noted t, is of the order of $(20.1H_{Fb}+10H_{Fb})/U_H$, and represents the streamwise length of the computational domain, $20.1H_{Fb}$, extended by its spanwise length, $10H_{Fb}$, to take into account the fluctuations and the deviations underwent by a particle during its residence time in the domain, divided by the particle velocity, U_H, estimated at the BE building height. The calculated time, t, results in a value of about 1 second.

The time step, Δt, is chosen by consideration of the Courant-Friedrichs-Lewy (CFL) number (Courant *et al.*, 1967) which assures the balance of the temporal and spatial scales when it is kept around 1 (Liu *et al.*, 2010b). The expression used for the time step estimation is $\Delta t = \mathrm{CFL}(\Delta x_{i_{\min}}/U_H)$ where $\Delta x_{i_{\min}}$ is the minimum grid spacing of the smallest cell in the domain. In physical sense, the time step represents the necessary time for a particle to cross the smallest cell of the domain. In other words, the time step should be able to capture correctly any particle and its fluctuations passing any cell through the domain regardless of the cell size. It is worth noting that a small time step is recommended for the accuracy of the results (Spalart, 2001). For a possible approach of CFL concept (i.e. to obtain a CFL value as close as possible to 1 in the entire domain), the value of the CFL number is set to 0.5 in the evaluation of the time step. Finally, since the minimum spacing grid, $\Delta x_{i_{\min}}$, in the domain is equal to $0.025H_{BE}$, a time step of 1×10^{-4} s is obtained. It gave a maximum CFL number of approximately 1.2 with smaller values than 1 in 99% of the cells.

Since the initial solution used for the DES approach has already converged to 10^{-5} with RANS realizable $k-\epsilon$ turbulence model before the primary circulation, the monitoring residuals have shown that 15 sub-iterations are sufficient for each time step to reach the convergence of the solution. The time is non-dimensionalized by U_H and H_{BE} and the flow is averaged, after the primary circulation, during $T = 400$ non-dimensional time units ($t^* = tU_H/H_{BE}$) which represents 40 000 time steps.

5.3 Consistency of DES simulations

5.3.1 Grid consistency

Plots of power spectral density (PSD) of velocity components, u_i, obtained in the three directions using a fast Fourier transform (FFT) algorithm are shown in Fig. 5.2. The velocity component data are recorded at a point A located in the centreline between the two buildings ($y = 0$) and at half-height of the BE building from the ground ($z = 1/2H_{BE}$) as indicated in Fig. 5.2. The curves represent the energy cascade which takes its origin from the large turbulent eddies and transfers that energy to small eddies. The phenomenon occurs mainly in

the massively separated regions where the dominant unsteady structures are resolved by LES modelling. The end of the cascade is controlled by the filter width which activates the SGS model (Squires, 2004). The range of frequencies associated with the inertial transfer during the energy cascade is clearly reached as shown in Fig. 5.2 by the slope -5/3. Therefore, the consistency of the constructed grid is demonstrated and justified.

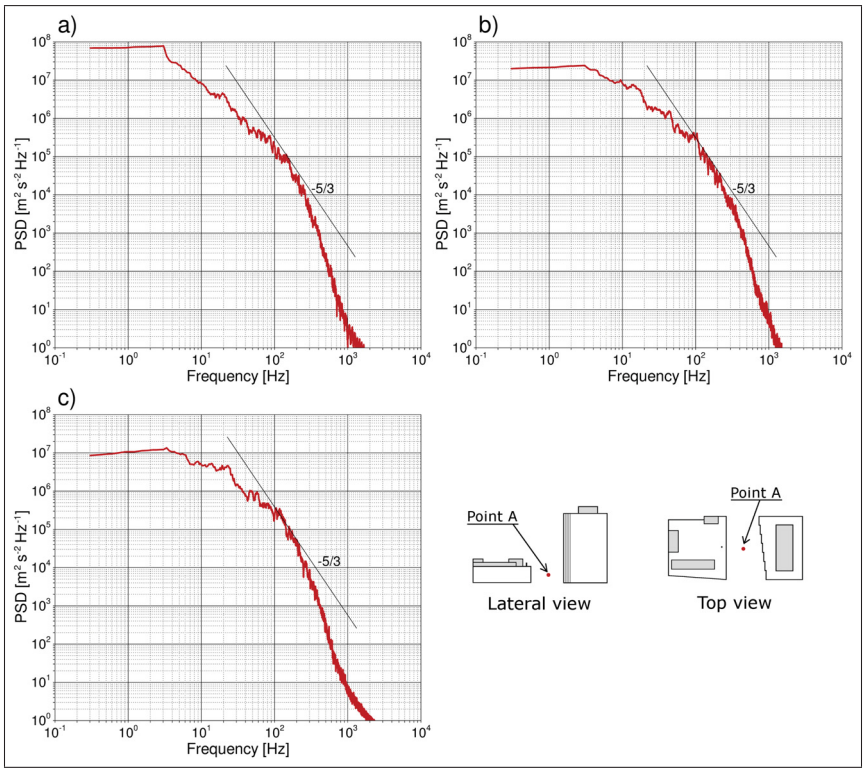

Figure 5.2 Power spectral density of velocity components in (a) streamwise, (b) spanwise, and (c) vertical directions, recorded at point A located in the centreline between the two buildings and at half-height of the BE building from the ground (i.e. $y = 0$ m, $x = 5H_{BE}$ and $z = 1/2H_{BE}$, as illustrated in Fig. 5.1b).

5.3.2 Statistical averaging period consistency

To ensure that the averaging period used to obtain statistical values is sufficiently acceptable, the average error, e_a, for simulated and experimental values of non-dimensional concentration, K, at various samplers located on the BE building roof and the top of the Faubourg tower

leeward wall are calculated. The expression of K is non-dimensionalized using the averaged time concentrations as follows:

$$K = \frac{\langle c \rangle}{\langle c_o \rangle} \tag{5.5}$$

where angular brackets $\langle\ \rangle$ denotes the time average, $\langle c \rangle$ is the pollutant concentration and $\langle c_o \rangle$ the reference concentration given by:

$$\langle c_o \rangle = \frac{Q_e}{H_{BE}^2 U_H} \tag{5.6}$$

where U_H is the mean wind velocity at the roof height of the BE building in [m s^{-1}], H_{BE} is the height of the BE building in [m] and Q_e is the pollutant emission rate in [m^3 s^{-1}].

The average error over all samplers is evaluated by the following equation:

$$e_a = \frac{1}{N} \sum_{i=1}^{N} \left| \frac{K_{i,num} - K_{i,exp}}{K_{i,exp}} \right| \tag{5.7}$$

with N defined as the total number of the concerned samplers (here N is equal to 15 as can be seen in Fig. 5.5 where all samplers are clearly illustrated), $K_{i,num}$ and $K_{i,exp}$ represent the concentration mesured numerically and experimentally at each sampler, respectively.

Fig. 5.3 shows the evolution of the average error, e_a, of K as a function of sampling time. The average error over all samplers is calculated at each 0.1 second and during a sampling time of 4 s. The distribution of e_a presents high fluctuations, in the first range of 2 seconds, mainly due to the transient period. Thereafter, a strong decrease of these fluctuations occurs throughout the following one second period. Finally, between 2.9 and 4 seconds, a clear stabilisation of the average error is established, therefore a statistical averaging period of 3.5 s is judged sufficient for obtaining statistically-steady mean values, which correspond to a full-scale averaging time of about 12 minutes. Consequently, the non-dimensional concentrations over such a statistical averaging period are presented in this paper.

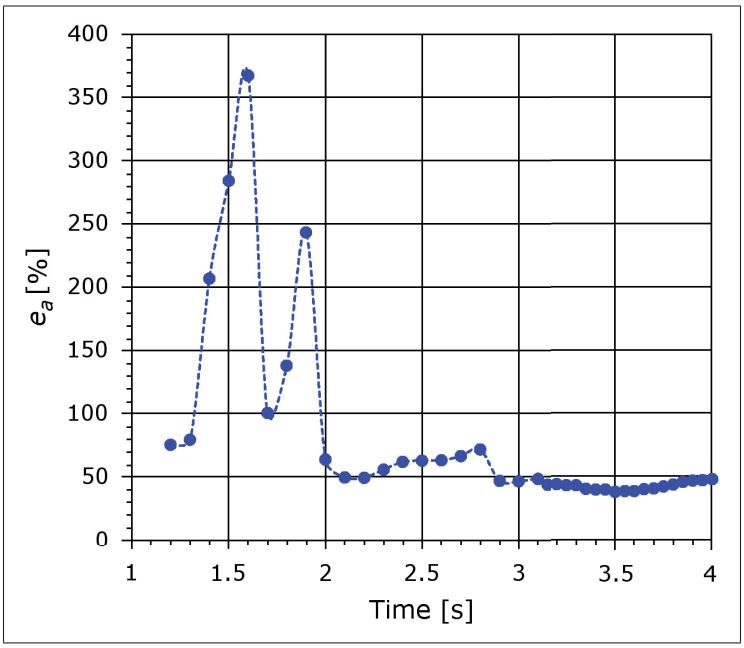

Figure 5.3 Average error between measured and calculated K over all samplers for time sampling between 1.2 and 4 seconds obtained with the case of $h_s = 1$ m and $M = 5$.

5.4 Results and validation

In this section, detailed results obtained with the DES turbulence model are described and compared to both RNG and wind tunnel results (Lateb *et al.*, 2013) to highlight the differences between the two modelling approaches (i.e. steady-state RNG $k - \epsilon$ and unsteady-state DES models). Firstly, the comparison focuses mainly on the mean concentration K values for the various results available from the wind tunnel experiments for the case selected and studied ($h_s = 1$ m and $M = 5$). Afterwards, other parameters such as flow-field structures and Reynolds stress components ($\langle u_i' u_j' \rangle$) are compared between DES and RNG approaches.

The basic strategy of LES is to resolve most of the turbulent kinetic energy, k, of the flow and modelling most of the dissipation ϵ (Fröhlich and von Terzi, 2008), and this possible separation arises from the fact that k is determined by the large scales of motion and ϵ by the small scales (Tennekes and Lumley, 1972). In addition, LES approach is well known to be superior to RANS when validating flow fields and turbulence structures against experimental results

(Tominaga and Stathopoulos, 2012). Since (i) the 11 million cells grid is rigorously made by considering the Taylor-microscale resolution (Liao and Cowen, 2010) and uses stretching ratios equal to 1 near walls and to 1.1 elsewhere, and (ii) the RLZ model is used for modelling the subgrid scales, known as one of best model among those of RANS $k-\epsilon$ models (Blocken *et al.*, 2008), one can consider that DES results are at least comparable to those that could be obtained with LES approach using the traditional Smagorinsky model which remains in wide use (O'Neil and Meneveau, 1997). Consequently, since no wind-flow field data is available from the experimental results, the use of DES results as the reference for the aim of comparison to RANS is justified.

5.4.1 Average error of sampler concentrations

Fig. 5.4 compares the dispersion of K values on the BE roof and the top of the tower leeward wall between wind tunnel and CFD simulation results obtained at different samplers (detailed sampler locations for the studied case are shown in Fig. 5.5). Good agreement with experimental concentrations is shown by RNG model at the top of the tower leeward wall samplers compared to DES model whereas both DES and RNG simulations showed approximately the same dispersion of K over the BE building roof. The average error, e_a, provided by DES and RNG was 37% and 38%, respectively. These values illustrate the insignificant difference between the two tested models, while the required simulation time is 30 times greater when using DES approach. The dashed lines on each side of the median line indicate the limit of values located within a range factor of 2. Eighty percent (80%) and 86% of the DES and RNG concentration K values are within that portion, respectively. However, the correlation coefficient R of the dispersion K values is 0.96 for DES model and 0.97 for RNG model.

5.4.2 Concentrations on the BE building roof and top of Faubourg tower leeward wall

Fig. 5.5 shows the concentration K values at different samplers located on the BE building roof and on the top of the tower leeward wall obtained with both numerical approaches and wind tunnel experiments. As noted previously through Fig. 5.4a, the DES model showed significant underestimation of K values at samplers (F_{B1} and F_{B3}) of the tower leeward wall compared to

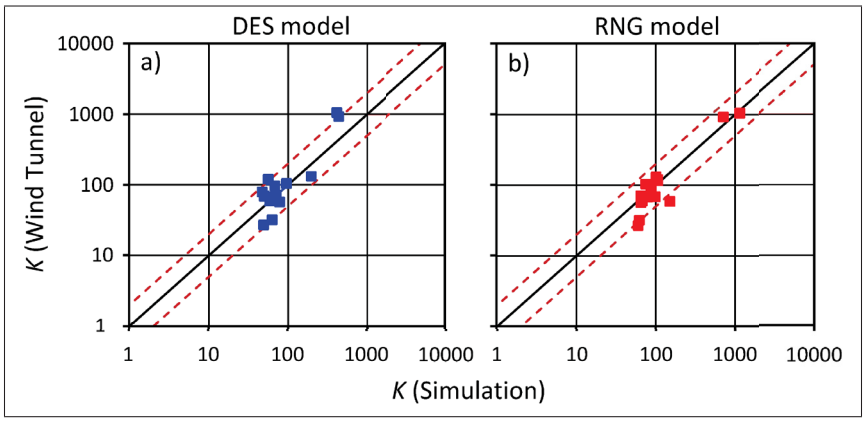

Figure 5.4 Scatter plots of simulation and wind tunnel K data obtained for the case of $h_s = 1$ m and $M = 5$ with (a) DES and (b) RNG models.

those obtained by the RNG model whereas the trend of simulation results obtained on the BE building roof varies from one sampler to the other for both models. Along the central line of the building roof, the RNG model shows better capability to approach the experimental values as detailed in Fig. 5.6; only at sampler P_2, located far in the back of the roof, DES approach has shown approximately the same result as RNG model. On the lateral samplers of the roof, the RNG model remains the best representation of the wind tunnel values at samplers R_{35}, R_{19} and S_5 as can be seen in Fig. 5.5 whereas at samplers R_{25} and S_1, DES yields better results. At samplers R_3 and R_6 located near the building upwind wall, DES shows better concordance with wind tunnel results.

5.4.3 Concentrations along the Faubourg tower leeward wall

Fig. 5.7 indicates the vertical distribution of concentrations K along the leeward wall of the Faubourg tower. The results displayed for RNG model and wind tunnel experiments are obtained with $h_s = 3$ m and $M = 4.5$ whereas those shown for DES model are obtained with $h_s = 1$ m and $M = 5$. Lateb *et al.* (2011) have studied the effect of stack height and pollutant exhaust velocity using the same two-building configuration. The authors have concluded that increasing the momentum ratio M with a small stack height h_s is similar than reducing the momentum ratio for higher h_s and conversely, especially on the leeward wall of the Faubourg

tower and the windward wall of the BE building. Therefore, the comparison between these two cases ($h_s = 1$ m with $M = 5$ and $h_s = 3$ m with $M = 4.5$) is intended to assess the vertical evolution of the concentrations using DES model since the case of $h_s = 3$ m and $M = 4.5$ was not considered in this study. The DES model results show good agreement with wind tunnel results, while the RNG model values overestimate clearly the experimental results. The vertical trend of K distribution is well reproduced by DES compared to RNG, which shows an opposite trend in the upper region.

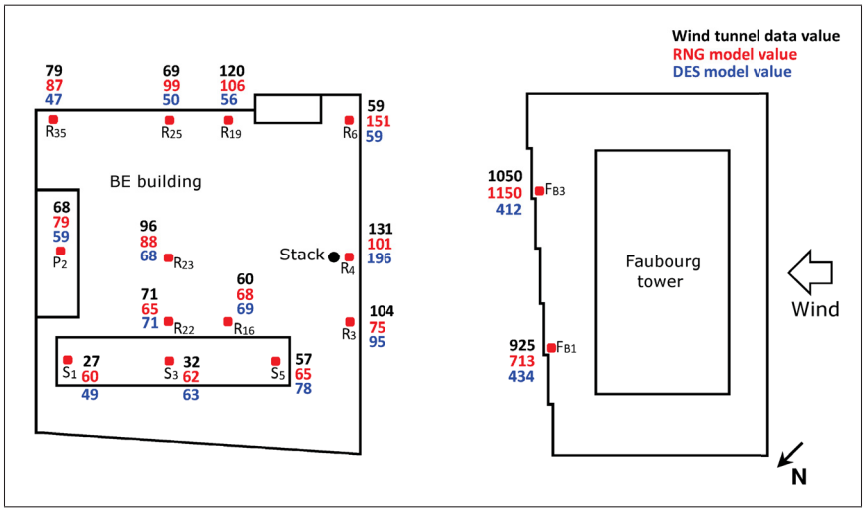

Figure 5.5 Simulation and wind tunnel values of K for $h_s = 1$ m and $M = 5$.

As partial deduction for this section of results, DES shows the same average error (37%) compared to RNG model (38%), while RNG provides better distribution of K values. At most samplers (F_{B1}, F_{B3}, R_4, R_{19}, R_{23}, R_{35} and S_5), RNG has produced closer results to experiment, whereas DES model provides better concordance with experimental values only at few samplers (R_{22}, R_3 and R_6). DES results depicted in Fig. 5.7 agreed well with the wind tunnel results along the Faubourg tower leeward wall while the RNG model overestimated significantly the experimental K values along the tower leeward wall.

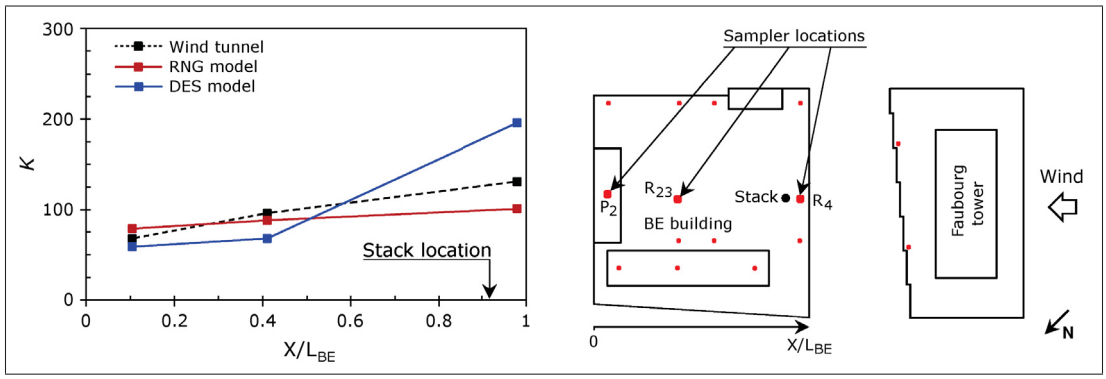

Figure 5.6 Measured and calculated variation of K at samplers R_4, R_{23} and P_2 along x axis on BE building roof for $h_s = 1$ m and $M = 5$.

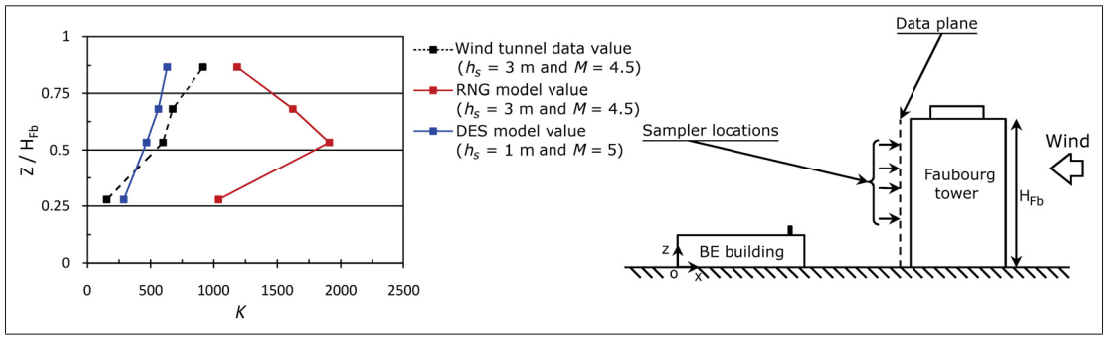

Figure 5.7 Vertical profiles of K on leeward wall of the Faubourg tower (Wind tunnel and RNG simulation values for $h_s = 3$ m and $M = 4.5$, and DES simulation values for $h_s = 1$ m and $M = 5$).

5.5 Analysis and discussion

5.5.1 Flow field analysis

Fig. 5.8 shows the streamlines by time averaged wind velocities in the vertical (x-z) plane through the stack position and the centreline of the domain. The well-known horseshoe vortex system (Liu *et al.*, 2010b; Blocken *et al.*, 2011) induced by the airflow pattern around the tower is well established in the upwind part of the tower – as shown in Fig. 5.8 by the vortex in front of the tower – with DES compared to RNG which displayed a very small horseshoe vortex. Two other vortices are apparent for DES, one between the two buildings and another in the BE building wake, while RNG showed only the recirculation zone between the two buildings.

However the other recirculation zone behind the BE building is included in the recirculation zone induced by the tower roof. In other words, the recirculation region generated by the tower roof was so extended that it reached the BE building wake, thus forming only one single recirculation zone in the vertical plane behind the Faubourg tower, as shown in Fig. 5.8 for RNG model.

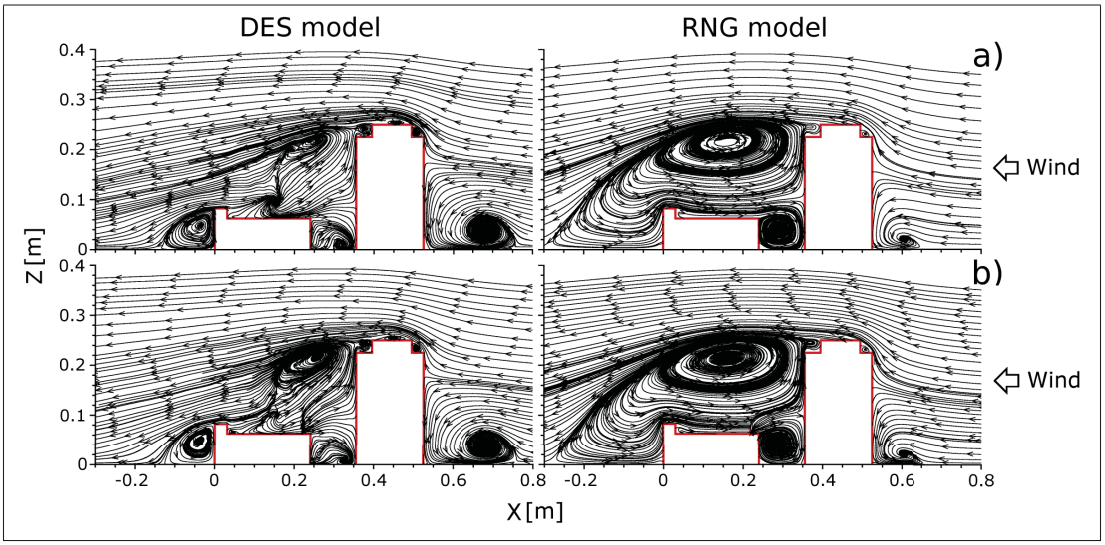

Figure 5.8 Vertical (x-z) plane distribution of streamlines by time averaged velocity for the case of $h_s = 1$ m and $M = 5$ through (a) the centre of the domain ($y = 0$ m) and (b) the stack position ($y = 0.0155$ m).

In order to gain an insight about the length of the recirculation zone behind the Faubourg tower, the recirculation cavity length, L_r, of the latter was evaluated using the approximate equation ($L_r = B_S^{0.67} B_L^{0.33}$) recommended for use by ASHRAE (2007); where B_S is the smaller of the tower upwind face dimensions (height or width) and B_L is the larger. The length L_r evaluated for the two-building configuration of interest is about 0.24 m. The RNG model shows clearly in Fig. 5.8 an overestimation of L_r value (= 0.6 m), while DES exhibits a complex recirculation zone, without borders clearly delimited. However, at height $z = 3/2 H_{BE}$ of the horizontal plan shown in Fig. 5.9a, an approximate recirculation length of 0.25 m is observed. In addition, this overestimation issue of recirculation region behind a building when using RANS models has been already stated by several authors (e.g. Rodi, 1997; Wright and Easom, 2003; Shira-

sawa *et al.*, 2008; Yoshie *et al.*, 2011). According to Yoshie *et al.* (2011), this overestimated reattachment length is mainly due to the steady-state approach of RANS models which did not reproduce the vortex shedding behind the tower. Consequently, very large velocities in streamwise direction are induced by the reversed flow (Wright and Easom, 2003).

When analysing the streamlines in the vertical plane passing by the stack presented in Fig. 5.8b, the exhausted pollutant velocity appears less disrupted by the wind flow above the stack with DES than does the RNG, because of the higher pollutant emission velocity ($M = 5$). Indeed, for RNG the pollutant is directed towards the tower leeward wall immediately when it expelled from the stack, while with DES the pollutant rose in height then directed towards the tower leeward wall. This could partly explain the correct approach of the concentration by RNG at samplers F_{B1} and F_{B3} – previously noticed in Fig. 5.5 – which is just a consequence of the overestimated recirculation zone that, in turn, resulted from the steady-state approach of the RNG model, as previously explained.

Recently Nozu and Tamura (2012) have noted that using RANS models favour the imprisonment of the pollutant in the wake regions since the solution lacks of periodic fluctuations. Therefore, this results in very high concentrations, particularly when the source emission is located in the wake zone. This observation is clearly illustrated in Fig. 5.7 since the distribution of K in the vertical direction along the tower leeward wall is quite overestimated. However, for DES modelling, the reversed flow interacting with the transient vortices and the tower leeward wall boundary forms a free shear layer, and fluctuated periodically because of Kelvin-Helmholtz-type instability (Hasama *et al.*, 2008). In additional, the Reynolds number of 2.5×10^4 – based on the BE building height – remains an important mixing parameter for flows in which the shear layers arising from separation of the boundary layers at the salient edges (Lim *et al.*, 2007), like those of the staircase shape of the tower leeward wall. Consequently, the pollutant carried by the reversed flow from the stack is well mixed and transported laterally. This could also explain the good agreement of K at samplers R_3 and R_6 shown in Fig. 5.5 and along the vertical direction of the tower leeward wall presented in Fig. 5.7.

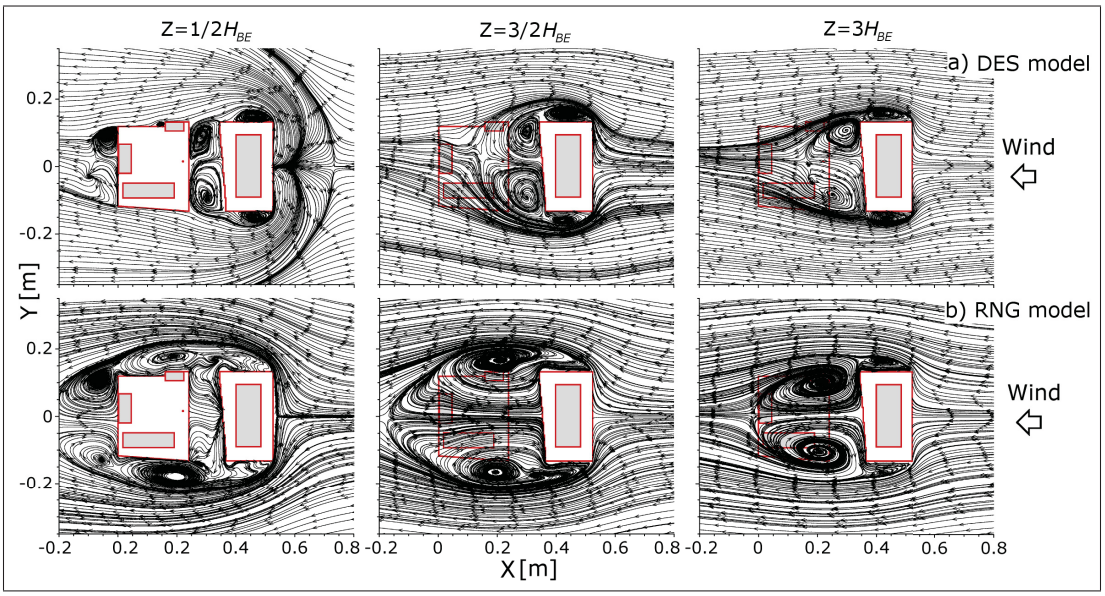

Figure 5.9 Horizontal (x-y) plane distribution of streamlines by time averaged velocity at different vertical positions for the case of $h_s = 1$ m and $M = 5$ obtained with (a) DES and (b) RNG models. Columns from left to right represent the results at height $z = 1/2H_{BE}$, $z = 3/2H_{BE}$ and $z = 3H_{BE}$ from the ground, respectively.

Fig. 5.9 shows the streamlines by time averaged wind velocities in the horizontal (x-y) plane at different vertical heights from the ground ($z = 1/2H_{BE}$, $3/2H_{BE}$ and $3H_{BE}$). The horseshoe phenomenon is well shown by DES through the horizontal plane ($z = 1/2H_{BE}$) in Fig. 5.9a. At higher levels ($z = 3/2H_{BE}$ and $3H_{BE}$) shown in Fig.5.9, two main vortices are clearly distinguished in the Faubourg tower wake for both models. Vortices illustrated by RNG in Fig. 5.9b appear more symmetrical than those depicted by DES; while the vortices configuration presented in Fig. 5.9a for DES simulations showed a north-west side vortex more significant than that of the south-east side. This is due to the difference in width between the two tower sides. Consequently, the wind-flow field produced by DES has better taken into account the horizontal staircase form of the tower leeward wall than RNG, which can be explained by the vortex shedding reproduced by DES but not with the RNG approach.

Despite the good agreement in concentration values between the RNG model and experimental results, at the BE roof samplers in general and at the top of the tower leeward wall samplers (i.e. F_{B1} and F_{B3}) in particular, three main anomalies are apparent in the wind-flow field

analysis: (i) significant overestimation of the recirculation zone length in the tower wake, (ii) non-consideration of the difference in width between the tower sides, and (iii) insignificant reproduction of the horseshoe phenomenon in the upstream part of the tower in spite of the strong wind-flow velocity. In principle, the lack of all these basic flow characteristics around an obstacle like the Faubourg tower indicates that the wind-flow structure has not been well simulated by RNG as opposed to DES which seems to reproduce the wind-flow configuration far better.

5.5.2 Distribution of Reynolds stress components

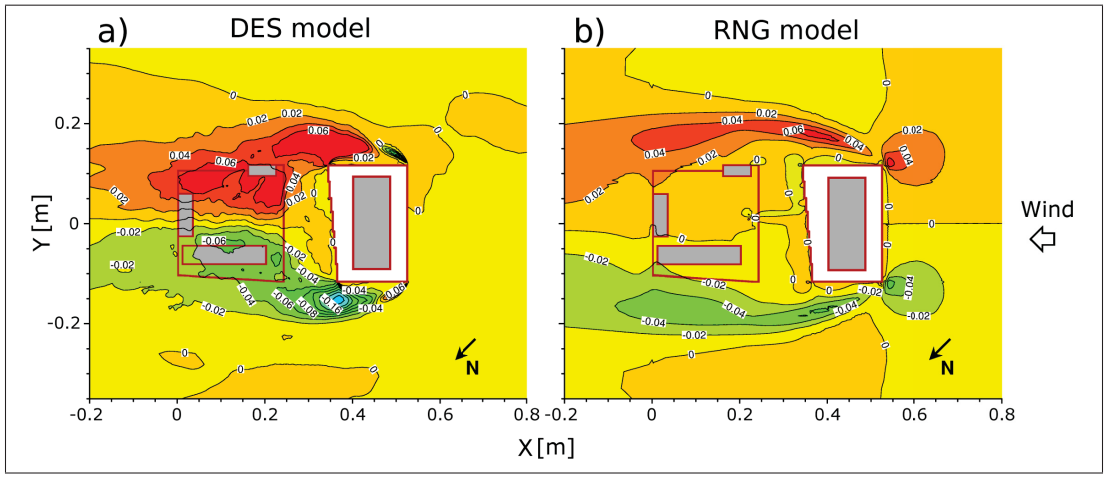

Figure 5.10 Distribution of non-dimensional shear stress component $\langle u_1' u_2' \rangle / U_H^2$ iso-contours on the horizontal plane (x-y) at height $z = 3/2 H_{BE}$ for the case of $h_s = 1$ m and $M = 5$ with (a) DES model and (b) RNG model.

The horizontal movement of the vortex shedding towards the lateral directions is mainly fulfilled by $\langle u_1' u_2' \rangle$ and $\langle u_2' u_2' \rangle$ shear stress components in the tower wake region. Therefore, Fig. 5.10 depicts the horizontal distribution of non-dimensional shear stress component $\langle u_1' u_2' \rangle / U_H^2$ at height $z = 3/2 H_{BE}$ to assess the vortex shedding production behind the tower. Note that the modelled part of $\langle u_1' u_2' \rangle$ values is less significant than those of the resolved part, nevertheless the non-dimensional values presented in Fig. 5.10 are estimated as the algebraic sum of the two parts ($\langle u_1' u_2' \rangle_{res}$ + $\langle u_1' u_2' \rangle_{SGS}$) when using DES. The distribution of $\langle u_1' u_2' \rangle / U_H^2$ values shows clearly the vortices induced by the Faubourg tower sides, directed towards the central

plane when following the absolute value of 0.04 and 0.02 with DES, see Fig. 5.10a. In contrast to the RNG approach shown in Fig. 5.10b, the absolute value of 0.04 remains outside the wake region, and the movement of vortices of which the absolute value is of 0.02 begins heading towards the central plane at the end of the extended wake region. The distribution between the north-west and the south-east leeward wall corners of the tower is clearly different for DES with significant absolute values of $\langle u_1' u_2' \rangle / U_H^2$ at the north-west leeward corner, while the distribution presented by RNG is rather similar at both tower leeward wall corners. This confirms the non-consideration of the horizontal staircase form of the tower leeward wall stated previously.

Figs. 5.11 and 5.12 show the distribution of the Reynolds normal stress components $\langle u_i' u_i' \rangle$ normalized by U_H^2 along the horizontal and vertical lines, respectively, located at four streamwise positions (i.e. $x/H_{BE} =$ -2, 0, 2 and 5 as illustrated in Fig. 5.1b). Horizontal lines are in plane (x-y) at height $z =$ 3/2H_{BE} and vertical lines are contained in the central plane ($y = 0$). For the RNG model, all non-dimensional component values vary between 0 and 0.125, while for DES the variation range lies within 0 and 0.235. The trend between the three $\langle u_i' u_i' \rangle$ components is almost the same for RNG model when comparing with DES results which, in turn, show significant difference in the Reynolds normal stress component distributions. However, the streamwise component $\langle u_1' u_1' \rangle$ distributions, in vertical and horizontal lines at the BE building leeward wall (i.e. $x/H_{BE} = 0$) shown in Figs. 5.11b and 5.12b with RNG, present small values because of the reversed flow and the lateral movements which occurred in that region (see Figs. 5.8a and 5.9b), and therefore promote the lateral and vertical components $\langle u_2' u_2' \rangle$ and $\langle u_3' u_3' \rangle$ as shown in Figs. 5.11 and 5.12. In region above the BE building behind the tower (i.e. $x/H_{BE} = 0$ and 2), the DES model showed very large values of $\langle u_2' u_2' \rangle$ component compared to $\langle u_1' u_1' \rangle$ and $\langle u_3' u_3' \rangle$ as can be seen in Figs. 5.11c and 5.12c.

In many regions of the flow-field structure, the RNG model shows large values of $\langle u_i' u_i' \rangle$ compared to DES. For instance, in the lower part along the vertical leeward wall of the BE building (i.e. $x/H_{BE} = 0$), the RNG model exhibits large $\langle u_1' u_1' \rangle$ values compared to those of DES (see Figs. 5.12a and b). This results from large velocities stated previously in the streamwise

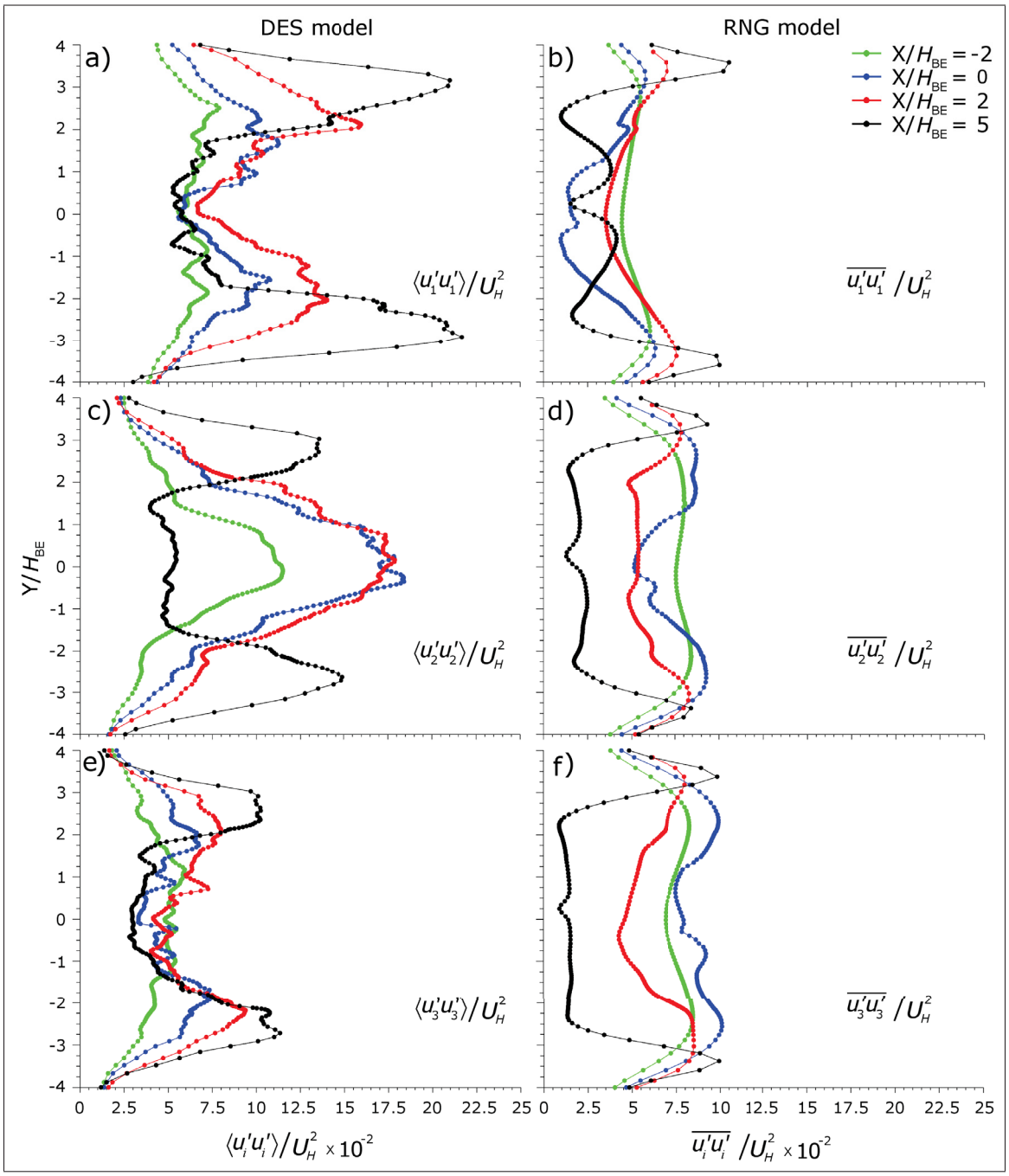

Figure 5.11 DES- and RNG-based distribution of non-dimensional Reynolds normal stress components ($\langle u_i' u_i' \rangle / U_H^2$) along horizontal lines at $z = 3/2 H_{BE}$ and for four streamwise positions (i.e. $x/H_{BE} =$ -2, 0, 2 and 5, as illustrated in Fig. 5.1b).

direction when using the RNG model. Far in the wake zone at side regions of the BE building

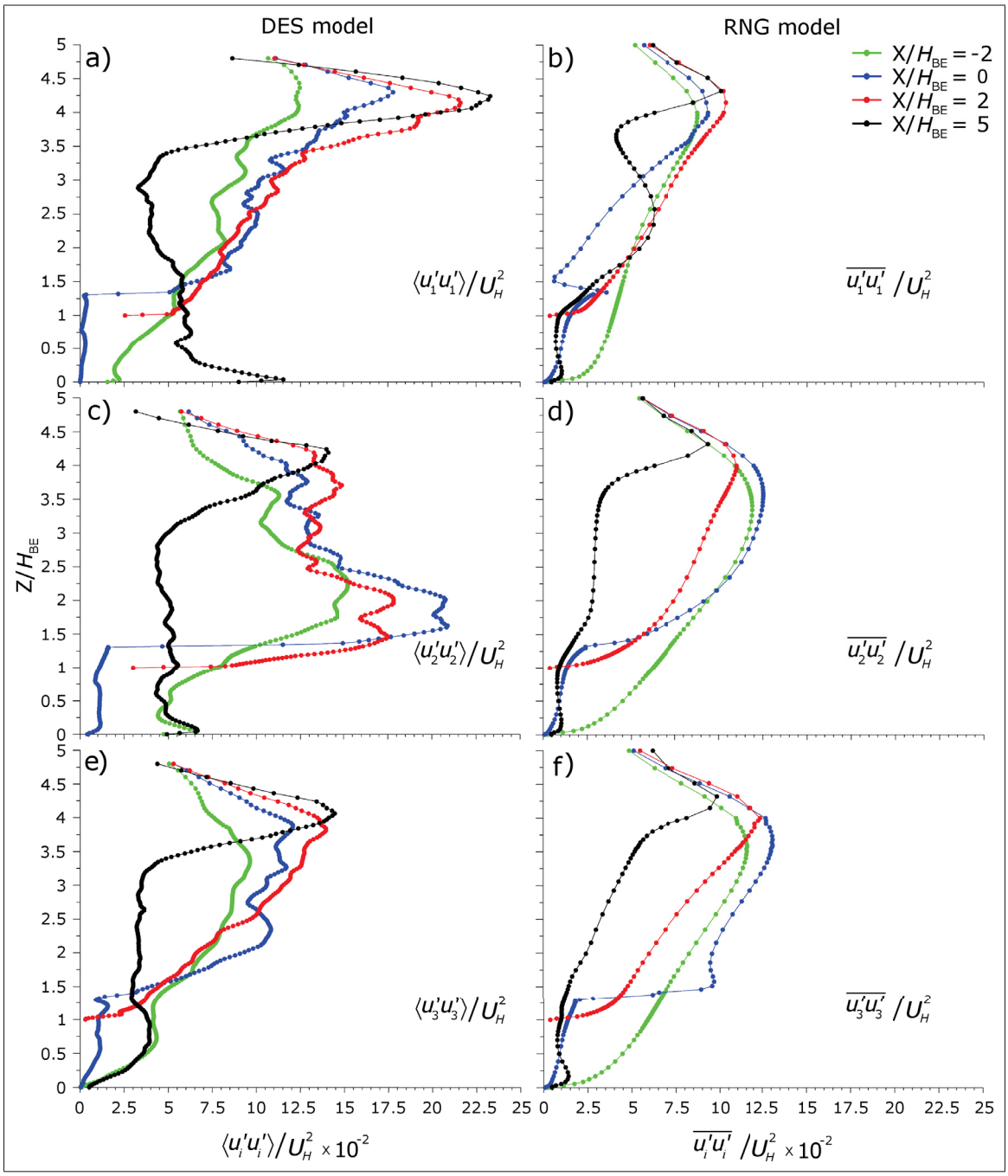

Figure 5.12 DES- and RNG-based distribution of non-dimensional Reynolds normal stress components ($\langle u_i' u_i' \rangle / U_H^2$) along vertical lines in the central plane ($y = 0$) and for four streamwise positions (i.e. x/H_{BE} = -2, 0, 2 and 5, as illustrated in Fig. 5.1b).

(i.e. x/H_{BE} = -2 and 0), the lateral, $\langle u_2' u_2' \rangle$, and vertical, $\langle u_3' u_3' \rangle$, components are also very large with RNG compared to those of DES as can be seen in Figs. 5.11c–f.

In summary, this section shows that the DES reproduces well the vortex shedding, while no such phenomenon is observed with RNG. Since it can be considered that the improvements in the prediction accuracies of normal stresses and shear stresses are correlated with each other (Shirasawa *et al.*, 2008), this observation reveals that the lateral momentum diffusion is insufficient so that it is impossible to reproduce correctly the tower wake region, and thus to accurately evaluate its reattachment length when using the RNG model. In addition, the anisotropy of the Reynolds normal stress components – that may be associated with the highly intermittent character of the wake region flow (Kang and Meneveau, 2001) – has been well taken into account by DES, whereas the RNG model has not considered it sufficiently. In other words, on the one hand, the underestimation and/or overestimation of the Reynolds stress components, when using the RNG approach, results in an incorrect reproduction of the flow-field structure. On the other hand, the steady-state methodology of RNG does not favour the vortex shedding production, therefore the lateral diffusion is highly underestimated especially in the immediate wake region. Furthermore, the transient flow plays a very important role when modelling a passive pollutant concentration field (Johnson and Hunter, 1998) and the dispersion of pollutant gases within urban environment is essentially unsteady (Chang and Meroney, 2003). Consequently, the steady-state RANS methodology, in general, cannot predict the turbulent pollutant transport process accurately since the dispersion field is closely related to flow-field behaviour (Tominaga and Stathopoulos, 2009). Nonetheless, one can say that RNG model remains an acceptable approach to estimate concentration values for dispersion where advection transport phenomena dominate – like over the BE roof region – while for regions where the turbulent diffusion process is more significant – like within the immediate wake zone behind the tower – DES model performs best.

5.6 Conclusions

In the present work, the dispersion of pollutants around a two-building configuration has been investigated using the unsteady-state detached-eddy simulation approach, and the results have been compared to steady-state RNG $k - \epsilon$ model as well as experimental wind tunnel data. The purpose is to evaluate the effects of the unsteadiness and the Reynolds stress component

anisotropy in reproducing the flow and dispersion fields when comparing between DES and RNG approaches. The main findings of the study can be summarized as follows.

- In terms of the flow field, DES approach seems to reproduce correctly the recirculation zone in the wake region, while the RNG model has clearly overestimated the recirculation region. The horseshoe vortex system induced by the airflow pattern around the upstream tower is well established with DES compared to RNG model. The vortex shedding induced by the tower sides in the wake region is not reproduced properly by RNG whereas this phenomenon is clearly observed with DES.

- In terms of pollutant dispersion, both models show approximately the same average error of concentrations calculated over all samplers. For concentration values at samplers F_{B1} and F_{B3} located at the top of the tower leeward wall, the RNG model shows better agreement with experimental values compared to DES. This good agreement is likely due to the large stream-wise velocities in the reversed flow that are a consequence of the steady-state methodology of RNG model (Wright and Easom, 2003). However the DES model reproduces with good agreement the distribution of concentrations in the vertical direction along the tower leeward wall, while the RNG approach exhibits a significant overestimation.

- The underestimation and/or overestimation of Reynolds stress components and the steady-state methodology of RNG $k-\epsilon$ model tend, respectively, to (i) distort and/or limit the Reynolds stress component values, and (ii) not reproduce contribution of periodic fluctuation due to the transient characteristics of the flow field, particularly in wake regions where high anisotropy is exhibited. Consequently, RANS approaches are generally unable to reproduce the wind-flow structure and the pollutant transport process accurately.

- In terms of CPU time, the DES model required approximately 30 times more computing time than the RNG model. Given the average errors of concentration obtained by the DES and RNG approaches, the steady-state RNG model remains an approach that can be used and trusted for obtaining an insight into the dispersion process at specific measurement points where dispersion is mainly dominated by the advection transport phenomenon. Finally, the

DES model has demonstrated that the unsteady-state approach is clearly better suited to understand the flow-field development and the dispersion process.

CONCLUSION

Numerical simulations have been performed for the study of pollutant dispersion around a two-building configuration in an urban area. The study is concerned with the transportation of pollutant emissions in the lower atmospheric boundary layer by wind flows especially in an urban environment. This topic is an important environmental problem since it is connected to the protection of indoor air quality as well as human health.

This study is based on experiments carried out at full-scale (1:1) and wind tunnel scale (1:200) in downtown Montreal and in the boundary layer wind tunnel of Concordia University, respectively. The geometry considered consists of two lined up buildings composed of a tower and a building in its wake from which a pollutant is emitted from a rooftop stack, with a wind blowing perpendicularly to the windward wall of the upstream tower. The numerical results are compared against experimental measurements in each part of the different chapters that compose this work and a number of conclusions are presented and recommendations for future works are outlined.

Following literature review in Chapter 1, Chapter 2 investigated various RANS $k-\epsilon$ turbulence models (i.e. standard, RNG and realizable $k-\epsilon$ models) in order to determine the best model to reproduce pollutant plume dispersion. The standard $k-\epsilon$ model showed the worst results compared to the other models. Indeed, the realizable $k-\epsilon$ model yielded the best agreement with experiments for the lower stack height and momentum ratio, while the RNG $k-\epsilon$ model performed best for higher stack and momentum ratio. The realizable model was the only model to provide a correct trend for concentration distribution in the lower region between the two buildings. Given the well-known excessive k-production of the standard $k-\epsilon$ model, it was generally found to be inadequate for reproducing the vertical concentration distribution and was the only model that failed to satisfy the realizability requirement, therefore reproducing non-physical results. For the configuration under investigation, favouring the turbulent mass diffusivity by decreasing the turbulent Schmidt number Sc_t values – as found by several authors (e.g. Tominaga and Stathopoulos, 2007; Blocken *et al.*, 2008; Chavez *et al.*, 2011; Gousseau *et al.*, 2011a) – did not bring improvements to the lack of lateral dispersion observed in the

wake region and neither significant variations in concentration values. Consequently, changes in Sc_t value did not have a major impact on pollutant dispersion with complex flows where strong separation/recirculation zones occur like wake zones. It is thought that the dispersion process is dominated by the advection transport phenomenon which, in turn, is strongly related to the correct reproduction of the wind-flow field. According to many authors, the inaccuracy of reproducing correctly the flow field is probably due to the incorrect simulation of the Reynolds stress components (Wright and Easom, 2003) and the steady-state methodology (Shirasawa *et al.*, 2008). Therefore, an unsteady turbulence model was recommended for use to shed light on the effects of steadiness on both the dispersion process and flow-field structure.

In Chapter 3, simulations at both scales (full-scale and wind tunnel scale 1:200) were carried out and the average relative error of all concentrations obtained at different samplers located on the BE roof and Faubourg tower leeward wall were evaluated. The results showed that numerical results obtained at wind tunnel scale are closer to experiment than those at field scale. Consequently, this clearly highlights the numerical approach capability to reproduce experiments better in controlled than non-controlled environments. The concentration distribution varied from one sampler to the other when compared to the experimental data for both scales tested. The CFD simulations did not reproduce well the wake zone observed in the experiments. However, the lower region between the two buildings seemed to be correctly reproduced. From these first simulations, the leeward wall of the BE building appeared to be the best location to install fresh-air intakes for this building with the configuration considered.

Chapter 4 dealing with the effects of stack height and exhaust velocity on the transportation of the pollutant showed clearly that increasing the stack height had an effect similar to that obtained by increasing the pollutant exhaust velocity, with some differences however depending mainly upon the wall of the building under consideration. Indeed, the iso-concentration contour distributions were investigated on the BE building roof and walls as well as on the Faubourg leeward wall. For instance, on the BE roof, a stack height of 3 metres with a momentum ratio of 2.2 generated approximately the same iso-concentration contour configurations when the stack height or the momentum ratio were increased by factors higher than 2. How-

ever, the reduction in highest iso-concentration contour value obtained on the tower leeward wall was 22% less when increasing the momentum ratio than when increasing stack height. On the BE building windward wall, the opposite tendency was observed: increasing momentum ratio provided an insignificant change in the highest iso-concentration contour value compared to increasing stack height. Therefore, given the differences found when increasing stack height or exhaust velocity, it would be worthwhile to study which parameter should be modified in order to reduce pollution in certain places and/or where to install fresh-air intakes. Neglecting some neighbourhood buildings, like the Faubourg tower upstream of the building of interest in the case studied, led to considerable errors in the pollutant dispersion pattern, hence major design errors regarding the location of fresh-air intakes. Varying these two parameters (i.e. stack height and pollutant exhaust velocity) did not sufficiently alter the concentration calculated on the emitting building leeward wall and their values remained the lower concentrations recorded on these BE building walls. Therefore the leeward wall of the emitting building appeared to be the best location for fresh-air intakes as opposed to the tower leeward wall where the fresh-air intakes should not be placed because of the high pollutant concentrations recorded there.

As a follow up to recommendations made in Chapter 2, an additional study was carried out and reported in Chapter 5 in which an unsteady model (i.e. detached-eddy simulation DES model) was presented and tested. Because of the long computing time required by the DES approach, only one case among those treated in Chapter 2 was studied ($h_s = 1$ m and $M = 5$). The results obtained were compared to those from the wind tunnel experiments and the RNG steady-state model, since the latter provided the best results among the various RANS models previously tested for the specific case. The study showed clearly the contribution of periodic fluctuations in the pollutant dispersion process due to the transient characteristics of the flow field in the wake region when using DES model whereas the steady-state methodology could not reproduce these transient wind-flow structures. Therefore, it is clear that RANS models are unable to reproduce accurately the flow-field patterns. Additionally, an underestimation/overestimation of the shear stress components was observed for the RNG model compared to DES approach in the wake region where high anisotropy was exhibited. Consequently, the underestimation/overestimation of the shear stress components and the lacking transient wind-flow

structures stated in the wake region made the RANS $k-\epsilon$ models generally inadequate to reproduce accurately the wind-flow field in highly anisotropic regions. Despite the shortcomings of RANS methodology to reproduce the wind-flow field with good accuracy, the small differences between the average error of the non-dimensional concentrations obtained with the two approaches (DES and RNG models) and the relatively short computing requirements of the RNG model made it, as well as the RANS $k-\epsilon$ models in general, acceptable and useful to obtain an insight of the dispersion field at specific point measurements. However, the DES approach demonstrated that the unsteady-state approach is clearly better suited to understand the flow-field configuration and consequently the dispersion processes since the two phenomena are closely related (Tominaga and Stathopoulos, 2009).

In summary, this thesis reports a detailed investigation of pollutant dispersion for a configuration frequently encountered in large towns, namely where a pollutant is emitted from a rooftop stack on a building completely engulfed in the wake region of another higher building upstream, by means of numerical simulations. After making a careful assessment of all requirements (e.g. grid design, computational domain size, homogeneity of the simulated flow, boundary conditions, wall treatment...) necessary for carrying out properly the numerical simulations, significant parameters were identified, i.e. stack height, pollutant exhaust velocity and turbulence model, and thoroughly investigated throughout this work for the correct reproduction of the wind flow and dispersion fields that are necessary to determine the best fresh-air intake locations.

Recommendations for future work

Urban pollutant dispersion is a complex phenomenon and thus many challenges remain for further study. The present work should therefore be seen as a contribution towards the better use of numerical simulation approaches for the understanding of pollutant dispersion in urban areas in terms of wind flow and dispersion fields around buildings in order to improve indoor air quality by means of carefully locating fresh-air intakes. For future work, a number of improvements to simulate better dispersion phenomena can be suggested as follows:

- In the past, many studies have emphasized the importance of the wind-building interactions on the wind-flow structure (e.g. Khanduri *et al.*, 1997, 1998) and the effects of neighbouring building characteristics on the dispersion field (e.g. Hajra *et al.*, 2011; Chavez *et al.*, 2011; Hajra and Stathopoulos, 2012; Chavez *et al.*, 2012). For instance, Khanduri *et al.* (1998) have concluded that adjacent buildings can drastically modify the wind load on buildings while Hajra and Stathopoulos (2012) have shown the importance of the adjacent building characteristics for reproducing the dispersion field in the case of urban areas where the emitting source is surrounded by a group of buildings. Throughout this research, only one incident wind direction was used, which corresponds to the dominant wind direction in downtown Montreal. Such assumption appears acceptable as a good initial step since the two-building configuration under study is in perfect tandem alignment with the wind direction. In future work, it would be interesting to generalise the dispersion field investigation for other wind directions, which will require taking into account the adjacent building characteristics.

- Regarding the insignificant changes in concentration values reported in Chapter 4 of this work when promoting the dispersion through low turbulent Schmidt number values, it would seem wise to investigate the impact of the turbulent diffusion and advection mass transport mechanisms that occur during the pollutant dispersion process. This orientation has already been suggested by several authors (e.g. Tominaga and Stathopoulos, 2007; Blocken *et al.*, 2008; Gousseau *et al.*, 2011a,b) to emphasize the effects of turbulence on mass transfer when it consists of turbulent flows. Gousseau *et al.* (2011b) have analysed the transport process of a pollutant in the turbulent wind-flow pattern around isolated buildings and clarified the role of convective and turbulent fluxes in the transport process and in the prediction accuracy of RANS and LES simulations. The study showed that, in separation regions and in the wake of buildings, the accuracy of LES is clearly better than RANS since, on the one hand, the convection is the dominant mechanism of mass transport and, on the other hand, LES model computes more accurate convective fluxes. The authors stated that the modification of turbulent Schmidt number influences the pollutant dispersion predicted by RANS models, which in turn, cannot compensate deficiencies of these models in terms of flow-field. Since no relation has been established in this study between the variation of the turbulent Schmidt number and the

dispersion field, it would appear necessary to conduct new research for understanding the mass transport mechanisms in order to explain better the observed findings.

- Most of the dispersion numerical studies assume that the contaminant particles are chemically and dynamically passive (Sini *et al.*, 1996). This assumption is most of the time not fully appropriate, already in the case of inert gases, since exhaust gases are generally warmer than the surrounding air when they exit from the stack. Consequently, neglecting the exiting temperature gradients that induce necessarily differences in density between pollutant particles and the air, may lead to inaccurate dispersion process simulations. Further study considering temperature effects may result in a better estimation of the transport mechanism, which could improve numerical simulation results significantly.

BIBLIOGRAPHY

Abohela, I., N. Hamza, and S. Dudek. 2013. " Effect of roof shape, wind direction, building height and urban configuration on the energy yield and positioning of roof mounted wind turbines ". *Renewable Energy*, vol. 50, p. 1106–1118.

Adair, D. 1990. " Numerical calculations of aerial dispersion from elevated sources ". *Applied Mathematical Modelling*, vol. 14, n° 9, p. 459–467.

AIAA. 1998. Guide for the verification and validation of computational fluid dynamics simulations. *American Institute of Aeronautics and Astronautics (AIAA)*, (ISBN: 978-1-56347-354-8), Reston, VA, USA.

AIAA. 2010. Guide to reference and standard atmosphere models. *American Institute of Aeronautics and Astronautics (AIAA)*, (ISBN: 978-1-60086-784-2), Reston, VA, USA.

An, K., J C H. Fung, and S H L. Yim. 2013. " Sensitivity of inflow boundary conditions on downstream wind and turbulence profiles through building obstacles using a CFD approach ". *Journal of Wind Engineering and Industrial Aerodynamics*, vol. 115, p. 137–149.

Antonacci, G. 2005. " Air pollution modelling over complex topography ". Ph.D thesis, Department of Civil and Environmental Engineering, Faculty of Engineering of the University of Trento, Italy.

ASHRAE. 1997. Chapter 15: Airflow around buildings. ASHRAE Handbook – Fundamentals. *American Society of Heating, Refrigerating and Air-conditioning Engineers*, Atlanta, USA.

ASHRAE. 2007. Chapter 44: Building air intake and exhaust design. ASHRAE Handbook – Heating, Ventilating, and Air-Conditioning Applications. *American Society of Heating, Refrigerating and Air-conditioning Engineers*, Atlanta, USA.

ASHRAE. 2009. Chapter 24: Airflow around buildings. ASHRAE Handbook – Fundamentals. *American Society of Heating, Refrigerating and Air-conditioning Engineers*, Atlanta, USA.

ASHRAE. 2011. Chapter 45: Building air intake and exhaust design. ASHRAE Handbook – Fundamentals. *American Society of Heating, Refrigerating and Air-conditioning Engineers*, Atlanta, USA.

ASME. 2009. Standard for verification and validation in computational fluid dynamics and heat transfer. *American Society of Mechanical Engineers (ASME)*, V&V 20-2009.

Assimakopoulos, V D., H M. ApSimon, and N. Moussiopoulos. 2003. " A numerical study of atmospheric pollutant dispersion in different two-dimensional street canyon configurations ". *Atmospheric Environment*, vol. 37, n° 29, p. 4037–4049.

Aubrun, S. and B. Leitl. 2004. "Unsteady characteristics of the dispersion process in the vicinity of a pig barn. Wind tunnel experiments and comparison with field data". *Atmospheric Environment*, vol. 38, p. 81–93.

Baldauf, R W., D. Heist, V. Isakov, S. Perry, G S W. Hagler, S. Kimbrough, R. Shores, K. Black, and L. Brixey. 2013. "Air quality variability near a highway in a complex urban environment". *Atmospheric Environment*, vol. 64, p. 169–178.

Barlow, J F. and O. Coceal. 2009. A review of urban roughness sublayer turbulence. Met office, meteorology research and development, (Technical Report No. 527), University of Reading, UK.

Basu, D., A. Hamed, and K. Das. 2005. DES and hybrid RANS/LES models for unsteady separated turbulent flow predictions. In: *Proceedings of the 43th AIAA Aerospace Sciences Meeting and Exhibit*, Pap. No. AIAA-2005-0503, Reno, NV, USA.

Bechmann, A. and N N. Sørensen. 2010. "Hybrid RANS/LES method for wind flow over complex terrain". *Wind Energy*, vol. 13, n° 1, p. 36–50.

Bitsuamlak, G T., A G. Chowdhury, and D. Sambare. 2010. "Application of a full-scale testing facility for assessing wind-driven-rain intrusion". *Building and Environment*, vol. 44, p. 2430–2441.

Blocken, B. and C. Gualtieri. 2012. "Ten iterative steps for model development and evaluation applied to Computational fluid dynamics for environmental fluid mechanics". *Environmental Modelling & Software*, vol. 33, p. 1–12.

Blocken, B. and T. Stathopoulos. 2008. On the use of CFD for modelling air pollutant dispersion around buildings. In: *Proceedings of the 4th International Conference on Advances in Wind and Structures (AWAS'08)*, Jeju, Korea.

Blocken, B., T. Stathopoulos, and J. Carmeliet. 2007. "CFD simulation of the atmospheric boundary layer: wall function problems". *Atmospheric Environment*, vol. 41, n° 2, p. 238–252.

Blocken, B., T. Stathopoulos, P. Saathoff, and X. Wang. 2008. "Numerical evaluation of pollutant dispersion in the built environment: Comparisons between models and experiments". *Journal of Wind Engineering and Industrial Aerodynamics*, vol. 96, n° 10-11, p. 1817–1831.

Blocken, B., T. Stathopoulos, J. Carmeliet, and J L M. Hensen. 2011. "Application of computational fluid dynamics in building performance simulation for the outdoor environment: an overview". *Journal of Building Performance Simulation*, vol. 4, n° 2, p. 157–184.

Blocken, B., W D. Janssen, and T. Van-Hooff. 2012. "CFD simulation for pedestrian wind comfort and wind safety in urban areas: general decision framework and case study for the Eindhoven University campus". *Environmental Modelling & Software*, vol. 30, p. 15–34.

Blocken, B., Y. Tominaga, and T. Stathopoulos. 2013. "CFD simulation of micro-scale pollutant dispersion in the built environment". *Building and Environment*, vol. 64, p. 225–230.

Bonner, C S., M C B. Ashley, X. Cui, L. Feng, X. Gong, J S. Lawrence, D M. Luong-Van, Z. Shang, J W V. Storey, L. Wang, H. Yang, X. Zhou, and Z. Zhu. 2010. "Thickness of the atmospheric boundary layer above dome A, Antartica, during 2009". *The Astronomical Society of the Pacific*, vol. 122, p. 1122–1131.

Brethouwer, G. and E. Lindborg. 2009. "Numerical study of vertical dispersion by stratified turbulence". *Journal of Fluid Mechanics*, vol. 631, p. 149-–163.

Britter, R. and M. Schatzmann. 2007. "Background and justification document to support the model evaluation guidance and protocol". *Cost Action 732*.

Brown, R J. and R W. Bilger. 1996. "An experimental study of a reactive plume in grid turbulence". *Journal of Fluid Mechanics*, vol. 312, p. 373–407.

Bunge, U., C. Mockett, and F. Thiele. 2007. "Guidelines for implementing detached-eddy simulation using different models". *Aerospace Science and Technology*, vol. 11, n° 5, p. 376–385.

Cai, X-M., J F. Barlow, and S E. Belcher. 2008. "Dispersion and transfer of passive scalars in and above street canyons – large-eddy simulations". *Atmospheric Environment*, vol. 42, p. 5885–5895.

Calhoun, R., F. Gouveia, J. Shinn, S. Chan, D. Stevens, R. Lee, and J. Leone. 2005. "Flow around a complex building: experimental and large-eddy simulation comparison". *Journal of Applied Meteorology*, vol. 44, p. 571–589.

Campos-Arriaga, L. 2009. "Wind energy in the built environment: a design analysis using CFD and wind tunnel modelling approach". Ph.D thesis, Department of Built Environment, University of Nottingham, England.

Canepa, E. 2004. "An overview about the study of downwash effects on dispersion of airborne pollutants". *Environmental Modelling & Software*, vol. 19, n° 12, p. 1077–1087.

Carpentieri, M., P. Hayden, and A G. Robins. 2012. "Wind tunnel measurements of pollutant turbulent fluxes in urban intersections". *Atmospheric Environment*, vol. 46, p. 669–674.

Caruelle, B. and F. Ducros. 2003. "Detached-eddy simulations of attached and detached boundary layers". *International Journal of Computational Fluid Dynamics*, vol. 17, n° 6, p. 433–451.

Casey, M. and T. Wintergerste. 2000. "Quality and trust in industrial CFD: Best practice guidelines". *ERCOFTAC Special Interest Group*.

Castro, I P. and A G. Robins. 1977. "The flow around a surface mounted cube in uniform and turbulent streams". *Journal of Fluid Mechanics*, vol. 79, n° 2, p. 307–335.

Celik, I B., U. Ghia, P J. Roache, C J. Freitas, H. Coleman, and P E. Raad. 2008. " Procedure for estimation and reporting of uncertainty due to discretization in CFD applications ". *Journal of Fluids Engineering*, vol. 130 (078001), p. 1–4.

Cermak, J E. and L S. Cochran. 1992. " Physical modelling of the atmospheric surface layer ". *Journal of Wind Engineering and Industrial Aerodynamics*, vol. 42, n° 1-3, p. 935–946.

Chang, C H. and R N. Meroney. 2001. " Numerical and physical modeling of bluff body flow and dispersion in urban street canyons ". *Journal of Wind Engineering and Industrial Aerodynamics*, vol. 89, n° 14-15, p. 1325–1334.

Chang, C H. and R N. Meroney. 2003. " Concentration and flow distributions in urban street canyons: wind tunnel and computational data ". *Journal of Wind Engineering and Industrial Aerodynamics*, vol. 91, n° 9, p. 1141–1154.

Chavez, M., B. Hajra, T. Stathopoulos, and A. Bahloul. 2011. " Near-field pollutant dispersion in the built environment by CFD and wind tunnel simulations ". *Journal of Wind Engineering and Industrial Aerodynamics*, vol. 99, n° 4, p. 330–339.

Chavez, M., B. Hajra, T. Stathopoulos, and A. Bahloul. 2012. " Assessment of near-field pollutant dispersion: Effect of upstream buildings ". *Journal of Wind Engineering and Industrial Aerodynamics*, vol. 104-106, p. 509–515.

Cheng, H. and I P. Castro. 2002. " Near wall flow over urban-like roughness ". *Boundary-Layer Meteorology*, vol. 104, n° 2, p. 229–259.

Cheng, Y., F S. Lien, E. Yee, and R. Sinclair. 2003. " A comparison of large-eddy simulation with a standard $k - \epsilon$ Reynolds-averaged Navier–Stokes model for the prediction of a fully developed turbulent flow over matrix of cubes ". *Journal of Wind Engineering and Industrial Aerodynamics*, vol. 91, p. 1301–1328.

Coceal, O., A. Dobre, T G. Thomas, and S E. Belcher. 2007. " Structure of turbulent flow over regular arrays of cubical roughness ". *Journal of Fluid Mechanics*, vol. 589, p. 375–409.

Contini, D., D. Cesari, A. Donateo, and A G. Robins. 2009. " Effects of Reynolds number on stack plume trajectories simulated with small scale models in a wind tunnel ". *Journal of Wind Engineering and Industrial Aerodynamics*, vol. 97, n° 9-10, p. 468–474.

Courant, R., K. Friedrichs, and H. Lewy. 1967. " On the partial difference equations of mathematical physics ". *IMB Journal of Research and Development*, vol. 11, n° 2, p. 215–234.

Crasto, G. 2007. " Numerical simulation of the atmospheric boundary layer ". Ph.D thesis, Department of Industrial Engineering, University of Perugia, Perugia, Italy.

Davidson, P A. 2004. Turbulence - an introduction for scientists and engineers. Oxford University Press,.

Deck, S. 2005. " Zonal-detached-eddy simulation of the flow around a high-lift configuration ". *AIAA Journal*, vol. 43, n° 11, p. 2372–2384.

Deck, S. 2012. “Recent improvements in the zonal-detached-eddy simulation (ZDES) formulation”. *Theoretical and Computational Fluid Dynamics*, vol. 26, n° 6, p. 523-–550.

Delaunay, D., D. Lakehal, C. Barré, and C. Sacré. 1997. “Numerical and wind tunnel simulation of gas dispersion around a rectangular building”. *Journal of Wind Engineering and Industrial Aerodynamics*, vol. 67-68, p. 721–732.

Di-Sabatino, S., R. Buccolieri, B. Pulvirenti, and R. Britter. 2007. “Simulations of pollutant dispersion within idealised urban-type geometries with CFD and integral models”. *Atmospheric Environment*, vol. 41, n° 37, p. 8316–8329.

Dobrescu, M A. 1994. “Effect of mismatching model and boundary layer scales in estimating pollutant dispersion around buildings”. M.Sc.A thesis, Department of Building, Civil and Environmental Engineering, Concordia University, Montreal, Canada.

Easom, G. 2000. “Improved turbulence models for computational wind engineering”. Ph.D thesis, School of Civil Engineering, University of Nottingham, England.

Efthimiou, G C. and J G. Bartiz. 2011. “Atmospheric dispersion and individual exposure of hazardous materials”. *Journal of Hazardous Materials*, vol. 188, p. 375–383.

EPA. 1978. Guideline on air quality models. *United State Environmental Protection Agency (EPA)*, EPA 450/2-78-027 Research Triangle Park, NC, USA.

EPA. 1981. Guideline for use of fluid modeling to determine good engineering practice stack height. *United State Environmental Protection Agency (EPA)*, EPA 450/4-81-003, Research Triangle Park, NC, USA.

Fernando, H J S., D. Zajic, S. Di-Sabatino, R. Dimitrova, B. Hedquist, and A. Dallman. 2010. “Flow, turbulence, and pollutant dispersion in urban atmospheres”. *Physics of Fluids*, vol. 22 (051301), p. 1–20.

Finn, D., K L. Clawson, R G. Carter, J D. Rich, C. Biltoft, and M. Leach. 2010. “Analysis of urban atmosphere plume concentration fluctuations”. *Boundary-Layer Meteorology*, vol. 136, p. 431–456.

Fisher, B., J. Kukkonen, M. Piringer, W. Rotach, and M. Schatzmann. 2006. “Meteorology applied to urban air pollution problems: concept from COST 715”. *Atmospheric Chemistry and Physics*, vol. 6, n° 2, p. 555–564.

Fluent. 2005. “Fluent 6.3 User’s Guide, Fluent Inc., Lebanon”.

Franke, J., C. Hirsch, A G. Jensen, H W. Krüs, M. Schatzmann, P S. Westbury, S D. Miles, J A. Wisse, and N G. Wright. 2004. Recommendations on the use of CFD in wind engineering. In: *Proceedings of the International Conference on Urban Wind Engineering and Building Aerodynamics*, Van-Beeck, J.P.A.J. (Ed.), Cost Action C14, Impact of Wind and Storm on City Life Built Environment, Von Karman Institute, Sint-Genesius-Rode, Belgium.

Franke, J., A. Hellsten, H. Schlünzen, and B. Carissimo. 2007. "Best practice guideline for the CFD simulation of flows in the urban environment". *Cost Action 732*.

Franke, J., A. Hellsten, H. Schlünzen, and B. Carissimo. 2011. "The COST 732 best practice guideline for CFD simulation of flows in the urban environment: a summary". *International Journal of Environment and Pollution*, vol. 44, n° 1-4, p. 419–427.

Franzese, P. and P. Huq. 2011. "Urban dispersion modelling and experiments in the daytime and nighttime atmosphere". *Boundary-Layer Meteorology*, vol. 139, n° 3, p. 395–409.

Fröhlich, D. and J. von Terzi. 2008. "Hybrid LES/RANS methods for the simulation of turbulent flows". *Progress in Aerospace Sciences*, vol. 44, p. 349–377.

Fung, J C H., J C R. Hunt, N A. Malik, and R J. Perkins. 1992. "Kinematic simulation of homogeneous turbulence by unsteady random Fourier modes". *J. Fluid Mech.*, vol. 236, p. 281–318.

Galvàn, S., M. Reggio, and F. Guibault. 2011. "Assessment study of $k - \epsilon$ turbulence models and near-wall modeling for steady state swirling flow analysis in draft tube using Fluent". *Engineering Applications of Computational Fluid Mechanics*, vol. 5, n° 4, p. 459–478.

Gao, Y. and W K. Chow. 2005. "Numerical studies on air flow around a cube". *Journal of Wind Engineering and Industrial Aerodynamics*, vol. 93, n° 2, p. 115–135.

Gavrilov, K., D. Morvan, G. Accary, D. Lyubimov, and S. Meradji. 2013. "Numerical simulation of coherent turbulent structures and of passive scalar dispersion in a canopy sub-layer". *Computers & Fluids*, vol. 78, p. 54–62.

Georgoulias, A K. and D K. Papanastasiou. 2009. "Statistical analysis of boundary layer height in suburban environment". *Meteorology Atmospheric Physics*, vol. 104, n° 1-2, p. 103–111.

Gomes, M S P., A A. Isnard, and J M C. Pinto. 2007. "Wind tunnel investigation on the retention of air pollutants in three-dimensional recirculation zones in urban areas". *Atmospheric Environment*, vol. 41, n° 23, p. 4949–4961.

Gorlé, C., J. Van-Beeck, P. Rambaud, and G V. Tendeloo. 2009. "CFD modelling of small particle dispersion: the influence of the turbulence kinetic energy in the atmospheric boundary layer". *Atmospheric Environment*, vol. 43, n° 3, p. 673–681.

Gousseau, P., B. Blocken, T. Stathopoulos, and G J F. Van-Heijst. 2011a. "CFD simulation of near-field pollutant dispersion on a high-resolution grid: A case study by LES and RANS for a building group in downtown Montreal". *Atmospheric Environment*, vol. 45, n° 2, p. 428–438.

Gousseau, P., B. Blocken, and G J F. Van-Heijst. 2011b. "CFD simulation of pollutant dispersion around isolated buildings: On the role of convective and turbulent mass fluxes in the prediction accuracy". *Journal of Hazardous Materials*, vol. 194, p. 422–434.

Gryning, S E., A A M. Holtslag, J S. Irwin, and B. Sivertsen. 1987. " Applied dispersion modelling based on meteorological scaling parameters ". *Atmospheric Environment (1967)*, vol. 21, n° 1, p. 79–89.

Gupta, A., T. Stathopoulos, and P. Saathoff. 2012. " Wind tunnel investigation of the downwash effect of a rooftop structure on plume dispersion ". *Atmospheric Environment*, vol. 46, p. 496–507.

Hadjisophocleous, G V. and C J. McCartney. 2005. " Guidelines for the use of CFD simulations for fire and smoke modeling ". *ASHRAE Transactions*, vol. 111, n° 2, p. 583–594.

Hajra, B. and T. Stathopoulos. 2012. " A wind tunnel study of the effect of downstream buildings on near-field pollutant dispersion ". *Building and Environment*, vol. 52, p. 19–31.

Hajra, B., T. Stathopoulos, and A. Bahloul. 2010. " Assessment of pollutant dispersion from rooftop stacks: ASHRAE, ADMS and wind tunnel simulation ". *Building and Environment*, vol. 45, n° 12, p. 2768–2772.

Hajra, B., T. Stathopoulos, and A. Bahloul. 2011. " The effect of upstream buildings on near-field pollutant dispersion in the built environment ". *Atmospheric Environment*, vol. 45, p. 4930–4940.

Hang, J. and Y. Li. 2012. " Macroscopic simulations of turbulent flows through high-rise building arrays using a porous turbulence model ". *Building and Environment*, vol. 49, p. 41–54.

Hang, J., Y. Li, M. Sandberg, R. Buccolieri, and S. Di-Sabatino. 2012. " The influence of building height variability on pollutant dispersion and pedestrian ventilation in idealized high-rise urban areas ". *Building and Environment*, vol. 56, p. 346–360.

Hargreaves, D M. and N G. Wright. 2007. " On the use of the $k - \epsilon$ model in commercial CFD software to model the neutral atmospheric boundary layer ". *Journal of Wind Engineering and Industrial Aerodynamics*, vol. 95, n° 5, p. 355–369.

Hasama, T., S. Kato, and R. Ooka. 2008. " Analysis of wind-induced inflow and outflow through a single opening using LES & DES ". *Journal of Wind Engineering and Industrial Aerodynamics*, vol. 96, n° 10-11, p. 1678–1691.

Haupt, S E., F J. Zajaczkowski, and L J. Peltier. 2011. " Detached-eddy simulation of atmospheric flow about surface mounted cube at high Reynolds number ". *Journal of Fluids Engineering*, vol. 133, p. 1–8.

Hefny, M. and R. Ooka. 2009. " CFD analysis of pollutant dispersion around buildings: Effect of cell geometry ". *Building and Environment*, vol. 44, n° 8, p. 1699–1706.

Hennemuth, B. and A. Lammert. 2006. " Determination of the atmospheric boundary layer height from radiosonde and lidar backscatter ". *Boundary-Layer Meteorology*, vol. 120, n° 1, p. 181–200.

Häggkvist, K., U. Svensson, and R. Taeslerd. 1989. "Numerical simulations of pressure fields around buildings". *Building and Environment*, vol. 24, n° 1, p. 65–72.

Holmes, J D. 2001. The atmospheric boundary layer and wind turbulence. *Wind Loading of Structures*. Spon Press, (978-0-419-24610-7).

Holmes, N S. and L. Morawska. 2006. "A review of dispersion modelling and its application to the dispersion of particles: an overview of different dispersion models available". *Atmospheric Environment*, vol. 40, p. 5902–5928.

Hoxey, R P., P J. Richards, and J L. Short. 2005. "A 6 m cube in an atmospheric boundary layer flow. Part 1: full-scale and wind-tunnel results". *Wind and Structures*, vol. 5, p. 165–176.

Hsieh, K J., F S. Lien, and E. Yee. 2007. "Numerical modeling of passive scalar dispersion in an urban canopy layer". *Journal of Wind Engineering and Industrial Aerodynamics*, vol. 95, p. 1611–1636.

Huang, M F., I W H. Lau, C M. Chan, K C S. Kwok, and G. Li. 2011. "A hybrid RANS and kinematic simulation of wind load effects on full-scale tall buildings". *Journal of Wind Engineering and Industrial Aerodynamics*, vol. 99, n° 11, p. 1126–1138.

Huang, Y., X. Hu, and N. Zeng. 2009. "Impact of wedge-shaped roofs on airflow and pollutant dispersion inside urban street canyons". *Building and Environment*, vol. 44, p. 2335–2347.

Huq, P. and P. Franzese. 2012. "Measurements of turbulence and dispersion in three idealized urban canopies with different aspect ratios and comparisons with a Gaussian plume model". *Boundary-Layer Meteorology*, vol. November, p. 1–19.

Iyengar, A K S. and C. Farell. 2001. "Experimental issues in atmospheric boundary layer simulations: roughness length and integral length scale determination". *Journal of Wind Engineering and Industrial Aerodynamics*, vol. 89, n° 11-12, p. 1059–1080.

Janssen, W D., B. Blocken, and T. Van-Hooff. 2013. "Pedestrian wind comfort around buildings: comparison of wind comfort criteria based on whole-flow field data for a complex case study". *Building and Environment*, vol. 59, p. 547–562.

Johnson, G T. and L J. Hunter. 1998. "Urban wind flows: wind tunnel and numerical simulations - a preliminary comparison". *Environmental Modelling & Software*, vol. 13, n° 3-4, p. 279–286.

Jones, W P. and B E. Launder. 1972. "The prediction of laminarization with a two-equation model of turbulence". *International Journal of Heat and Mass Transfer*, vol. 15, n° 2, p. 301–314.

Kaimal, J C. and J J. Finnigan. 1994. Atmospheric boundary layer flows: their structure and measurement. Oxford University Press, Inc.

Kang, H S. and C. Meneveau. 2001. “ Passive scalar anisotropy in a heated turbulent wake: new observations and implications for large-eddy simulations ”. *Journal of Fluid Mechanics*, vol. 442, p. 161–170.

Kawamoto, T., T-T-P. Pham, T. Matsuda, T. Oyama, M. Tanaka, H S. Yu, and I. Uchiyama. 2011. “ Historical review on development of environmental quality standards and guideline values for air pollutants in Japan ”. *International Journal of Hygiene and Environmental Health*, vol. 214, p. 296–304.

Khanduri, A C., C. Bédard, and T. Stathopoulos. 1997. “ Modelling wind-induced interference effects using backpropagation neural networks ”. *Journal of Wind Engineering and Industrial Aerodynamics*, vol. 72, p. 71–79.

Khanduri, A C., T. Stathopoulos, and C. Bédard. 1998. “ Wind-induced interference effects on buildings – a review of the state-of-the-art ”. *Engineering Structures*, vol. 20, n° 7, p. 617–630.

Kossmann, M., R. Vögtlin, U. Corsmeier, B. Vogel, F. Fiedler, H J Binder, N. Kalthoff, and F. Beyrich. 1998. “ Aspects of the convective boundary layer structure over complex terrain ”. *Atmospheric Environment*, vol. 32, n° 7, p. 1323–1348.

Kraichnan, R. 1970. “ Diffusion by a random velocity field ”. *Physics of Fluids*, vol. 13, n° 1, p. 22–31.

Krajnovic, S. and L. Davidson. 2002. “ Large-eddy simulation of the flow around a bluff body ”. *AIAA Journal*, vol. 40, n° 5, p. 927–936.

Köse, D A. and E. Dick. 2010. “ Prediction of the pressure distribution on a cubical building with implicit LES ”. *Journal of Wind Engineering and Industrial Aerodynamics*, vol. 98, n° 10-11, p. 628–649.

Kukadia, V. and J. Palmer. 1998. “ The effect of external atmospheric pollution on indoor air quality: a pilot study ”. *Energy and Buildings*, vol. 27, n° 3, p. 223–230.

Lakehal, D. and W. Rodi. 1997. “ Calculation of the flow past a surface-mounted cube with two-layer turbulence models ”. *Journal of Wind Engineering and Industrial Aerodynamics*, vol. 67-68, p. 65–78.

Lateb, M., C. Masson, T. Stathopoulos, and C. Bédard. 2010a. “ Numerical simulation of pollutant dispersion around a building complex ”. *Building and Environment*, vol. 45, n° 8, p. 1788–1798.

Lateb, M., C. Masson, T. Stathopoulos, and C. Bédard. 2010b. Influence of turbulence models on pollutant dispersion studies around a building complex. In: *Proceedings of the Fifth International Symposium on Computational Wind Engineering (CWE2010)*, Chapel Hill, NC, USA.

Lateb, M., C. Masson, T. Stathopoulos, and C. Bédard. 2011. "Effect of stack height and exhaust velocity on pollutant dispersion in the wake of a building". *Atmospheric Environment*, vol. 45, n° 29, p. 5150–5163.

Lateb, M., C. Masson, T. Stathopoulos, and C. Bédard. 2013. "Comparison of various types of $k - \epsilon$ models for pollutant emissions around a two-building configuration". *Journal of Wind Engineering and Industrial Aerodynamics*, vol. 115, p. 9–21.

Lazure, L., P. Saathoff, and T. Stathopoulos. 2002. "Air intake contamination by building exhausts: tracer gas investigation of atmospheric dispersion models in the urban environment". *Journal of the Air & Waste Management Association*, vol. 52, n° 2, p. 160–166.

Li, W W. and R N. Meroney. 1983a. "Gas dispersion near a cubical model building: Part I. Mean concentration measurements". *Journal of Wind Engineering and Industrial Aerodynamics*, vol. 12, n° 1, p. 15–33.

Li, W W. and R N. Meroney. 1983b. "Gas dispersion near a cubical model building: Part II. Concentration fluctuation measurements". *Journal of Wind Engineering and Industrial Aerodynamics*, vol. 12, n° 1, p. 35–47.

Li, X X., C H. Liu, D Y C. Leung, and K M. Lam. 2006. "Recent progress in CFD modelling of wind field and pollutant transport in street canyons". *Atmospheric Environment*, vol. 40, p. 5640–5658.

Li, Y. and T. Stathopoulos. 1997. "Numerical evaluation of wind-induced dispersion of pollutants around building". *Journal of Wind Engineering and Industrial Aerodynamics*, vol. 67-68, p. 757–766.

Liao, Q. and E. A. Cowen. 2010. "Relative dispersion of a scalar plume in a turbulent boundary layer". *Journal of Fluid Mechanics*, vol. 661, p. 412–445.

Lien, F S. and E. Yee. 2004. "Numerical modelling of the turbulent flow developing within and over a 3-D building array, part I: a high-resolution Reynolds-averaged Navier–Stokes". *Boundary-Layer Meteorology*, vol. 112, n° 3, p. 427–466.

Lien, F S., E. Yee, and Y. Cheng. 2004. "Simulation of mean flow and turbulence over a 2D building array using high-resolution CFD and a distributed drag force approach". *Journal of Wind Engineering and Industrial Aerodynamics*, vol. 92, n° 2, p. 117–158.

Lien, F S., E. Yee, H. Ji, A. Keats, and K J. Hsieh. 2006. "Progress and challenges in the development of physically-based numerical models for prediction of flow and contaminant dispersion in the urban environment". *International Journal of Computational Fluid Dynamics*, vol. 20, n° 5, p. 323–337.

Lien, F S., E. Yee, H. Ji, and K J. Hsieh. 2008. "Partially resolved numerical simulation and RANS modeling of flow and passive scalar transport in an urban environment". *Journal of Wind Engineering and Industrial Aerodynamics*, vol. 96, p. 1832–1842.

Lim, H C., I P. Castro, and R P. Hoxey. 2007. “Bluff bodies in deep turbulent boundary layers: Reynolds-number issues”. *Journal of Fluid Mechanics*, vol. 571, p. 97–118.

Liu, G., J. Xuan, and S. Park. 2003. “A new method to calculate wind profile parameters of the wind tunnel boundary layer”. *Journal of Wind Engineering and Industrial Aerodynamics*, vol. 19, p. 1155–1162.

Liu, X P., J L. Niu, K C S. Kwok, J H. Wang, and B Z. Li. 2010a. “Investigation of indoor air pollutant dispersion and cross-contamination around a typical high-rise residential building: wind tunnel tests”. *Building and Environment*, vol. 45, n° 8, p. 1769–1778.

Liu, Z., Y. Xiong, Z. Wang, and S. Wang. 2010b. “Numerical simulation and experimental study of the new method of horseshoe vortex control”. *Journal of Hydrodynamics*, vol. 22, n° 4, p. 572–581.

Ma, X., X. Shao, X. Li, and Y. Lin. 2012. “An analytical expression for transient distribution of passive contaminant under steady flow field”. *Building and Environment*, vol. 50, p. 98–106.

MacDonald, R W. 2000. “Modelling the mean velocity profile in the urban canopy layer”. *Boundary-Layer Meteorology*, vol. 97, n° 1, p. 25–45.

Maple, R C. 2002. Adaptive harmonic balance method for unsteady, nonlinear, one-dimensional periodic flows. PhD thesis, Department of the air force, Air Force Institute of Technology, Ohio, USA.

Martinuzzi, R. and C. Tropea. 1993. “The flow around surface-mounted prismatic obstacle placed in a fully developed channel flow”. *Journal of Fluids Engineering*, vol. 115, p. 85–92.

Mavroidis, I., R F. Griffiths, and D J. Hall. 2003. “Field and wind tunnel investigations of plume dispersion around single surface obstacles”. *Energy and Buildings*, vol. 37, n° 21, p. 2903–2918.

Meinders, E R. and K. Hanjalic. 1999. “Vortex structure and heat transfer in turbulent flow over a wall-mounted matrix of cubes”. *International Journal of Heat and Fluid Flow*, vol. 20, n° 3, p. 255–267.

Meroney, R N. 1987. “Guidelines for fluid modeling of dense gas cloud dispersion”. *Journal of Hazardous Materials*, vol. 17, n° 1, p. 23–46.

Meroney, R N., B M. Leitl, S. Rafailidis, and M. Schatzmann. 1999. “Wind-tunnel and numerical modeling of flow and dispersion about several building shapes”. *Journal of Wind Engineering and Industrial Aerodynamics*, vol. 81, n° 1-3, p. 333–345.

Mockett, C. and F. Thiele. 2007. Overview of detached-eddy simulation for external and internal turbulent flow applications. In: *Proceedings of the Fifth International Conference on Fluid Mechanics*, Shanghai, China.

Montazeri, H. and B. Blocken. 2013. “CFD simulation of wind-induced pressure coefficients on buildings with and without balconies: validation and sensitivity analysis”. *Building and Environment*, vol. 60, p. 137–149.

Moonen, P., T. Defraeye, V. Dorer, B. Blocken, and J. Carmeliet. 2012a. “Urban physics: effect of the micro-climate on comfort, health and energy demand”. *Frontiers of Architectural Research*, vol. 1, n° 3, p. 197–228.

Moonen, P., V. Dorer, and J. Carmeliet. 2012b. “Effect of flow unsteadiness on the mean wind flow pattern in an idealized urban environment”. *Journal of Wind Engineering and Industrial Aerodynamics*, vol. 104-106, p. 389–396.

Morris, S C., S R. Stolpa, P E. Slaboch, and J C. Klewicki. 2007. “Near-surface particle image velocimetry measurements in a transitionally rough-wall atmospheric boundary layer”. *Journal of Fluid Mechanics*, vol. 580, p. 319-–338.

Murakami, S. 1993. “Comparison of various turbulence models applied to a bluff body”. *Journal of Wind Engineering and Industrial Aerodynamics*, vol. 46, n° 47, p. 21–36.

Murakami, S. 1998. “Overview of turbulence models applied in CWE–1997”. *Journal of Wind Engineering and Industrial Aerodynamics*, vol. 74-76, p. 1–24.

Murakami, S. and A. Mochida. 1988. “3-D numerical simulation of airflow around a cubic model by means of the $k - \epsilon$ model”. *Journal of Wind Engineering and Industrial Aerodynamics*, vol. 31, p. 283–303.

Murakami, S. and A. Mochida. 1989. “Three-dimensional numerical simulation of turbulent flow around buildings using the $k - \epsilon$ turbulence model”. *Building and Environment*, vol. 24, n° 1, p. 51–64.

Murakami, S., A. Mochida, Y. Hayashi, and K. Hibi. 1991. “Numerical simulation of velocity field and diffusion field in an urban area”. *Energy and Buildings*, vol. 15, n° 3-4, p. 345–356.

Nakiboglu, G., C. Gorlé, I. Horváth, J V. Beeck, and B. Blocken. 2009. “Stack gas dispersion measurements with large scale-PIV, aspiration probes and light scattering techniques and comparison with CFD”. *Atmospheric Environment*, vol. 43, n° 21, p. 3396–3406.

Nallasamy, M. 1987. “Turbulence models and their applications to the prediction of internal flows: A review”. *Computers & Fluids*, vol. 15, n° 2, p. 151–194.

Nozu, T. and T. Tamura. 2012. “LES of turbulent wind and gas dispersion in a city”. *Journal of Wind Engineering and Industrial Aerodynamics*, vol. 104-106, p. 492–499.

Oberkampf, W L. and T G. Trucano. 2002. “Verification and validation in computational fluid dynamics”. *Progress in Aerospace Sciences*, vol. 38, n° 3, p. 209–272.

Oberkampf, W L., T G. Trucano, and C. Hirsch. 2004. " Verification, validation, and predictive capability in computational engineering and physics ". *Applied Mechanics Reviews*, vol. 57, n° 5, p. 345–384.

Oke, T R. 1988. " Street design and urban canopy layer climate ". *Energy and Buildings*, vol. 11, p. 103–113.

Onbasioglu, S U. 2001. " On the simulation of the plume from stacks of buildings ". *Building and Environment*, vol. 36, n° 4, p. 543–559.

O'Neil, J. and C. Meneveau. 1997. " Subgrid-scale stresses and their modelling in a turbulent plane wake ". *Journal of Fluid Mechanics*, vol. 349, p. 253–293.

O'Sullivan, J P., R A. Archer, and R G J. Flay. 2011. " Consistent boundary conditions for flows within the atmospheric boundary layer ". *Journal of Wind Engineering and Industrial Aerodynamics*, vol. 99, n° 1, p. 65–77.

Paik, J., F. Sotiropoulos, and F. Porté-Angel. 2009. " Detached-eddy simulation of flow around two wall-mounted cubes in tandem ". *International Journal of Heat and Fluid Flow*, vol. 30, p. 286–305.

Panofsky, H A. and J A. Dutton. 1984. Atmospheric turbulence. John Wiley & Sons, New York.

Parente, A., C. Gorlé, J. Van-Beeck, and C. Benocci. 2011. " Improved $k - epsilon$ model and wall function formulation for the RANS simulation of ABL flows ". *Journal of Wind Engineering and Industrial Aerodynamics*, vol. 99, n° 4, p. 267–278.

Pasquill, F. 1961. " The estimation of the dispersion of windborne material ". *The Meteorological Magazine*, vol. 90, n° 1063, p. 33–49.

Patankar, S V. and D B. Spalding. 1972. " A calculation procedure for heat, mass and momentum transfer in three-dimensional parabolic flows ". *International Journal of Heat and Mass Transfer*, vol. 15, n° 10, p. 1787–1806.

Paterson, D A. and C J. Apelt. 1990. " Simulation of flow past a cube in a turbulent boundary layer ". *Journal of Wind Engineering and Industrial Aerodynamics*, vol. 35, p. 149–176.

Philips, D A. 2011. " Modeling Scalar Dispersion in Urban Environments ". Ph.D thesis, Department of Mechanical Engineering, Stanford University, CA, USA.

Philips, D A., R. Rossi, and G. Iaccarino. 2013. " Large-eddy simulation of passive scalar dispersion in an urban-like canopy ". *Journal of Fluid Mechanics*, vol. 723, p. 404–428.

Piringer, M., S. Joffre, A. Baknalov, A. Christen, M. Deserti, K. De-Ridder, S. Emeis, P. Mestayer, M. Tombrou, D. Middleton, K. Baumann-Stanzer, A. Dandou, A. Karppinen, and J. Burzynski. 2007. " The surface energy balance and the mixing height in urban areas - activities and recommendations of COST-Action 715 ". *Boundary-Layer Meteorology*, vol. 124, n° 1, p. 3–24.

Pope, S B. 2000. Turbulent flows. Combridge University Press.

Poreh, M. and J E. Cermak. 1990. " Small scale modeling of line integrated concentration fluctuations ". *Journal of Wind Engineering and Industrial Aerodynamics*, vol. 36, p. 665–673.

Pournazeri, S., M. Princevac, and A. Venkatram. 2012. " Scaling of buildings affected plume rise and dispersion in water channels and wind tunnels - revisit of an old problem ". *Journal of Wind Engineering and Industrial Aerodynamics*, vol. 103, p. 16–30.

Qu, Y. 2011. " Computational study of wind flow and pollutant dispersion near tree canopies ". Ph.D thesis, Department of Science, Engineering and Environment, University of Paris-Est, Paris, France.

Ramponi, R. and B. Blocken. 2012a. " CFD simulation of cross-ventilation for a generic isolated building: impact of computational parameters ". *Building and Environment*, vol. 53, p. 34–48.

Ramponi, R. and B. Blocken. 2012b. " CFD simulation of cross-ventilation flow for different isolated building configurations: validation with wind tunnel measurements and analysis of physical and numerical diffusion effects ". *Journal of Wind Engineering and Industrial Aerodynamics*, vol. 104-106, p. 408–418.

Ratcliff, M A. and E. Sandru. 1999. Dilution calculations for determining laboratory exhaust stack height. American Society of Heating, Refrigerating and Air-conditioning Engineering (ASHRAE), CH-99-7-1, Atlanta, USA.

Razak, A A., A. Hagishima, N. Ikegaya, and j. Tanimoto. 2013. " Analysis of airflow over building arrays for assessment of urban wind environment ". *Building and Environment*, vol. 59, p. 56–65.

Ricciardelli, F. and S. Polimeno. 2006. " Some characteristics of the wind flow in the lower Urban Boundary Layer ". *Journal of Wind Engineering and Industrial Aerodynamics*, vol. 94, n° 11, p. 815–832.

Richards, P. and S. Norris. 2011. " Appropriate boundary conditions for computational wind engineering models revisited ". *Journal of Wind Engineering and Industrial Aerodynamics*, vol. 99, n° 4, p. 257–266.

Richards, P J. and R P. Hoxey. 1993. " Appropriate boundary conditions for computational wind engineering models using the $k-\epsilon$ turbulence model ". *Journal of Wind Engineering and Industrial Aerodynamics*, vol. 46-47, p. 145–153.

Richards, P J. and R P. Hoxey. 2008. " Wind loads on the roof of a 6 m cube ". *Journal of Wind Engineering and Industrial Aerodynamics*, vol. 96, n° 6-7, p. 984–993.

Richards, P J. and R P. Hoxey. 2012. " Pressures on a cubic building - part 1: full-scale results ". *Journal of Wind Engineering and Industrial Aerodynamics*, vol. 102, p. 72–86.

Riddle, A., D. Carruthers, A. Sharpe, C. McHugh, and J. Stocker. 2004. "Comparisons between FLUENT and ADMS for atmospheric dispersion modelling". *Atmospheric Environment*, vol. 38, n° 7, p. 1029–1038.

Roache, P J. 1994. "Perspective: a method for uniform reporting of grid refinement studies". *Journal of Fluids Engineering*, vol. 116, n° 3, p. 405–413.

Roache, P J. 1997. "Quantification of uncertainty in computational fluid dynamics". *Annual Review of Fluids Mechanics*, vol. 29, p. 123–160.

Robin, A. 2003. "Wind tunnel dispersion modelling some recent and not so recent achievements". *Journal of Wind Engineering and Industrial Aerodynamics*, vol. 91, p. 1777–1790.

Rock, B A. and K A. Moylan. 1999. "Placement of ventilation air intakes for improved IAQ". *ASHRAE Transactions*, vol. 105, n° 1, p. 1–9.

Rodi, W. 1997. "Comparison of LES and RANS calculations of the flow around bluff bodies". *Journal of Wind Engineering and Industrial Aerodynamics*, vol. 69-71, p. 55–75.

Rodriguez, L M., P E. Bieringer, and T. Warner. 2013. "Urban transport and dispersion model sensitivity to wind direction uncertainty and source location". *Atmospheric Environment*, vol. 64, p. 25–39.

Rohdin, P. and B. Moshfegh. 2011. "Numerical modelling of industrial indoor environments: a comparison between different turbulence models and supply systems supported by field measurements". *Building and Environment*, vol. 46, p. 2365–2374.

Rossi, R. and G. Iaccarino. 2009. "Numerical simulation of scalar dispersion downstream of a square obstacle using gradient-transport type models". *Atmospheric Environment*, vol. 43, n° 16, p. 2518–2531.

Rotach, M W. 1993a. "Turbulence close to a rough urban surface Part I: Reynolds stress". *Boundary-Layer Meteorology*, vol. 65, n° 1-2, p. 1–28.

Rotach, M W. 1993b. "Turbulence close to a rough urban surface part II: variances and gradients". *Boundary-Layer Meteorology*, vol. 66, n° 1-2, p. 75–92.

Rotach, M W. 1999. "On the influence of the urban roughness sublayer on turbulence and dispersion". *Atmospheric Environment*, vol. 33, n° 24-25, p. 4001–4008.

Roth, M. 2000. "Review of atmospheric turbulence over cities". *Quarterly Journal of the Royal Meteorological Society*, vol. 126, p. 941–990.

Roy, C J. 2005. "Review of code and solution verification procedures for computational simulation". *Journal of Computational Physics*, vol. 205, n° 1, p. 131–135.

Roy, C J. 2010. Review of discretization error estimators in scientific computing. In: *Proceedings of the 48th AIAA Aerospace Science Meeting Including the New Horizons Forum and Aerospace Exposition*, Orlando, FL, USA.

Saathoff, P. and T. Stathopoulos. 1997. “Dispersion of exhaust gases from roof-level stacks and vents on a laboratory building: discussion”. *Atmospheric Environment*, vol. 31, n° 7, p. 1087–1089.

Saathoff, P J., T. Stathopoulos, and M. Dobrescu. 1995. “Effects of model scale in estimating pollutant dispersion near buildings”. *Journal of Wind Engineering and Industrial Aerodynamics*, vol. 54-55, p. 549–559.

Sada, K. and A. Sato. 2002. “Numerical calculation of flow and stack-gas concentration fluctuation around a cubical building”. *Atmospheric Environment*, vol. 36, n° 35, p. 5527–5534.

Salim, S M. 2011. “Computational study of wind flow and pollutant dispersion near tree canopies”. Ph.D thesis, Division of Environment, University of Nottingham Malaysia Campus, Malaysia.

Salim, S M., R. Buccolieri, A. Chan, and S. Di-Sabatino. 2011. “Numerical simulation of atmospheric pollutant dispersion in an urban street canyon: Comparison between RANS and LES”. *Journal of Wind Engineering and Industrial Aerodynamics*, vol. 99, n° 2-3, p. 103–113.

Santos, J M., N C. Reis, E V. Goulart, and I. Mavroidis. 2009. “Numerical simulation of flow and dispersion around an isolated cubical building: the effect of the atmospheric stratification”. *Atmospheric Environment*, vol. 43, n° 34, p. 5484–5492.

Schatzmann, M. and R. Britter. 2005. Quality assurance of micro-scale meteorological models. COST 732 Report, European Science Foundation (ISBN: 3-00-018312-4).

Schatzmann, M. and B. Leitl. 2002. “Validation and application of obstacle-resolving urban dispersion models”. *Atmospheric Environment*, vol. 36, n° 30, p. 4811–4821.

Schatzmann, M. and B. Leitl. 2011. “Issues with validation of urban flow and dispersion CFD models”. *Journal of Wind Engineering and Industrial Aerodynamics*, vol. 99, n° 4, p. 169–186.

Schatzmann, M., S. Rafailidis, and M. Pavageau. 1997. “Some remarks on the validation of small-scale dispersion models with field and laboratory data”. *Journal of Wind Engineering and Industrial Aerodynamics*, vol. 67-68, p. 885–893.

Schatzmann, M., B. Leitl, and J. Liedtke. 2000. “Dispersion in urban environment; comparison of field measurements with wind tunnel results”. *Environmental Monitoring and Assessment*, vol. 65, n° 1-2, p. 249–257.

Shih, T H., W W. Liou, A. Shabbir, Z. Yang, and J. Zhu. 1995a. “A new $k - \epsilon$ eddy viscosity model for high Reynolds number turbulent flows”. *Computers & Fluids*, vol. 24, n° 3, p. 227–238.

Shih, T H., J. Zhu, and J L. Lumley. 1995b. "A new Reynolds stress algebraic equation model". *Computer Methods in Applied Mechanics and Engineering*, vol. 125, n° 1-4, p. 287–302.

Shirasawa, T., R. Yoshie, H. Takana, T. Kobayashi, A. Mochida, and Y. Endo. 2008. Cross comparison of CFD results of gas diffusion in weak wind region behind a high-rise building. In: *Proceedings of the 4th International Conference on Advances in Wind and Structures (AWAS'08)*, Jeju, Korea.

Shur, M., P R. Spalart, M. Strelets, and A. Travin. 1999. Detached-eddy simulation of an airfoil at high angle of attack. In *Engineering Turbulence Modelling and Experiments 4*, Ed. W. Rodi, D. Laurence, Oxford, Elsevier Sci., 669-–678.

Sini, J F., S. Anquetin, and P G. Mestayer. 1996. "Pollutant dispersion and thermal effects in urban street canyons". *Atmospheric Environment*, vol. 30, n° 15, p. 2659–2677.

Smirnov, R., S. Shi, and I. Celik. 2001. "Random flow generation technique for large-eddy simulations and particle-dynamics modeling". *Journal of Fluids Engineering*, vol. 123, n° 2, p. 359–371.

Snyder, W H. 1981. Guideline for fluid modeling of atmospheric diffusion. *United State Environmental Protection Agency (EPA)*, EPA-600/8-81-009, Research Triangle Park, NC, USA.

Spalart, P R. 2001. Young-person's guide to detached-eddy simulation grids. Technical report, NASA/CR-2001-211032, NASA Center for AeroSpace Information, MD, USA.

Spalart, P R. 2009. "Detached-eddy simulation". *Annual Review of Fluid Mechanics*, vol. 41, p. 181–202.

Spalart, P R. and K D. Squires. 2004. The status of detached-eddy simulation for bluff bodies. In: *Direct and large-eddy simulation*, p. 29–45.

Spalart, P R., W H. Jou, M. Strelets, and S R. Allmaras. 1997. Comments on the feasibility of LES for wings, and on a hybrid RANS/LES approach. In: Advances in DNS/LES, Ed. C. Liu and Z. Liu, Columbus, OH: Greydon Press, p. 137–147.

Spalart, P R., S. Deck, M L. Shur, K D. Squires, M K. Strelets, and A Travin. 2006. "A new version of detached-eddy simulation, resistant to ambiguous grid densities". *Theoretical and Computational Fluid Dynamics*, vol. 20, n° 3, p. 181–195.

Squires, K D. 2004. Detached-eddy simulation: current status and perspectives. In: *Direct and large-eddy simulation*, Ed. R. Friedrich, B.J Geurt and O Métais, Kluwer, Dordrecht.

Stathopoulos, T. 1997. "Computational wind engineering: past achievements and future challenges". *Journal of Wind Engineering and Industrial Aerodynamics*, vol. 67-68, p. 509–532.

Stathopoulos, T. 2006. "Pedestrian level winds and outdoor human comfort". *Journal of Wind Engineering and Industrial Aerodynamics*, vol. 94, n° 11, p. 769–780.

Stathopoulos, T., L. Lazure, P. Saathoff, and X. Wei. 2002. "Dilution of exhaust from a rooftop stack on a cubical building in an urban environment". *Atmospheric Environment*, vol. 36, n° 29, p. 4577–4591.

Stathopoulos, T., L. Lazure, P. Saathoff, and A. Gupta. 2004. The effect of stack height, stack location and rooftop structures on air intake contamination: A laboratory and full-scale study. Institut de recherche Robert-Sauvé en santé et en sécurité du travail (IRSST), IRSST/Report-392, Montreal, Canada.

Stathopoulos, T., B. Hajra, and A. Bahloul. 2008. Analytical evaluation of dispersion of exhaust from rooftop stacks on buildings. Institut de recherche Robert-Sauvé en santé et en sécurité du travail (IRSST), IRSST/Report-576, Montreal, Canada.

Sterling, E. 1988. Overview of detached-eddy simulation for external and internal turbulent flow applications. In: *Proceedings of the Symposium on Indoor Air Quality*, San Carlos de Bariloche, Argentina.

Stern, F., R V. Wilson, H W. Coleman, and E G. Paterson. 2001. "Comprehensive approach to verification and validation of CFD simulations–part 1: methodology and procedures". *Journal of Fluids Engineering*, vol. 123, n° 4, p. 793–802.

Straw, M P. 2000. "Computation and measurement of wind induced ventilation". Ph.D thesis, School of Civil Engineering, University of Nottingham, England.

Straw, M P., C J. Baker, and A P. Robertson. 2000. "Experimental measurements and computations of the wind-induced ventilation of a cubic structure". *Journal of Wind Engineering and Industrial Aerodynamics*, vol. 88, n° 2-3, p. 213–230.

Stull, R B. 1998. An introduction to boundary layer meteorology. Kluwer Academic Publishers.

Tennekes, H. and J L. Lumley. 1972. A first course in turbulence. The MIT Press.

Tominaga, Y. and T. Stathopoulos. 2007. "Turbulent Schmidt numbers for CFD analysis with various types of flowfield". *Atmospheric Environment*, vol. 41, n° 3, p. 8091–8099.

Tominaga, Y. and T. Stathopoulos. 2009. "Numerical simulation of dispersion around an isolated cubic building: Comparison of various types of $k - \epsilon$ models". *Atmospheric Environment*, vol. 43, n° 20, p. 3200–3210.

Tominaga, Y. and T. Stathopoulos. 2010. "Numerical simulation of dispersion around an isolated cubic building: Model evaluation of RANS and LES". *Building and Environment*, vol. 45, n° 10, p. 2231–2239.

Tominaga, Y. and T. Stathopoulos. 2012. “CFD modeling of pollution dispersion in building array: Evaluation of turbulent scalar flux modeling in RANS model using LES results”. *Journal of Wind Engineering and Industrial Aerodynamics*, vol. 104–106, p. 484–491.

Tominaga, Y., A. Mochida, R. Yoshie, H. Kataoka, T. Nozu, M. Yoshikawa, and T. Sharasawa. 2008. “AIJ guidelines for practical applications of CFD to pedestrian wind environment around buildings”. *Journal of Wind Engineering and Industrial Aerodynamics*, vol. 96, n° 10-11, p. 1749–1761.

Travin, A., M. Shur, M. Strelets, and P. Spalart. 1999. “Detached-eddy simulations past a circular cylinder”. *Flow, Turbulence and Combustion*, vol. 63, n° 1-4, p. 293–313.

Tseng, Y H., C. Meneveau, and M B. Parlange. 2006. “Modeling flow around bluff bodies and predicting urban dispersion using large-eddy simulation”. *Environmental Science & Technology*, vol. 40, n° 8, p. 2653–2662.

Tutar, M. and G. Ogguz. 2004. “Computational modeling of wind flow around a group of buildings”. *International Journal of Computational Fluid Dynamics*, vol. 18, n° 8, p. 651–670.

Van-Hooff, T. and B. Blocken. 2010. “On the effect of wind direction and urban surroundings on natural ventilation of a large semi-enclosed stadium”. *Computers & Fluids*, vol. 39, p. 1146–1155.

Van-Pul, W A J., A A M. Holtslag, and D P J. Swart. 1994. “A comparison of ABL height inferred routinely from lidar and radiosondes at noontime”. *Boundary-Layer Meteorology*, vol. 68, n° 1-2, p. 173–191.

Vardoulakis, S., R. Dimitrova, K. Richards, D. Hamlyn, G. Camilleri, M. Weeks, J F. Sini, R. Britter, C. Borrego, M. Schatzmann, and N. Moussiopoulos. 2011. “Numerical model inter-comparison for wind flow and turbulence around single-block buildings”. *Environmental Modeling & Assessment*, vol. 16, n° 2, p. 169–181.

Varshney, K. and K. Poddar. 2011. “Experiments on integral length scale control in atmospheric boundary layer wind tunnel”. *Theoretical and Applied Climatology*, vol. 106, n° 1-2, p. 127–137.

Vincont, J Y., S. Simoëns, M. Ayrault, and J M. Wallace. 2000. “Passive scalar dispersion in a turbulent boundary layer from a line source at the wall and downstream of an obstacle”. *Journal of Fluid Mechanics*, vol. 424, p. 127–167.

Wagaman, S A., K A. Rainwater, K C. Mehta, and R H. Ramsey. 2002. “Full-scale flow visualization over a low-rise building”. *Journal of Wind Engineering and Industrial Aerodynamics*, vol. 90, n° 1, p. 1–8.

Wang, K. and T. Stathopoulos. 2007. “Exposure model for wind loading of buildings”. *Journal of Wind Engineering and Industrial Aerodynamics*, vol. 95, n° 9-11, p. 1511–1525.

Wang, M., C H. Lin, and Q. Chen. 2011. "Determination of particle deposition in enclosed spaces by detached-eddy simulation with the Lagrangian method". *Atmospheric Environment*, vol. 45, n° 30, p. 5376–5384.

Wang, P. and H. Mu. 2010. "Numerical simulation of pollutant flow and dispersion in different street layouts". *International Journal of Environmental Studies*, vol. 67, n° 2, p. 155–167.

Wang, X. 2006. "Numerical simulation of wind – Induced dispersion of emissions from rooftop stacks". M.Sc.A thesis, Department of Building, Civil and Environmental Engineering, Concordia University, Montreal, Canada.

Wang, Y. and P W. James. 1999. "On the effect of anisotropy on the turbulent dispersion and deposition of small particles". *International Journal of Multiphase Flow*, vol. 25, n° 3, p. 551–558.

Weil, J C., P P. Sullivan, E G. Patton, and C-H. Moeng. 2012. "Statistical variability of dispersion in the convective boundary layer: ensembles of simulations and observations". *Boundary-Layer Meteorology*, vol. 145, p. 185–210.

White, A B. and C J. Senff. 1999. "A comparison of mixing depths observed by ground-based wind profilers and an airborne lidar". *Journal of Atmospheric and Ocean Technology*, vol. 16, p. 584–590.

White, B R. 2000. Physical modeling of atmospheric flow and environmental applications. In: *Proceedings of the 51st Anniversary Conference of* K*orean* S*ociety of* M*echanical* E*ngineers (KSME)*.

White, B R. 2003. Wind-tunnel study of atmospheric dispersion of near-field exhaust from a stack. American Society of Heating, Refrigerating and Air-conditioning Engineering (ASHRAE), IN-91-3-5, Atlanta, USA.

White, B R. and W. Stein. 1990. "Wind-tunnel studies of variable stack heights for a low-profile building". *Journal of Wind Engineering and Industrial Aerodynamics*, vol. 36, n° 1-3, p. 675–687.

Wilson, D J. and B K. Lamb. 1994. "Dispersion of exhaust gases from roof-level stacks and vents on a laboratory building". *Atmospheric Environment*, vol. 28, n° 19, p. 3099–3111.

Wright, N G. and G J. Easom. 2003. "Non-linear $k-\epsilon$ turbulence model results for flow over a building at full-scale". *Applied Mathematical Modelling*, vol. 27, n° 12, p. 1013–1033.

Xie, X., Z. Huang, and J-S. Wang. 2005. "Impact of building configuration on air quality in street canyon". *Atmospheric Environment*, vol. 39, n° 25, p. 4519–4530.

Xie, Z T. and I P. Castro. 2006. "LES and RANS for turbulent flow over arrays of wall-mounted obstacles". *Flow Turbulence Combustion*, vol. 76, p. 291–312.

Xie, Z T., P. Hayden, and C R. Wood. 2013. "Large-eddy simulation of approaching-flow stratification on dispersion over arrays of buildings". *Atmospheric Environment*, vol. 71, p. 64–74.

Yakhot, A., T. Anor, H. Liu, and N. Nikitin. 2006. "Direct numerical simulation of turbulent flow around a wall-mounted cube: spatio-temporal evolution of large-scale vortices". *Journal of Fluid Mechanics*, vol. 566, p. 1–9.

Yakhot, V., S A. Orszag, S. Thangam, T B. Gatski, and C G. Speziale. 1992. "Development of turbulence models for shear flows by a double expansion technique". *Physics of Fluids*, vol. A4, p. 1510–1520.

Yang, W., Y. Quan, X. Jin, Y. Tamura, and M. Gu. 2005. "Influences of equilibrium atmosphere boundary layer and turbulence parameter on wind loads of low-rise buildings". *Journal of Wind Engineering and Industrial Aerodynamics*, vol. 96, n° 10-11, p. 2080–2092.

Yang, Y. and Y. Shao. 2008. "Numerical simulations of flow and pollution dispersion in urban atmospheric boundary layers". *Environmental Modelling & Software*, vol. 23, n° 7, p. 906–921.

Yang, Y., M. Gu, S. Chen, and X. Jin. 2009. "New inflow boundary conditions for modelling the neutral equilibrium atmospheric boundary layer in computational wind engineering". *Journal of Wind Engineering and Industrial Aerodynamics*, vol. 97, n° 2, p. 88–95.

Yassin, M F. 2013. "A wind tunnel study on the effect of thermal stability on flow and dispersion of rooftop stack emissions in the near wake of a building". *Atmospheric Environment*, vol. 65, p. 89–100.

Yassin, M F., S. Kato, R. Ooka, T. Takahashi, and R. Kouno. 2005. "Field and wind-tunnel study of pollutant dispersion in a built-up area under various meteorological conditions". *Journal of Wind Engineering and Industrial Aerodynamics*, vol. 93, n° 5, p. 361–382.

Yassin, M F., R. Kellnerova, and Z. Janour. 2008. "Impact of street intersections on air quality in an urban environment". *Atmospheric Environment*, vol. 42, n° 20, p. 4948—4963.

Yoshie, R., G. Jiang, T. Shirasawa, and J. Chung. 2011. "CFD simulations of gas dispersion around high-rise building in non-isothermal boundary layer". *Journal of Wind Engineering and Industrial Aerodynamics*, vol. 99, n° 4, p. 279–288.

Zhai, Z J., Z. Zhang, W. Zhang, and Q Y. Chen. 2007. "Evaluation of various turbulence models in predicting airflow and turbulence in enclosed environments by CFD: part 1–summary of prevalent turbulence models". *HVAC&R Research*, vol. 13, n° 6, p. 853–870.

Zhang, A., C. Gao, and L. Zhang. 2005. "Numerical simulation of the wind field around different building arrangements". *Journal of Wind Engineering and Industrial Aerodynamics*, vol. 93, n° 12, p. 891—904.

Zhou, J. and C N. Kim. 2010. Numerical investigation of indoor CO_2 concentration distribution in an apartment. In: *Proceedings of the 3rd International Symposium on Sustainable Healthy Buildings (SHB2010)*, Seoul, Korea.

Zhou, Y. and T. Stathopoulos. 1997. " A new technique for the numerical simulation of wind flow around buildings ". *Journal of Wind Engineering and Industrial Aerodynamics*, vol. 72, p. 137–147.